

Quantum Transport through Conjugated Organic Molecular Junctions

Norah Theafallh Algethami

PhD Thesis in Physics



Submitted in partial fulfilment of the requirements for the degree of Doctor of Philosophy

January 2019

Declaration

Except where stated otherwise, this thesis is a result of the author's original work and has not been submitted in whole or in part for the award of a higher degree elsewhere.

This thesis documents work carried out between October 2015 and January 2019 at Lancaster University, UK, under the supervision of Prof. Colin J. Lambert and funded by Taif University, Saudi Arabia.

Norah Algethami

January 2019

*I dedicate this thesis to
My beloved parents and husband, My Kids
for their love, endless support, Encouragement and sacrifices.*

Abstract

Understanding the electronic transport properties of junctions consisting of a scattering region such as a nanoscale object or molecule connected to electrodes is the central basis for future nano and molecular scale applications. In this thesis, I shall discuss the theoretical methods needed to describe such junctions and the present three studies of the electronic properties of molecular junction.

High electrical conductance molecular nanowires are highly desirable components for future molecular-scale circuitry, but typically molecular wires act as tunnel barriers and their conductance decays exponentially with length. In chapter 4, I demonstrate that the conductance of fused-oligo-porphyrin nanowires can be either length independent or increase with length at room temperature. I show that this negative attenuation is an intrinsic property of fused-oligo-porphyrin nanowires, but its manifestation depends on the electrode material or anchor groups. This highly-desirable, non-classical behaviour signals the quantum nature of transport through such wires. It arises, because with increasing length, the tendency for electrical conductance to decay is compensated by a decrease in their HOMO-LUMO gap. This study reveals the potential of these molecular wires as interconnects in future molecular-scale circuitry.

Identification of structure-property relationships that govern single-molecule conductance is key to the continued development of molecular electronics. To realise new quantum-interference-based molecular junction, there is a need to establish simple and intuitive rules for synthesizing molecules with flexible and controllable chemical structures. In chapter 5, I demonstrate methoxyl groups (-OMe) induce destructive quantum interference (DQI) tuning in meta-phenylene ethylene-type oligomers (m-OPE). My calculation reveals that the conductance of single molecules with -OMe pendant groups is sensitive to the position of the -OMe. This result is in agreement

with recently developed magic ratio and orbital product rules and demonstrates that destructive QI can be tuned by changing the –OMe position. This novel method of DQI tuning provides a new design strategy for creating single-molecule junctions with desirable functions.

The design and development of metal/single-molecule/metal junctions with a conductance response to external stimuli has been a strong driving force in molecular electronics community. Reproducible conductance increase (or decrease) of a junction in response to external stimuli have been exploited. Mechanoresistive metal-molecule-metal junctions, whose electrical conductance depends on the mechanical separation of the two electrodes, allow further control, which could be exploited to fabricate junctions responsive to multiple stimuli (e.g. electrochemical potential and electrode separation). Furthermore, knowledge of the structure-property relationships of mechanosensitive junctions provides a wealth of information about the nature, strength and configuration of metal-molecule interactions at the contact interface, which can be applied to fundamental studies of surface science and can be exploited to improve the design of molecular junction. In chapter 6, I demonstrate the metal/single-molecule/metal junctions give a mechanoresistive behaviour with enhanced sensitivity, based on (methylthio)thiophene contacting groups. The effect arises from localised interactions between the thienyl sulfurs and the electrodes, which allows the junction to transition from a monodentate to a bidentate contact configuration as the junction is compressed, resulting in a up to two order of magnitude in the (methylthio)thiophene-terminated molecule higher conductance compared with the (methylthio)benzene counterpart.

Acknowledgments

First and foremost, I would like to thank ALLAH for giving me the strength, knowledge and ability to achieve my dream.

During the completion of this thesis, there were many kinds of supports I have got I would like to express the deepest appreciation to my supervisor, Professor Colin J. Lambert, who has the attitude and the substance of a genius: he continually and convincingly adds a special flavour and spirit of adventure in regard to research by intensive fruitful discussion and excitement in regard to teaching over these years.

My deep gratitude goes to my co-supervisor Dr. Hatef Sadeghi, for his excellent guidance, caring, patience, answering questions and providing me with many useful suggestions.

The good advice, support and friendship of my second co-supervisor, Dr. Sara Sangtarash has been invaluable on both an academic and a personal level, for which I am extremely grateful for her.

I would like to thank the all collaborating experimental groups in (Liverpool University), (Xiamen University, China), (University of Western Australia) and (Durham University) for their synthesis and measurements.

I am also so grateful for Dr. Steven Bailey and Dr. Iain Grace for providing the help tutorials.

I would like also to thank my sponsor, the Ministry of Higher Education in Saudi Arabia and Saudi culture mission in London, Taif University in Saudi Arabia, for given me this fantastic opportunity to study a Ph.D. in the United Kingdom.

I would thank my beloved husband, Talal who gives me the largest support, endless love, care, encouragement and understanding for everything. I am really grateful for his patience, tolerance and love.

I also would like to extend my gratitude to **all** my PhD colleagues and my friends in Colin's group for their kind help and support.

Last but not the least, I would like to thank my parent, brothers (Mohammed and Dr. Saad), sisters (♥Meaad, Sara, Eiyda, Foz, Maha, Lateefa, Areej♥) and all friends especially my soul friend which my gratitude to her is beyond words.

Publications

- 1- **Algethami, N.**, Sadeghi, H., Sangtarash, S., & Lambert, C. J. (2018). The conductance of porphyrin-based molecular nanowires increases with length. *Nano letters*. 2018, 18 (7), 4482–4486.
- 2- Nicolò Ferri, **Norah Algethami**, Andrea Vezzoli, Sara Sangtarash, Maeve McLaughlin, Hatef Sadeghi, Colin J. Lambert, Richard J. Nichols and Simon J. Higgins. (2018). Large-Amplitude, High-Frequency Single-Molecule Switch. (Submitted)
- 3- Feng Jiang, Douglas I. Trupp, **Norah Algethami**, Haining Zheng, Sara Sangtarash, Wenxiang He, Afaf Alqorashi, Chenxu Zhu, Chun Tang, Ruihao Li, Junyang Liu, Hatef Sadeghi, Jia Shi, Ross Davidson, Masnun Naher, Paul J. Low, Wenjing Hong, Colin J. Lambert.(2018). Ringing the changes: Quantum Interference Tuning in Single Molecular Junctions. (Submitted)

Contents

1. Chapter 1: Introduction	
1.1: Molecular Electronics	10
1.2: Thesis Outline	13
Bibliography	14
2. Chapter 2: Density Functional Theory	
2.1. Introduction	22
2.2. The Many-Body Problem	23
2.3. The Hohenberg-Kohn theorems	25
2.4. The Kohn-Sham Method	25
2.5. The Exchange Correlation functional	27
2.5.1. Local Density Approximation	28
2.5.2. Generalized Gradient Approximation	28
2.6. SIESTA	29
2.6.1. The Pseudopotential Approximation	29
2.6.2. SIESTA Basis Sets	30
2.6.3. Calculating binding energy using the counter poisemethod	31
Bibliography	33
3. Chapter 3: Single Particle Theory	
3.1. Introduction	36
3.2. Schrödinger Equation	37
3.3. The Landauer Formula	38
3.4. Tight-Binding Model	41
3.5. Scattering Theory	43
3.5.1. One dimensional (1-D) linear crystalline lattice (infinite)	43
3.5.2. Retarded Green's Function	44
3.5.3. One-Dimensional (1-D) Scattering	46
3.6. Transport through an arbitrary scattering region	50
3.7. Features of the Transport Curve	53
3.7.1. Breit-Wigner Resonance	53
Bibliography	56

4. Chapter 4: The Conductance of Porphyrin-Based Molecular Nanowires Increases with Length	
4.1. Introduction	59
4.2. Molecular Structure	60
4.3. Results and discussion	63
4.3.1. A simple model based on coupling of a chain of monomers	74
Bibliography	79
5. Chapter5: Quantum Interference Tuning in Single Molecular Junctions	
5.1. Introduction	85
5.2. Molecular Structure	86
5.3. Results and discussion	86
Bibliography	93
6. Chapter 6: Large amplitude, high-frequency single-molecule switch.	
6.1. Introduction	99
6.2. Molecular Structure	99
6.3. Results and discussion	100
Bibliography	108
7. Chapter 7: Conclusion, Future work	
7.1. Conclusions	111
7.2. Future Works	113
Bibliography	114

Chapter 1

1. Introduction

1.1. Molecular Electronics

Molecular electronics is a field of science that investigates the electronic transport properties of systems in which individual molecules are used as a basic building block. The dimensions of some molecular systems are a few nanometres, and therefore molecular electronics should be viewed as a subfield of nanotechnology¹.

The idea of using single molecules as building block to design and fabricate molecular electronic components has been around for more than 40 years², but only recently it has attracted huge scientific interest to explore their unique properties and opportunities. Molecular electronics, including self-assembled monolayers³ and single-molecule junctions⁴ are of interest not only for their potential to deliver logic gates⁵, sensors⁶ and memories⁷ with ultralow power requirements and sub-10-nm device footprints, but also for their ability to probe room-temperature quantum properties at a molecular scale such as quantum interference⁸.

In the last couple of years and especially since the rise of graphene⁹ in materials science and condensed-matter physics¹⁰, one can think of graphene-molecule-graphene junctions¹¹. Graphene with its low resistance is a very attractive candidate that

offers different anchoring modalities^{12,13} compared to metallic electrodes such as gold. It has attracted enormous interest due to its fascinating properties, including high charge mobility, transparency, mechanical strength and flexibility.

Graphene, a single-layer of a hexagonal lattice of carbon atoms, is a two-dimensional zero band gap semimetal carbon material and has received worldwide attention since its discovery by Geim and Novoselov et al. in 2004¹⁴. It has emerged as a fascinating system for fundamental studies in condensed matter physics, as well as the promising candidate material for future application in nanoelectronics and molecular devices¹⁰. It has a high specific surface structure¹⁵ and excellent thermal, mechanical and electrical properties¹⁶⁻¹⁸. Nano-sized graphene nanoribbons have been cut out of graphene sheets with two basic shapes for the edges: armchair and zigzag, which have distinct electronic transport properties^{19,20}.

This thesis involves theoretical studies focused on electronic properties of electrode-molecule-electrode junctions. Two main techniques have been used to study the junctions in this thesis; density functional theory (DFT), which is implemented in the SIESTA code²¹, and the non-equilibrium Green's function formalism of transport theory²², which is implemented in the Gollum code²³.

The main focus in this thesis, is on finding molecules with desirable properties. Among different organic molecules, porphyrins are an attractive class of organic molecules to investigate for molecular electronic functions²⁴. The porphyrin molecule consists of four pyrrole cores (the inner ring π -system), and is an attractive building block for molecular-scale devices, because it is highly-conjugated, has a rigid planar geometry and is chemically stable^{25,26}. Therefore, we can use it as a basis for wires, switches, transistors, and photodiodes²⁷⁻²⁹.

The search for molecular nanowires, whose electrical conductance decays slowly with length has been subject to many studies in the last couple of decades^{27,30–34}. Single-molecule wires typically act as tunnel barriers and their conductance decays exponentially by molecular length^{35,36}. Molecular wires usually possess a high beta factor, which limits their potential as interconnects in future molecular-scale circuitry. For example, measured room-temperature values of positive beta factor for OPEs³⁷, OAEs³⁸, OPVs³⁹, acenes⁴⁰, for oligoynes^{39,41} and alkanes⁴² depending on their precise anchor groups to gold electrodes.

One of the most interesting aspects of single-molecular electronics is the phenomena of room-temperature quantum interference (QI), which has attracted increasing attention due to its potential for tuning charge transport through molecules^{43–47}. QI affects electron transport, because when a molecule is bonded to the electrodes, the de Broglie waves of electrons passing through the molecule from one side to the other side, causes complicated interference patterns within the molecule^{8,48,49}.

In the co-tunneling regime, where a single molecule is weakly connected to compound electrodes via sites *i* and *j*, electrons passing through the molecule from one electrode to the other can remain phase coherent, even at room temperature^{38,50}. This means that quantum interference QI will determine the electrical conductance of single molecules^{51,52}, as was confirmed in a series of recent experiments revealing room-temperature signatures of QI^{53,54}. These signatures are described by counting rules^{55,56} which identify conditions for the occurrence of destructive quantum interference, while recently-developed mid-gap theory and Magic ratio rule (MRR) can be used to account for constructive interference. The MRR is an exact formula for conductance ratios of tight-binding representations of molecules in the weak coupling limit, when the Fermi energy is located at the centre of the HOMO-LUMO (H-L) gap. It captures the

complexity of interference patterns created by electrons at the center of HOMO-LUMO gap and allow the prediction of conductance ratios.^{5,57,58}

1.2. Thesis Outline

The theoretical approach used in this thesis includes two main techniques, Density Functional Theory in chapter (2), which is implemented in the SIESTA code and the non-equilibrium Greens function formalism of transport theory in chapter (3). Both of these methods are used to extensively study a family of molecules.

Chapter four presents the unusual behaviour of porphyrin molecular wires, whose conductance increases with length. This is in contrast with classical conductors and most molecular wires, whose conductance decays with length.

In the fifth chapter, I will introduce the effect of external substituent groups on the (phenylene ethylene-type oligomers) molecular wires, when placed in different positions and compare their behaviour with the effect of heteroatoms placed in different positions.

The sixth chapter will present a novel strategy for the introduction of electromechanical functionality in molecular wires and highlights the importance of weak interactions at the electrode interface by designed and characterised a series of single-molecule switch. Finally, the seventh chapter presents conclusions and suggestions for future works.

Bibliography

- (1) Elke, S.; Carlos, C. J. *Molecular Electronics: An Introduction to Theory and Experiment*; World Scientific, 2017; Vol. 15.
- (2) Scheer, E. Visions for a Molecular Future. *Nat. Nanotechnol.* **2013**, 8 (6), 386.
- (3) Love, J. C.; Estroff, L. A.; Kriebel, J. K.; Nuzzo, R. G.; Whitesides, G. M. Self-Assembled Monolayers of Thiolates on Metals as a Form of Nanotechnology.
- (4) Aradhya, S. V; Venkataraman, L. Single-Molecule Junctions beyond Electronic Transport. *Nat. Nanotechnol.* **2013**, 8 (6), 399.
- (5) Sangtarash, S.; Huang, C.; Sadeghi, H.; Sorohhov, G.; Hauser, J.; Wandlowski, T.; Hong, W.; Decurtins, S.; Liu, S.-X.; Lambert, C. J. Searching the Hearts of Graphene-like Molecules for Simplicity, Sensitivity, and Logic. *J. Am. Chem. Soc.* **2015**, 137 (35), 11425–11431.
- (6) Sadeghi, H.; Algaragholy, L.; Pope, T.; Bailey, S.; Visontai, D.; Manrique, D.; Ferrer, J.; Garcia-Suarez, V.; Sangtarash, S.; Lambert, C. J. Graphene Sculpturene Nanopores for DNA Nucleobase Sensing. *J. Phys. Chem. B* **2014**, 118 (24), 6908–6914.
- (7) Themistoklis, P. C. T.; Chua, L. Two Centuries of Memristors. *Nat. Mater.* **2012**, 11, 478–481.
- (8) Lambert, C. J. Basic Concepts of Quantum Interference and Electron Transport in Single-Molecule Electronics. *Chem. Soc. Rev.* **2015**, 44 (4), 875–888.
- (9) Novoselov, K. S.; Geim, A. K.; Morozov, S. V; Jiang, D. A.; Zhang, Y.; Dubonos, S. V; Grigorieva, I. V; Firsov, A. A. Electric Field Effect in Atomically Thin Carbon Films. *Science* (80-.). **2004**, 306 (5696), 666–669.

- (10) Schedin, F.; Geim, A. K.; Morozov, S. V.; Hill, E. W.; Blake, P.; Katsnelson, M. I.; Novoselov, K. S. Detection of Individual Gas Molecules Adsorbed on Graphene. *Nat. Mater.* **2007**, *6* (9), 652.
- (11) Jo, G.; Choe, M.; Lee, S.; Park, W.; Kahng, Y. H.; Lee, T. The Application of Graphene as Electrodes in Electrical and Optical Devices. *Nanotechnology* **2012**, *23* (11), 112001.
- (12) Elias, D. C.; Nair, R. R.; Mohiuddin, T. M. G.; Morozov, S. V.; Blake, P.; Halsall, M. P.; Ferrari, A. C.; Boukhvalov, D. W.; Katsnelson, M. I.; Geim, A. K.; et al. Control of Graphene's Properties by Reversible Hydrogenation: Evidence for Graphane. *Science* (80-.). **2009**, *323* (5914), 610–613.
- (13) Loh, K. P.; Bao, Q.; Ang, P. K.; Yang, J. The Chemistry of Graphene. *J. Mater. Chem.* **2010**, *20* (12), 2277–2289.
- (14) Novoselov, K. S. KS Novoselov, AK Geim, SV Morozov, D. Jiang, Y. Zhang, SV Dubonos, IV Grigorieva, and AA Firsov, *Science* 306, 666 (2004). *Science* (80-.). **2004**, *306*, 666.
- (15) Ojha, R. P.; Lemieux, P.-A.; Dixon, P. K.; Liu, A. J.; Durian, D. J. Statistical Mechanics of a Gas-Fluidized Particle. *Nature* **2004**, *427* (6974), 521.
- (16) Berger, C.; Song, Z.; Li, T.; Li, X.; Ogbazghi, A. Y.; Feng, R.; Dai, Z.; Marchenkov, A. N.; Conrad, E. H.; First, P. N.; et al. Ultrathin Epitaxial Graphite: 2D Electron Gas Properties and a Route toward Graphene-Based Nanoelectronics. *J. Phys. Chem. B* **2004**, *108* (52), 19912–19916.
- (17) Hirata, M.; Gotou, T.; Horiuchi, S.; Fujiwara, M.; Ohba, M. Thin-Film Particles of Graphite Oxide 1: High-Yield Synthesis and Flexibility of the Particles.

Carbon N. Y. **2004**, 42 (14), 2929–2937.

- (18) Neto, A. H. C.; Guinea, F.; Peres, N. M. R.; Novoselov, K. S.; Geim, A. K. The Electronic Properties of Graphene. *Rev. Mod. Phys.* **2009**, 81 (1), 109.
- (19) Nakada, K.; Fujita, M.; Dresselhaus, G.; Dresselhaus, M. S. Edge State in Graphene Ribbons: Nanometer Size Effect and Edge Shape Dependence. *Phys. Rev. B* **1996**, 54 (24), 17954.
- (20) Brey, L.; Fertig, H. A. Edge States and the Quantized Hall Effect in Graphene. *Phys. Rev. B* **2006**, 73 (19), 195408.
- (21) Li, J.-C.; Wu, J.-Z.; Gong, X. Conductance Switching and Photovoltaic Effect of Ru (II) Complex Molecular Junctions: Role of Complex Properties and the Metal/Molecule Interface. *J. Phys. Chem. Lett.* **2014**, 5 (6), 1017–1021.
- (22) Sadeghi, H. Theory of Electron, Phonon and Spin Transport in Nanoscale Quantum Devices. *Nanotechnology* **2018**.
- (23) Sakamoto, R.; Katagiri, S.; Maeda, H.; Nishihara, H. Bis (Terpyridine) Metal Complex Wires: Excellent Long-Range Electron Transfer Ability and Controllable Intrawire Redox Conduction on Silicon Electrode. *Coord. Chem. Rev.* **2013**, 257 (9–10), 1493–1506.
- (24) Noori, M. Quantum Theory of Electron Transport Through Photo-Synthetic Porphyrins, Lancaster University, 2017.
- (25) Auwärter, W.; Écija, D.; Klappenberger, F.; Barth, J. V. Porphyrins at Interfaces. *Nat. Chem.* **2015**, 7 (2), 105.
- (26) Jurow, M.; Schuckman, A. E.; Batteas, J. D.; Drain, C. M. Porphyrins as Molecular Electronic Components of Functional Devices. *Coord. Chem. Rev.*

2010, 254 (19–20), 2297–2310.

- (27) Sedghi, G.; Sawada, K.; Esdaile, L. J.; Hoffmann, M.; Anderson, H. L.; Bethell, D.; Haiss, W.; Higgins, S. J.; Nichols, R. J. Single Molecule Conductance of Porphyrin Wires with Ultralow Attenuation. *J. Am. Chem. Soc.* **2008**, 130 (27), 8582–8583.
- (28) Sena, A. M. P.; Brázdová, V.; Bowler, D. R. Density Functional Theory Study of the Iron-Based Porphyrin Haem (b) on the Si (111): H Surface. *Phys. Rev. B* **2009**, 79 (24), 245404.
- (29) Cho, S.; Yoon, M.-C.; Kim, K. S.; Kim, P.; Kim, D. Electron Delocalization in Various Triply Linked Zinc (II) Porphyrin Arrays: Role of Antiaromatic Junctions between Aromatic Porphyrins. *Phys. Chem. Chem. Phys.* **2011**, 13 (36), 16175–16181.
- (30) Sadeghi, H.; Sangtarash, S.; Lambert, C. J. Robust Molecular Anchoring to Graphene Electrodes. *Nano Lett.* **2017**, 17 (8), 4611–4618.
- (31) Fan, F. R. F.; Yang, J.; Cai, L.; Price, D. W.; Dirk, S. M.; Kosynkin, D. V.; Yao, Y.; Rawlett, A. M.; Tour, J. M.; Bard, A. J. Charge Transport through Self-Assembled Monolayers of Compounds of Interest in Molecular Electronics. *J. Am. Chem. Soc.* **2002**, 124 (19), 5550–5560.
- (32) Bergren, A. J.; McCreery, R. L.; Stoyanov, S. R.; Gusarov, S.; Kovalenko, A. Electronic Characteristics and Charge Transport Mechanisms for Large Area Aromatic Molecular Junctions. *J. Phys. Chem. C* **2010**, 114 (37), 15806–15815.
- (33) Ferreira, Q.; Bragança, A. M.; Alcácer, L.; Morgado, J. Conductance of Well-Defined Porphyrin Self-Assembled Molecular Wires up to 14 Nm in Length. *J.*

Phys. Chem. C **2014**, *118* (13), 7229–7234.

- (34) Ashwell, G. J.; Urasinska, B.; Wang, C.; Bryce, M. R.; Grace, I.; Lambert, C. J. Single-Molecule Electrical Studies on a 7 Nm Long Molecular Wire. *Chem. Commun. (Camb)*. **2006**, No. 45, 4706–4708.
- (35) Shankar, R. *Principles of Quantum Mechanics*; Springer Science & Business Media, 2012.
- (36) Sangtarash, S.; Vezzoli, A.; Sadeghi, H.; Ferri, N.; Brien, H. M. O. Gateway State-Mediated, Long-Range Tunnelling in Molecular Wires. 1 , 2. *Nanoscale* **2018**, *10*, 3060–3067.
- (37) Kaliginedi, V.; Moreno-García, P.; Valkenier, H.; Hong, W.; García-Suárez, V. M.; Buitter, P.; Otten, J. L. H. H.; Hummelen, J. C.; Lambert, C. J.; Wandlowski, T. Correlations between Molecular Structure and Single-Junction Conductance: A Case Study with Oligo(Phenylene-Ethynylene)-Type Wires. *J. Am. Chem. Soc.* **2012**, *134* (11), 5262–5275.
- (38) Zhao, X.; Huang, C.; Gulcur, M.; Batsanov, A. S.; Baghernejad, M.; Hong, W.; Bryce, M. R.; Wandlowski, T. Oligo(Aryleneethynylene)s with Terminal Pyridyl Groups: Synthesis and Length Dependence of the Tunneling-to-Hopping Transition of Single-Molecule Conductances. *Chem. Mater.* **2013**, *25* (21), 4340–4347.
- (39) Moreno-García, P.; Gulcur, M.; Manrique, D. Z.; Pope, T.; Hong, W.; Kaliginedi, V.; Huang, C.; Batsanov, A. S.; Bryce, M. R.; Lambert, C.; et al. Single-Molecule Conductance of Functionalized Oligoynes: Length Dependence and Junction Evolution. *J. Am. Chem. Soc.* **2013**, *135* (33), 12228–12240.

- (40) Kim, B.; Beebe, J. M.; Jun, Y.; Zhu, X. Y.; Frisbie, G. D. Correlation between HOMO Alignment and Contact Resistance in Molecular Junctions: Aromatic Thiols versus Aromatic Isocyanides. *J. Am. Chem. Soc.* **2006**, *128* (15), 4970–4971.
- (41) Sadeghi, H.; Sangtarash, S.; Lambert, C. J. Oligoynes Molecular Junctions for Efficient Room Temperature Thermoelectric Power Generation. *Nano Lett.* **2015**, *15* (11), 7467–7472.
- (42) Liu, H.; Wang, N.; Zhao, J.; Guo, Y.; Yin, X.; Boey, F. Y. C.; Zhang, H. Length-Dependent Conductance of Molecular Wires and Contact Resistance in Metal-Molecule-Metal Junctions. *ChemPhysChem* **2008**, *9* (10), 1416–1424.
- (43) Garner, M. H.; Li, H.; Chen, Y.; Su, T. A.; Shangguan, Z.; Paley, D. W.; Liu, T.; Ng, F.; Li, H.; Xiao, S.; et al. Comprehensive Suppression of Single-Molecule Conductance Using Destructive-Interference. *Nature* **2018**, *1*.
- (44) Cardamone, D. M.; Stafford, C. A.; Mazumdar, S. Controlling Quantum Transport through a Single Molecule. *Nano Lett.* **2006**, *6* (11), 2422–2426.
- (45) Frisenda, R.; Janssen, V. A. E. C.; Grozema, F. C.; van der Zant, H. S. J.; Renaud, N. Mechanically Controlled Quantum Interference in Individual π -Stacked Dimers. *Nat. Chem.* **2016**, *8* (12), 1099.
- (46) Guédon, C. M.; Valkenier, H.; Markussen, T.; Thygesen, K. S.; Hummelen, J. C.; Van Der Molen, S. J. Observation of Quantum Interference in Molecular Charge Transport. *Nat. Nanotechnol.* **2012**, *7* (5), 305.
- (47) Aradhya, S. V.; Meisner, J. S.; Krikorian, M.; Ahn, S.; Parameswaran, R.; Steigerwald, M. L.; Nuckolls, C.; Venkataraman, L. Dissecting Contact

Mechanics from Quantum Interference in Single-Molecule Junctions of Stilbene Derivatives. *Nano Lett.* **2012**, *12* (3), 1643–1647.

- (48) Su, T. A.; Neupane, M.; Steigerwald, M. L.; Venkataraman, L.; Nuckolls, C. Chemical Principles of Single-Molecule Electronics. *Nat. Rev. Mater.* **2016**, *1* (3), 16002.
- (49) Xiang, D.; Wang, X.; Jia, C.; Lee, T.; Guo, X. Molecular-Scale Electronics: From Concept to Function. *Chem. Rev.* **2016**, *116* (7), 4318–4440.
- (50) Sedghi, G.; García-Suárez, V. M.; Esdaile, L. J.; Anderson, H. L.; Lambert, C. J.; Martín, S.; Bethell, D.; Higgins, S. J.; Elliott, M.; Bennett, N.; et al. Long-Range Electron Tunnelling in Oligo-Porphyrin Molecular Wires. *Nat. Nanotechnol.* **2011**, *6* (8), 517–523.
- (51) Mol, J. A.; Lau, C. S.; Lewis, W. J. M.; Sadeghi, H.; Roche, C.; Cnossen, A.; Warner, J. H.; Lambert, C. J.; Anderson, H. L.; Briggs, G. A. D. Graphene-Porphyrin Single-Molecule Transistors. *Nanoscale* **2015**, *7* (31), 13181–13185.
- (52) Magoga, M.; Joachim, C. Conductance of Molecular Wires Connected or Bonded in Parallel. *Phys. Rev. B* **1999**, *59* (24), 16011.
- (53) Prins, F.; Barreiro, A.; Ruitenbergh, J. W.; Seldenthuis, J. S.; Aliaga-Alcalde, N.; Vandersypen, L. M. K.; van der Zant, H. S. J. Room-Temperature Gating of Molecular Junctions Using Few-Layer Graphene Nanogap Electrodes. *Nano Lett.* **2011**, *11* (11), 4607–4611.
- (54) Hong, W.; Valkenier, H.; Mészáros, G.; Manrique, D. Z.; Mishchenko, A.; Putz, A.; García, P. M.; Lambert, C. J.; Hummelen, J. C.; Wandlowski, T. An MCBJ Case Study: The Influence of π -Conjugation on the Single-Molecule

Conductance at a Solid/Liquid Interface. *Beilstein J. Nanotechnol.* **2011**, *2*, 699.

- (55) Xia, J.; Capozzi, B.; Wei, S.; Strange, M.; Batra, A.; Moreno, J. R.; Amir, R. J.; Amir, E.; Solomon, G. C.; Venkataraman, L.; et al. Breakdown of Interference Rules in Azulene, a Nonalternant Hydrocarbon. *Nano Lett.* **2014**, *14* (5), 2941–2945.
- (56) Markussen, T.; Stadler, R.; Thygesen, K. S. The Relation between Structure and Quantum Interference in Single Molecule Junctions. *Nano Lett.* **2010**, *10* (10), 4260–4265.
- (57) Geng, Y.; Sangtarash, S.; Huang, C.; Sadeghi, H.; Fu, Y.; Hong, W.; Wandlowski, T.; Decurtins, S.; Lambert, C. J.; Liu, S.-X. Magic Ratios for Connectivity-Driven Electrical Conductance of Graphene-like Molecules. *J. Am. Chem. Soc.* **2015**, *137* (13), 4469–4476.
- (58) Sangtarash, S.; Sadeghi, H.; Lambert, C. J. Exploring Quantum Interference in Heteroatom-Substituted Graphene-like Molecules. *Nanoscale* **2016**, *8* (27), 13199–13205.

Chapter 2

2. Density Functional Theory

2.1. Introduction

The electrical properties of molecular electronics devices can be understood by investigating their structural and electronic properties using density function theory (DFT). The aim of this chapter is to give a brief introduction to density functional theory (DFT) and its implementation in the SIESTA code (Spanish Initiative for Electronic Simulations with Thousands of Atoms)¹, which I have used as a theoretical tool to investigate the structures of molecules as well as calculating charge densities, band structures, mean-field Hamiltonian and binding energies.

The physical theories that support the fundamental assertion of density functional theory were introduced by Hohenberg and Kohn² and then expanded by Kohn and Sham³ to solve the intractable many-body problem of interacting electrons in an external potential to a tractable problem of non-interacting electrons in an effective potential. This has led DFT to become one of the main tools in theoretical physics, molecular chemistry and biology⁴.

2.2. Many-body problem

To find a method to solve the many-body problem we use the theoretical physics in quantum statistical mechanics⁵. The task is to find the eigenvalues and eigenstates of the full Hamiltonian operator of a general system by solving the Schrodinger equation:

$$H\psi_i(\vec{r}_1, \vec{r}_2, \dots, \vec{r}_N, \vec{R}_1, \vec{R}_2, \dots, \vec{R}_M) = E_i\psi_i(\vec{r}_1, \vec{r}_2, \dots, \vec{r}_N, \vec{R}_1, \vec{R}_2, \dots, \vec{R}_M) \quad (2.1.1)$$

Here H represents the time-independent Hamiltonian operator of the system consisting of N -electrons and M -nuclei which describes the interaction of particles with each other, ψ_i is the wavefunction of the i^{th} state of the system and E_i is the numerical value of the energy of the i^{th} state described by ψ_i . The many-body Hamiltonian can be written as:

$$H = -\sum_i \frac{\hbar^2}{2m_e} \nabla_i^2 + \frac{1}{8\pi\epsilon_0} \sum_{i \neq j} \frac{e^2}{|r_i - r_j|} - \sum_I \frac{\hbar^2}{2m_I} \nabla_I^2 + \frac{1}{8\pi\epsilon_0} \sum_{I \neq J} \frac{Z_I Z_J e^2}{|R_I - R_J|} - \frac{1}{4\pi\epsilon_0} \sum_{iI} \frac{Z_I e^2}{|r_i - R_I|} \quad (2.1.2)$$

Where m_I , Z_I and R_I are the mass, atomic number and position of the I -th atom in the solid respectively. The position of i -th electron is denoted by r_i and m_e is the mass of a single electron. The Hamiltonian of the many-body problem is divided into five terms: the first term is the electron kinetic energy, the second term is electron-electron interactions, the third term is the nuclei kinetic energy, the fourth term is nuclei-nuclei interactions and the last term is electron-nuclei interactions.

The Schrodinger equation (2.1.1) cannot be solved as it stands because there are too many variables unless apart from the hydrogen atom or a small number of electrons.

However, an approximate, but very accurate solutions may be found if the equation is simplified using the Born-Oppenheimer approximation⁶ by recognizing that the nuclei and the electrons differ greatly in mass and, as a result, differ greatly in their relative speeds of motion. They assume the nuclei are much heavier than an electron and consequently, masses of the nuclei move much slower than the electrons, which reveal that we can consider the electrons as moving in the field of fixed nuclei, i.e. the nuclear kinetic energy is zero and their potential energy is a constant. Thus, the electronic Hamiltonian reduces to:

$$H = -\sum_i \frac{\hbar^2}{2m_e} \nabla_i^2 + \frac{1}{8\pi\epsilon_0} \sum_{i \neq j} \frac{e^2}{|r_i - r_j|} - \frac{1}{4\pi\epsilon_0} \sum_{I} \frac{Z_I e^2}{|r_i - R_I|} \quad (2.1.3)$$

Here, the Schrodinger equation is solved for the electron degrees of freedom only. Once we know the electronic structure of a molecular system, we can calculate classical forces on the nuclei and minimize these forces to find the ground state geometry. With the Born-Oppenheimer approximation the assumption that the nuclei wave-function is independent of the electron position, the equation (2.1.3) can be rewritten as follows:

$$H = T_e + U_{e-e} + V_{e-nuc} \quad (2.1.4)$$

Here first term T_e is the kinetic energy of all electrons, the second term U_{e-e} is the interaction between electrons and the last term V_{e-nuc} describes the interaction between electrons and nuclei.

Therefore, the corresponding time independent Schrödinger equation will read:

$$H\psi_i(\vec{r}_1, \vec{r}_2, \dots, \vec{r}_i, \dots) = E_i\psi_i(\vec{r}_1, \vec{r}_2, \dots, \vec{r}_i, \dots) \quad (2.1.5)$$

Despite the Born-Oppenheimer approximation minimizing the size of the system, it is still difficult to solve equation (2.1.5). Therefore, Density functional theory solves this

problem by expressing the physical quantities in terms of the ground-state density, the electron density of a general many body states characterized by a wave function $\psi(r_1, r_2, \dots, r_i)$ is defined as:

$$\rho(r) = \int d^3r_3 d^3r_2 \dots d^3r_i |\psi(r_1, r_2, \dots, r_i)|^2 \quad (2.1.6)$$

2.3. The Hohenberg-Kohn theorems

Essentially, Density Functional Theory evolved significantly depending on two important theories developed by the Hohenberg and Kohn in 1964², where the electron density $\rho(r)$ is used to calculate the ground state energy⁷.

From the first theorem, for any system of interacting particles in an external potential $V_{\text{ext}}(r)$, the potential $V_{\text{ext}}(r)$ is determined uniquely, except for a constant, by the ground state particle density $\rho_0(r)$.

The second theorem of the Hohenberg-Kohn states that a universal functional for the energy $E[\rho]$ in terms of the density can be defined, valid for any external potential $V_{\text{ext}}(r)$. For any particular $V_{\text{ext}}(r)$, the exact ground state of the system is the global minimum value of this functional, and the density $\rho(r)$ that minimizes the functional is the exact ground state density $\rho_0(r)$.

2.4. The Kohn-Sham ansatz

The Kohn–Sham formalism³ enables DFT to solve the many-body problem. The many body interactions in the external potential are modelled as a set of non-interacting particles in a new effective external potential V_{ext} . By comparing the result of a non-interacting system and an interacting system, we can find the effective external

potential. In 1965 there was a solution introduced by Kohn and Sham³ to replace the original Hamiltonian of the system by an effective Hamiltonian of non-interacting particles in an effective external potential that has the same ground-state density as the original system^{8,9}.

The form of the energy functional of the Kohn-Sham is:

$$E_{KS}[\rho] = T_{KS}[\rho] + \int dr V_{ext}(r)\rho(r) + E_H[\rho] + E_{xc}[\rho] \quad (2.1.7)$$

Here, T_{KS} is the kinetic energy of the non-interacting system. The difference between the energy of the non-interacting and interacting system is referred to the exchange correlation functional E_{xc} . Also, E_H represents the Hartree function, which describes the electron-electron interaction and it is given by:

$$E_H[\rho] = \frac{1}{2} \iint \frac{\rho(r)\rho(r')}{|r-r'|} dr dr' \quad (2.1.8)$$

The above equation represents an approximate version of internal interactions of the electrons E_{int} . So, the exchange correlation functional E_{xc} represents the differences between the exact and approximated solutions to both the kinetic energy term and the electron-electron interaction terms that definition follows:

$$E_{xc}[\rho] = (E_{int}[\rho] - E_H[\rho]) + (T[\rho] - T_{KS}[\rho]) \quad (2.1.9)$$

If we take the functional derivatives of the last three terms of (2.1.9) then we can define an effective single particle potential V_{eff} as:

$$V_{eff}(r) = V_{ext}(r) + \frac{\partial}{\partial \rho}(E_H[\rho] + E_{xc}[\rho]) \quad (2.1.10)$$

Using this potential, we can write down a single particle Hamiltonian:

$$H_{KS} = T_{KS}[\rho] + V_{eff} \quad (2.1.11)$$

The corresponding Schrödinger equation:

$$H_{KS}\psi^{KS} = E\psi^{KS} \quad (2.1.12)$$

This equation called the Kohn-Sham equation, and the goal of solving the Kohn-Sham is to find the ground state density, as shown in figure (2.1.1). Normally, the solutions are obtained by an iteration step which starts by assuming an arbitrary density and then calculates an initial effective potential which is then used to solve a single particle Schrödinger equation. This solution is used to obtain the next density that will be considered as the initial value of density in the next loop. So, after several steps of iteration the density reaches the ground state density. The final density yields the implemented self-consistent effective potential for non-interacting electrons. Therefore, this method will be a successful approach to give an accurate ground state density when we have the exact E_{xc} , which is determined as described in the next section.

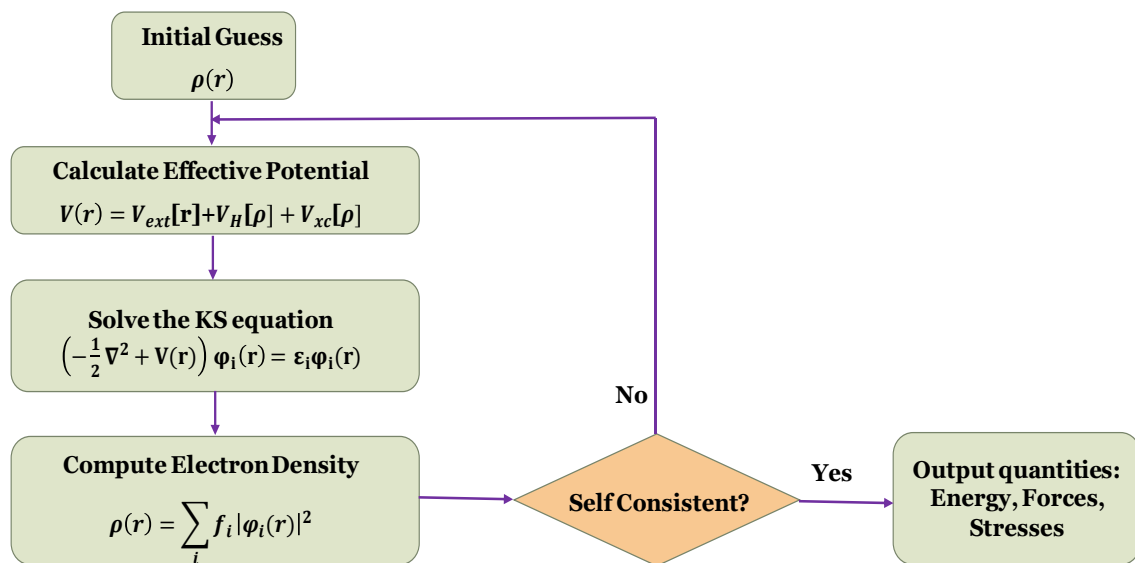


Figure 2.1.1: Schematic of the self-consistency process within SIESTA

2.5. The Exchange Correlation functional

DFT has been successful to reduce the quantum mechanical ground-state many-electron problem to self-consistent one-electron form, by the Kohn-Sham equations¹⁰. This method is formally precise, while for practical calculations, the exchange-correlation

energy, E_{xc} , as a functional of the density has to be approximated. There are numerous proposed forms for the exchange and correlation in the literature^{11,12}. The most commonly implemented approximation is Local Density Approximation (LDA)¹³ and generalized gradient approximation (GGA)¹⁴. To give more information about the Local Density Approximation and the Generalized Gradient Approximation, the following section will briefly describe it.

2.5.1. Local Density Approximation

The LDA approximation assumes that the exchange-correlation functional depends only on the local density and it is in some sense the simplest form one could imagine for the exchange and correlation energies. It is a powerful functional which is known to be accurate for systems where the electron density is not rapidly changing. The functional of the approximation is:

$$E_{xc}^{LDA}[\rho] = \int dr \rho(r) \left(\epsilon_x^{hom}(\rho(r)) + \epsilon_c^{hom}(\rho(r)) \right) \quad (2.1.13)$$

Where the exchange and correlation for the homogeneous electron gas can be defined by terms ϵ_x^{hom} and ϵ_c^{hom} , respectively.

2.5.2. Generalized gradient approximation

The GGA approximation extends the LDA by involving the derivatives of the density into the functional form of the exchange and correlation energies. In the GGA approximation, there is no closed form for the exchange term of the functional, but it has been calculated along with the correlation contribution by using numerical methods. The exchange-correlation energy is given by:

$$E_{xc}^{GGA} = E_x^{GGA}[\rho] + E_c^{GGA}[\rho] \quad (2.1.14)$$

And the exchange term is:

$$E_x^{GGA}[\rho] = \int \epsilon_x(\rho(r)) V_x(\rho(r) \nabla \rho(r)) \rho(r) dr \quad (2.1.15)$$

2.6. SIESTA

The DFT electronic structure calculations in this thesis have been performed using the SIESTA code¹. SIESTA is a set of methods and a complete software package that can be used to perform DFT calculations on a huge system consisting of thousands of atoms. It uses the standard Kohn-Sham self-consistent density function method. In addition, the functionals that are used in SIESTA include the Local Density Approximation (LDA) and the Generalized Gradient Approximation (GGA).

2.6.1. The Pseudopotential Approximation

The Kohn-Sham equation simplifies the large interacting problem, but the calculation for the many-body Schrödinger equation for practical purposes is still very large and has the potential to be computationally intensive. One method to solve the computational problem is to reduce the number of electrons by introducing the pseudopotential approximation which was proposed by Fermi in 1934^{15,16}. The idea is to solve this problem by removing the core electrons from an atom¹⁷.

The electrons in an atom can be split into two types: valence and core, where the valence electrons lie in partially filled shells, but core electrons lie within filled atomic shells. The core electrons are spatially localized about the nucleus and the valence electrons are outside the core region. When the atoms interact only the valence electrons overlap, and the core electrons could be removed and replaced by a

pseudopotential. This will reduce the number of electrons in a system and also, save the time and memory required to calculate properties of molecules that contain a large number of electrons¹⁸.

2.6.2. SIESTA Basis Sets

In order to turn the partial differential equations (e.g. the Schrodinger equation (2.1.1)) into algebraic equations suitable for efficient implementation on a computer, a set of functions (called basis functions) is used to represent the electronic wave function¹⁸. In order to find the ground state energy, the Hamiltonian of the system should be diagonalized. This process involves the inversion of a large matrix¹ whose computation time scales with the number of non-zero elements. To minimize the size of the Hamiltonian, SIESTA utilises a linear combination of atomic orbital (LCAO) basis set which are constrained to be zero outside of a certain radius (cut-off radius). Furthermore, this generates the required sparse form for the Hamiltonian, and that reduces the overlap between basis functions. Therefore, a minimal size basis set can produce characteristics which model that of the studied system.

The simplest form of the atomic basis set for an atom is single- ζ which corresponds to a single basis function per electron orbital $\Psi_{nlm}(r)$ (i.e. 1 for an s -orbital, 3 for a p -orbital, etc...). In this case, each basis function consists of a product of one radial wavefunction ϕ_{nl}^1 , and one spherical harmonic Y_{lm} :

$$\Psi_{nlm}(r) = \phi_{nl}^1(r)Y_{lm}(\varphi, \vartheta) \quad (2.1.16)$$

The radial part in equation (2.1.16) of the wavefunction is found by using the Sankey method¹⁹.

For higher accuracy basis sets (multiple- ζ) are formed by adding another radial wavefunctions for each included for each electron orbital. Further accuracy (multiple- ζ polarised) can be obtained by including wavefunctions with different angular momenta corresponding to orbitals which are unoccupied in the atom. Table (2.1.1) shows the number of basis orbitals for a selected number of atoms for single- ζ (SZ), double- ζ (DZ), Single- ζ Polarised (SZP) and double- ζ polarized (DZP) basis set in all DFT calculations.

Table 2.1.1: Example of the number of radial basis functions per atom as used within the SIESTA for different degrees of precisions.

Atoms	SZ	SZP	DZ	DZP
H	1	4	2	5
C	4	9	8	13
N	4	9	8	13
O	4	9	8	13
S	4	9	8	13
Au	6	9	12	15

2.6.3. Calculating binding energy using the counter poise method

Using the DFT approach to calculate the ground state geometry of different system configurations allows us also to calculate the binding energy between different parts of the system. However, these calculations are subject to errors, due to the use of localized basis sets which are centred on the nuclei. If atoms are moved, then, their basis functions will overlap which might cause artificial strengthening of atomic interactions and this will give an inaccurate total energy of the system. In general, to solve this type of error, the Basis Set Superposition Error correction (BSSE)²⁰ or the counterpoise correction (CP)²¹ must be performed in calculations when utilizing the linear

combination of atomic orbitals. The energy of interaction of two systems a and b can be expressed as:

$$\Delta E(ab) = E_{ab}^{ab} - (E_a^a + E_b^b) \quad (2.1.17)$$

Where E_{ab}^{ab} is the total energy for the dimer system a and b , and the E_a^a and E_b^b are the total energy of the two isolated systems. So, to perform these corrections inside SIESTA, I use ‘ghost’ states (basis set functions which have no electrons or protons) to evaluate the total energy of the systems a or b in the dimer basis.

$$\Delta E(ab) = E_{ab}^{ab} - (E_a^{ab} + E_b^{ab})$$

where E_a^{ab} and E_b^{ab} is the energy of system, a and b evaluated in the basis of the dimer.

This method provides accurate results for different systems to give reliable and realistic results²²⁻²⁴.

Bibliography

- (1) Soler, J. M.; Artacho, E.; Gale, J. D.; Garcia, A.; Junquera, J.; Ordejón, P.; Sánchez-Portal, D. The SIESTA Method for Ab Initio Order-N Materials Simulation. *J. Phys. Condens. Matter* **2002**, *14* (11), 2745.
- (2) Hohenberg, P.; Kohn, W. Inhomogeneous Electron Gas. *Phys. Rev.* **1964**, *136* (3B), B864.
- (3) Kohn, W.; Sham, L. J. Self-Consistent Equations Including Exchange and Correlation Effects. *Phys. Rev.* **1965**, *140* (4A), A1133.
- (4) van Mourik, T.; Bühl, M.; Gageot, M.-P. Density Functional Theory across Chemistry, Physics and Biology. The Royal Society 2014.
- (5) Lee, T. D.; Yang, C. N. Many-Body Problem in Quantum Statistical Mechanics. I. General Formulation. *Phys. Rev.* **1959**, *113* (5), 1165.
- (6) Born, M.; Oppenheimer, R. On the Quantum Theory of Molecules. In *Quantum Chemistry: Classic Scientific Papers*; World Scientific, 2000; pp 1–24.
- (7) Parr, R. G.; Yang, W. Density-Functional Theory of Atoms and Molecules Vol. 16. 1994: Oxford University Press. USA.
- (8) Levy, M. Electron Densities in Search of Hamiltonians. *Phys. Rev. A* **1982**, *26* (3), 1200.
- (9) Lieb, E. H. Thomas-Fermi and Related Theories of Atoms and Molecules. In *The Stability of Matter: From Atoms to Stars*; Springer, 1997; pp 259–297.
- (10) Kohn, W.; Becke, A. D.; Parr, R. G. Density Functional Theory of Electronic Structure. *J. Phys. Chem.* **1996**, *100* (31), 12974–12980.
- (11) Engel, E.; Dreizler, R. M. Density Functional Theory, Vol. 2011. Springer Verlag 2011.
- (12) Harrison, N. M. An Introduction to Density Functional Theory. *Nato Sci. Ser.*

- Sub Ser. III Comput. Syst. Sci.* **2003**, 187, 45–70.
- (13) Ceperley, D. M.; Alder, B. J. Ground State of the Electron Gas by a Stochastic Method. *Phys. Rev. Lett.* **1980**, 45 (7), 566.
- (14) Perdew, J. P.; Burke, K.; Ernzerhof, M. Generalized Gradient Approximation Made Simple. *Phys. Rev. Lett.* **1996**, 77 (18), 3865.
- (15) Fermi, E.; others. Motion of Neutrons in Hydrogenous Substances. *Ric. sci* **1936**, 7, 13–52.
- (16) Fermi, E. Sopra Lo Spostamento per Pressione Delle Righe Elevate Delle Serie Spettrali. *Nuovo Cim.* **1934**, 11 (3), 157–166.
- (17) Zunger, A.; Cohen, M. L. Erratum: Self-Consistent Pseudopotential Calculation of the Bulk Properties of Mo and W. *Phys. Rev. B* **1983**, 27 (2), 1376.
- (18) Sadeghi, H. Theory of Electron, Phonon and Spin Transport in Nanoscale Quantum Devices. *Nanotechnology* **2018**.
- (19) Sankey, O. F.; Niklewski, D. J. Ab Initio Multicenter Tight-Binding Model for Molecular-Dynamics Simulations and Other Applications in Covalent Systems. *Phys. Rev. B* **1989**, 40 (6), 3979.
- (20) Jansen, H. B.; Ros, P. Non-Empirical Molecular Orbital Calculations on the Protonation of Carbon Monoxide. *Chem. Phys. Lett.* **1969**, 3, 140–143.
- (21) Boys, S. F.; Bernardi, F. de. The Calculation of Small Molecular Interactions by the Differences of Separate Total Energies. Some Procedures with Reduced Errors. *Mol. Phys.* **1970**, 19 (4), 553–566.
- (22) Haynes, P. D.; Skylaris, C.-K.; Mostofi, A. A.; Payne, M. C. Elimination of Basis Set Superposition Error in Linear-Scaling Density-Functional Calculations with Local Orbitals Optimised in Situ. *Chem. Phys. Lett.* **2006**, 422 (4–6), 345–349.

- (23) Daza, M. C.; Dobado, J. A.; Molina, J. M.; Salvador, P.; Duran, M.; Villaveces, J. L. Basis Set Superposition Error-Counterpoise Corrected Potential Energy Surfaces. Application to Hydrogen Peroxide? X (X= F-, Cl-, Br-, Li+, Na+) Complexes. *J. Chem. Phys.* **1999**, *110* (24), 11806–11813.
- (24) Boese, A. D.; Jansen, G.; Torheyden, M.; Höfener, S.; Klopper, W. Effects of Counterpoise Correction and Basis Set Extrapolation on the MP2 Geometries of Hydrogen Bonded Dimers of Ammonia, Water, and Hydrogen Fluoride. *Phys. Chem. Chem. Phys.* **2011**, *13* (3), 1230–1238.

Chapter 3

3. Single Particle Transport

3.1. Introduction

In this chapter, I will introduce the theory of single particle transport as the main numerical tool. In molecular electronics, the aim is to understand the electrical behaviour and characteristics of molecular junctions and how to connect the molecular structures to electrodes to investigate electronic properties. The coupling strength between the molecule and the metallic electrodes in most cases is weak which leads to scattering processes from the electrode to the molecule or inside the molecule. One of the main theoretical methods to study scattering in these systems is the Green's function formalism.

I will start with a brief overview of Schrödinger equation and the Landauer formalism with a simple derivation. Following this, I will introduce the concept of Green's functions for a simple one-dimensional tight binding chain to describe the transport of arbitrarily complex geometry which presents the general methodology used to describe the transmission coefficient $T(E)$ in a molecular junction for electrons with energy E traversing from one electrode to the other.

3.2. Schrödinger Equation

The most general Schrödinger equation¹ describes the evolution of physical properties of a system in time and was proposed by the Austrian physicist Erwin Schrödinger in 1926 as:

$$i\hbar \frac{\partial}{\partial t} \psi(r, t) = \hat{H} \psi(r, t) \quad (3.2.1)$$

Where ψ is the wave function of the quantum system, and \hat{H} is the Hamiltonian operator which characterizes the total energy of any given wave function and \hbar is the reduced Planck constant ($\frac{h}{2\pi}$), r and t are the position vector and time respectively.

For a single particle moving in an electric field:

$$i\hbar \frac{\partial}{\partial t} \psi(r, t) = \left[\frac{-\hbar^2}{2m} \nabla^2 + V(r, t) \right] \psi(r, t) \quad (3.2.2)$$

Separating the variables, where $\psi(r, t) = \psi(r) f(t)$. The Schrodinger equation then becomes two ordinary differential equations:

$$\frac{1}{f(t)} \frac{d}{dt} f(t) = -\frac{iE}{\hbar} \quad (3.2.3)$$

And

$$\hat{H} \psi(r) = E\psi(r) \quad (3.2.4)$$

The solution of equation (3.2.3) could be written as:

$$f(t) = e^{-iEt/\hbar} \quad (3.2.5)$$

Then, the time dependent Schrodinger equation solution is obtained:

$$\psi(r, t) = \psi(r) e^{-iEt/\hbar} \quad (3.2.6)$$

Where, the most general solution is:

$$\psi(r, t) = \sum_i c_i \psi_i(r) e^{-iEt/\hbar} \quad (3.2.7)$$

Equation (3.2.4) is called the time independent Schrödinger equation and it is an eigenvalue problem where E 's are eigenvalues of the Hamiltonian \hat{H} .

3.3. The Landauer Formula

The Landauer formula^{2,3} is the standard theoretical model to describe transport phenomena in ballistic mesoscopic systems. This formula is the most popular way to describe coherent transport in nanodevices because it is a simple expression for the relation between the transmission probability of the electron and the electronic conductance in one-dimensional structures with two terminals. To begin with, I assume that the system connects two large reservoirs (or contacts) with a scattering region, as shown in figure 3.3.1. The chemical potentials for the reservoirs are slightly different $\mu_L > \mu_R \Rightarrow \mu_L - \mu_R = \delta E > 0$, which will drive electrons from the left to the right reservoir.

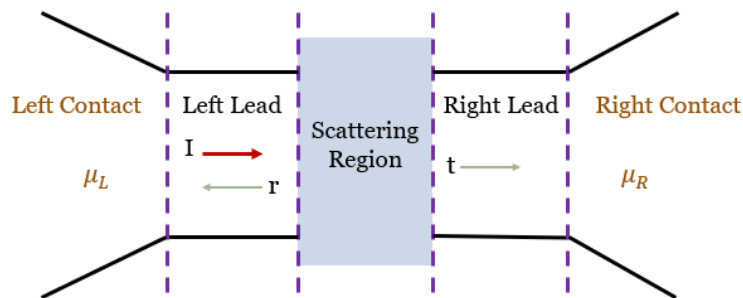


Figure 3.3.1: A mesoscopic scatterer connected to contacts by ballistic leads, where the chemical potential in the contacts is μ_L (left) and μ_R (right) respectively.

The incident current (δI^{in}) passing through this system from the left to the right reservoir is:

$$\delta I = ev \left(\frac{\partial n}{\partial E} \right) (\mu_L - \mu_R) \quad (3.3.1)$$

Where e is the electron charge, v is the group velocity, and $\frac{\partial n}{\partial E}$ is density of states (DOS).

For one-dimensional system:

$$\frac{\partial n}{\partial E} = \frac{\partial n}{\partial k} \frac{\partial k}{\partial E} = \frac{\partial n}{\partial k} \frac{1}{v\hbar} \quad (3.3.2)$$

As in one-dimension, $\frac{\partial n}{\partial k} = \frac{1}{\pi}$ and $\frac{\partial n}{\partial E} = \frac{1}{v\hbar}$, since the group velocity is $v = \frac{1}{\hbar} \frac{dE}{dk}$, which simplifies equation (3.3.1) to:

$$\delta I = \frac{2e}{h} (\mu_L - \mu_R) = \frac{2e^2}{h} \delta V \quad (3.3.3)$$

Where δV represents the voltage corresponding to the chemical potential difference and number 2 is a factor for spin dependency. From equation (3.3.3), it is clear that the conductance for one open channel in the absence of a scattering region is $\left(\frac{e^2}{h}\right)$, which is around $77.5 \mu S$, or the resistance $\left(\frac{h}{e^2}\right)$ about $12.9 \text{ k}\Omega$. On the other hand, if the system has a scattering region, the current is partially reflected with a probability $R = |r|^2$ and partially transmitted with a probability $T = |t|^2$. The current passing through the scatterer to the right lead will be:

$$\delta I = \frac{2e^2}{h} T \delta V \Rightarrow \frac{\delta I}{\delta V} = G = \frac{2e^2}{h} T \quad (3.3.4)$$

This equation is the Landauer formula, where the conductance $G = \frac{I}{V} = \left(\frac{2e^2}{h}\right) T$. and the transmission is evaluated at the Fermi energy⁴.

At zero voltage and finite temperature the conductance is:

$$G = \frac{I}{V} = G_0 \int_{-\infty}^{\infty} dE T(E) \left(-\frac{df(E)}{dE} \right) \quad (3.3.5)$$

Where $G_0 = \left(\frac{2e^2}{h}\right)$ which is the quantum of conductance, $f(E)$ is the Fermi-Dirac distribution function and the quantity $-\frac{df(E)}{dE}$ is a normalised probability distribution of width approximately equal to $k_B T$, centred on the Fermi energy E_F , where k_B is Boltzmann constant $k_B = 8.62 \times 10^{-5} \frac{eV}{K}$, T here is the Temperature.

The integral in equation (3.3.5) represents a thermal average of the transmission function $T(E)$ over an energy window of the width ($k_B T = 25$ meV at room temperature)⁵. at zero voltage and zero temperature:

$$G = G_0 \times T(E_F) \quad (3.3.6)$$

In the case where there is more than one open channel, the Landauer formula has been extended by Büttiker³, where the sum of all the transmission amplitudes which describe electrons incoming from the left contact and arriving to the right contact:

$$\frac{\delta I}{\delta V} = G = \frac{2e^2}{h} \sum_{i,j} |t_{i,j}|^2 = \frac{2e^2}{h} \text{Trace}(tt^\dagger) \quad (3.3.7)$$

Here, $t_{i,j}$ represents the amplitude of transmission describing scattering from the j^{th} channel of the left lead to i^{th} channel of the right lead and G is the electrical conductance. Also, the reflection amplitudes $r_{i,j}$ describe the electron passing through scattering region but in the opposite direction. Combination of the amplitudes of transmission and reflection will make the scattering S matrix as follows:

$$S = \begin{pmatrix} r & t' \\ t & r' \end{pmatrix} \quad (3.3.8)$$

Here, r and t represent the electrons transferring from the left, also r' and t' describe electrons coming from the right. In equation (3.3.7) r , t , r' and t' are matrices for more than one open channel, and due to charge conservation satisfaction, the S matrix be unitary $SS^+ = I$.

3.4. Tight-Binding Model

Tight binding has existed for many years as a convenient and transparent model for the description of the electronic structure in molecules and solids⁶. In this work, I will also use the tight binding model (TBM) which assume that the electrons in a solid are sufficiently tightly bound that I need only consider nearest neighbours. This will be true in many physical problems when the wave function at the individual atomic sites decay to zero before they reach the second nearest neighbour.

A simple TB description of system could be constructed by assigning a *Hückel* parameter to on-site energy ε of each atom in the molecule connected to the nearest neighbours with a single Hückel parameter (hopping matrix element) γ as shown in figure (3.4.1).

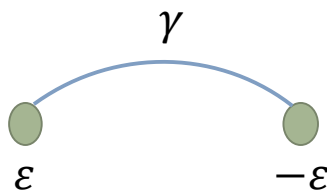


Figure 3.4.1: A simple Tight Binding Hamiltonian for a close system of two single-orbital sites with on-site energies ε and $-\varepsilon$ coupled to each other by the hopping integral γ .

Here, I will present a simplest example to find the eigenvalues and eigenvector by using tight binding method. The Hamiltonian of such system is written as: $H = \begin{pmatrix} \varepsilon & \gamma \\ \gamma^* & -\varepsilon \end{pmatrix}$, then the Schrödinger equation reads:

$$\begin{pmatrix} \varepsilon & \gamma \\ \gamma^* & -\varepsilon \end{pmatrix} \begin{pmatrix} \psi \\ \phi \end{pmatrix} = E \begin{pmatrix} \psi \\ \phi \end{pmatrix} \quad (3.4.1)$$

The eigenvalues E are calculated by solving $\det(H-EI)=0$. Where $I = \begin{pmatrix} 1 & 0 \\ 0 & 1 \end{pmatrix}$ is the identity matrix.

The eigenvalues from the Hamiltonian are:

$$E_{\pm} = \pm \sqrt{\varepsilon^2 + |\gamma|^2} \quad (3.4.2)$$

Corresponding to each eigenvalue there must be orthogonal eigenvectors $\begin{pmatrix} \psi_+ \\ \phi_+ \end{pmatrix}, \begin{pmatrix} \psi_- \\ \phi_- \end{pmatrix}$.

By substituting equation (3.4.2) into (3.4.1) I get:

$$\frac{\psi_{\pm}}{\phi_{\pm}} = \frac{\gamma}{E_{\pm} - \varepsilon} = \frac{E_{\pm} + \varepsilon}{\gamma^*} \quad (3.4.3)$$

If $\varepsilon = 0$ and $E = \pm\gamma$, simplest normalised eigenstates could be written as:

$$\begin{pmatrix} \psi_+ \\ \phi_+ \end{pmatrix} = \frac{1}{\sqrt{2}} \begin{pmatrix} 1 \\ 1 \end{pmatrix}, \quad \begin{pmatrix} \psi_- \\ \phi_- \end{pmatrix} = \frac{1}{\sqrt{2}} \begin{pmatrix} 1 \\ -1 \end{pmatrix} \quad (3.4.4)$$

If $\gamma = 0$ and $E = \pm\varepsilon$, the wave functions are fully localised on each site:

$$\begin{pmatrix} \psi_+ \\ \phi_+ \end{pmatrix} = \frac{1}{\sqrt{2}} \begin{pmatrix} 0 \\ 1 \end{pmatrix}, \quad \begin{pmatrix} \psi_- \\ \phi_- \end{pmatrix} = \frac{1}{\sqrt{2}} \begin{pmatrix} 1 \\ 0 \end{pmatrix} \quad (3.4.5)$$

3.5. Scattering Theory

3.5.1. One dimensional (1-D) linear crystalline lattice (infinite).

In order to calculate transport properties in a perfect wire I am going to use the Green's function technique to obtain the transmission coefficient, I will start by a simple infinite one-dimensional chain with on-site energies ϵ_0 and real hopping parameters $-\gamma$ as shown in figure (3.5.1).

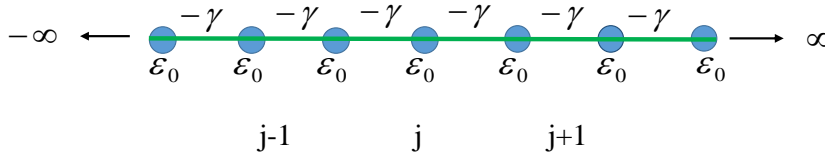


Figure 3.5.1: One-dimensional periodic lattice tight-binding approximation with on-site energies ϵ_0 and hopping parameters $-\gamma$.

First, the Schrödinger equation describing the system's wavefunction with the Hamiltonian H is:

$$H|\psi\rangle = E|\psi\rangle \quad (3.5.1)$$

To solve Schrödinger equation in (3.5.1) for the system in figure (3.5.1), I need to define the Hamiltonian matrix for this system as:

$$H = \begin{pmatrix} \ddots & -\gamma & 0 & 0 \\ -\gamma & \epsilon_0 & -\gamma & 0 \\ 0 & -\gamma & \epsilon_0 & -\gamma \\ 0 & 0 & -\gamma & \ddots \end{pmatrix} \quad (3.5.2)$$

The Schrödinger equation at a lattice site j in terms of the energy and wavefunction ψ_j is given by :

$$(E - H)\psi = 0 \quad (3.5.3)$$

$$\varepsilon_0\psi_j - \gamma\psi_{j+1} - \gamma\psi_{j-1} = E\psi_j \quad (3.5.4)$$

Where ψ is the wavefunction, and equation (3.5.2) satisfied for all j going from $+\infty$ to $-\infty$. I can get the Recurrent Relation by factored out the term ψ_{j+1} as:

$$\psi_{j+1} = \left(\frac{\varepsilon_0 - E}{\gamma}\right)\psi_j - \psi_{j-1} \quad (3.5.5)$$

By using the Bloch's theorem

$$\psi_j = \frac{1}{\sqrt{v}} e^{ikj} \quad , -\pi \leq k < \pi \quad (3.5.6)$$

I can define the wave function for the perfect lattice chain. The Schrödinger equation (3.5.5) can be solved to obtain the dispersion relation:

$$E = \varepsilon_0 - 2\gamma\cos k \quad (3.5.7)$$

The group velocity can be obtained by:

$$v = \frac{\partial E}{\partial k} = 2\gamma \sin(k) \quad (3.5.8)$$

Where k is the wavenumber. It is clear that for a given energy I can see there are two wavefunctions that satisfy equation (3.5.1), and their k and v have opposite signs.

3.5.2. Retarded Green's Function

To calculate the retarded Green's function $g(j, j')$, which is closely related to the wavefunction, the following equation is solved:

$$(E - H)g(j, j') = \delta_{j, j'} \quad (3.5.9)$$

Here, $\delta_{j, j'}$ is Kronecker delta $\delta_{j, j'} = 1$ if $j = j'$ and $\delta_{j, j'} = 0$ if $j \neq j'$.

In general, the retarded Green's function $g(j, j')$ explains the response of a system at a point j due to an excitation (a source) at point j' . In reality, the excitation give rise to two waves, which travel outwards with amplitudes A and B as shown in figure (3.5.2).

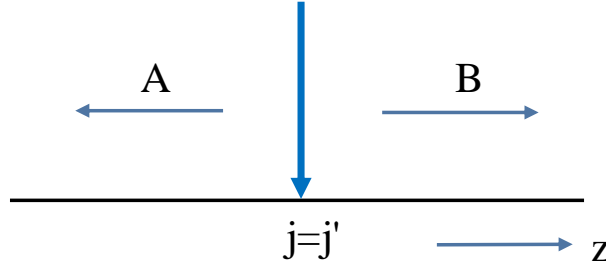


Figure 3.5.2: Retarded Green's function of an infinite one-dimensional lattice. The excitation at $j = j'$ causes waves to propagate left and right with amplitudes A and B respectively.

The waves can be presented as:

$$g(j', j) = \begin{cases} B e^{ikj} & j > j' \\ A e^{-ikj} & j < j' \end{cases} \quad (3.5.10)$$

In this equation, the solution satisfies equation (3.5.9) at every point except $j = j'$.

Since the Green's function must be continuous in equation (3.5.10), I equate the two at $j = j'$:

$$[g(j, j')]_{j=j' \text{ left}} = [g(j, j')]_{j=j' \text{ right}} \quad (3.5.11)$$

$$B e^{ikj'} = A e^{-ikj'} \Rightarrow A = B e^{2ikj'} \quad (3.5.12)$$

By substituting equation (3.5.12) into the Green's function equation (3.5.10), I find as shown:

$$g(j', j) = \begin{cases} B e^{ikj} & = B e^{ikj'} e^{ik(j-j')} & j \geq j' \\ B e^{2ikj'} e^{-ikj} & = B e^{ikj'} e^{ik(j'-j)} & j \leq j' \end{cases} \quad (3.5.13)$$

I can rewrite the equation (3.3.13) as:

$$g(j, j') = B e^{ikj'} e^{ik|j-j'|} \quad (3.5.14)$$

To find the value of the constant B, I use equation (3.5.9) and equation (3.5.6) which for $j = j'$ given:

$$(\varepsilon_0 - E)B - \gamma B e^{ik} - \gamma B e^{ik} = 1 \quad (3.5.15)$$

$$\gamma B (2 \cos k - 2 e^{ik}) = 1$$

$$B = \frac{1}{2i\gamma \sin k} = \frac{1}{i\hbar v}$$

Where the group velocity, found from the dispersion relation equation (3.5.7), is:

$$v = \frac{1}{\hbar} \frac{\partial E(k)}{\partial k} = \frac{2i\gamma \sin k}{\hbar} \quad (3.5.16)$$

I can rewrite the retarded Green's function as shown:

$$g^R(j, j') = \frac{1}{i\hbar v} e^{ik|j-j'|} \quad (3.5.17)$$

If the two waves incoming from left and right enter the point j' , so j' is a sink not a source, then the corresponding Green's function is called the advanced Green's function.

3.5.3. One-Dimensional (1-D) Scattering

In this section, I will obtain the Green's function of a system that has two one-dimensional tight binding semi-infinite leads, connected by a coupling element α . The two leads have equal on-site potentials ε_0 and hopping elements $-\gamma$, as shown in figure (3.5.3).

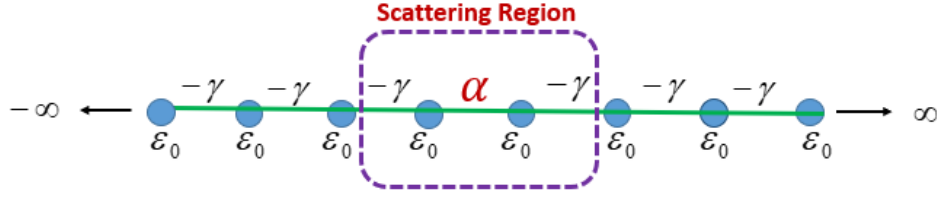


Figure 3.5.3: Simple tight-binding model of a one-dimensional scatterer attached to one-dimensional leads.

To solve this problem, I will derive the transmission and reflection amplitudes for an electron moving from the left lead to right lead through the scattering region. First, the Hamiltonian that takes the form of an infinite matrix, is given by:

$$H = \begin{pmatrix} \ddots & -\gamma & 0 & 0 & 0 & 0 \\ -\gamma & \varepsilon_0 & -\gamma & 0 & 0 & 0 \\ 0 & -\gamma & \varepsilon_0 & \alpha & 0 & 0 \\ 0 & 0 & \alpha & \varepsilon_0 & -\gamma & 0 \\ 0 & 0 & 0 & -\gamma & \varepsilon_0 & -\gamma \\ 0 & 0 & 0 & 0 & -\gamma & \ddots \end{pmatrix} = \begin{pmatrix} H_L & V_c \\ V_c^\dagger & H_R \end{pmatrix} \quad (3.5.18)$$

Here, H_L and H_R denote the Hamiltonians of the leads, which are the semi-infinite equivalent of the Hamiltonian that is shown in equation (3.5.4), and V_c is the coupling parameter connecting them. If γ is real, then the dispersion relation corresponding to the leads which is introduced above in equation (3.5.7), and also the group velocity was written in equation (3.5.16). By calculating the Green's function of this problem, I can obtain the scattering amplitudes. So, the form for the solution of equation (3.5.9), which is given as:

$$G = (E - H)^{-1} \quad (3.5.19)$$

This equation can be singular if the energy E is equal to eigenvalues of the Hamiltonian H , to deal with this it is practical to consider the limit:

$$G_{\mp} = \lim_{\eta \rightarrow 0} (E - H \pm i\eta)^{-1} \quad (3.5.20)$$

Here, η denotes a positive number and G_{\mp} represents the retarded (advanced) Green's function. In what follows, the retarded Green's function has been used, and the positive sign only has been chosen. For the infinite one-dimensional chain, the retarded Green's function can be defined in equation (3.5.17), which is given as:

$$g_{j,j'}^{\infty} = \frac{1}{i\hbar v} e^{ik|j-j'|} \quad (3.5.21)$$

Hence, j and j' denote the labels of the sites in the chain and sufficient boundary conditions, which are needed to give the Green's function of a semi-infinite lead. The lattice is semi-infinite; therefore, the chain should be terminated at a given point j_0 as shown in figure (3.5.4).

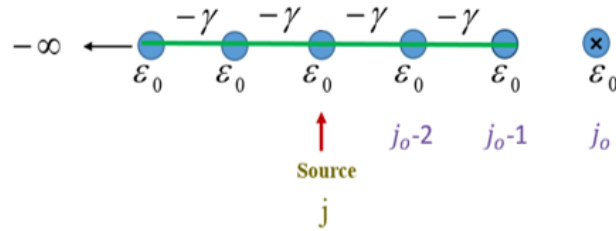


Figure 3.5.4: Tight-binding approximation of a semi-infinite one-dimensional chain with on-site energies ϵ_0 and couplings $-\gamma$.

The boundary condition is achieved by adding a wavefunction to the Green's function.

To get the appropriate boundary condition thus I have to add:

$$\Psi_{j,j'}^{j_0} = -\frac{e^{ik(j+j'-2j_0)}}{i\hbar v} \quad (3.5.22)$$

The Green's function ($g_{jj'} = g_{jj'}^{\infty} + \Psi_{j,j'}^{j_0}$) will have the following simple form at the

boundary $j = j' = j_0 - 1$:

$$g_{j_0-1,j_0-1} = -\frac{e^{ik}}{\gamma} \quad (3.5.23)$$

In the case where the two leads are decoupled, $\alpha = 0$, the total Green's function of the scattering region can be given as:

$$g = \begin{pmatrix} -\frac{e^{ik}}{\gamma} & 0 \\ 0 & -\frac{e^{ik}}{\gamma} \end{pmatrix} = \begin{pmatrix} g_L & 0 \\ 0 & g_R \end{pmatrix} \quad (3.5.24)$$

Here, g is the decoupled Green's function.

If I consider a switch on of the interaction, then to obtain the Green's function of the coupled leads of this system, Dyson's equation is written:

$$G^{-1} = (g^{-1} - V) \quad (3.5.25)$$

Where the operator V describing the interaction connecting the two leads, which has the form:

$$V = \begin{pmatrix} 0 & V_c \\ V_c^\dagger & 0 \end{pmatrix} = \begin{pmatrix} 0 & -\alpha \\ -\alpha^* & 0 \end{pmatrix} \quad (3.5.26)$$

By solving the Dyson's equation (3.5.25), I will obtain:

$$G = \frac{1}{\alpha^2 - \gamma^2 e^{-2ik}} \begin{pmatrix} \gamma e^{-ik} & -\alpha \\ -\alpha & \gamma e^{-ik} \end{pmatrix} \quad (3.5.27)$$

Here, I can calculate the transmission (t) and the reflection (r) amplitudes from the Green's function equation (3.5.27). This is obtained by using the Fisher-Lee relation,^{7,8} which relates the scattering amplitudes of a scattering problem to the Green's function of the problem. The Fisher-Lee relations for our case is given:

$$r = i\hbar v G_{1,1}^{-1} \quad (3.5.28)$$

And
$$t = i\hbar v G_{1,2} e^{ik} \quad (3.5.29)$$

These amplitudes correspond to particles incident from the left. Similar expressions could be used for the transmission (\tilde{t}') and reflection (\tilde{r}') amplitudes for the particles are travelling from the right. Based on these coefficients, the probability is defined as:

$$T = |t|^2, \quad T' = |t'|^2 \quad \text{and} \quad R = |r|^2, \quad R' = |r'|^2 \quad (3.5.10)$$

Since I am now in the possession of the full scattering matrix, so I can use the Landauer formula equation (3.3.4) to calculate the zero-bias conductance.

3.6. Transport through an arbitrary scattering region

In this section I will derive the most general formula for the transmission probability for an arbitrarily scattering structure. Here I will use a different approach starting with the wave functions leading to the surface Green's function and ending up with a general formula for the transmission probability.

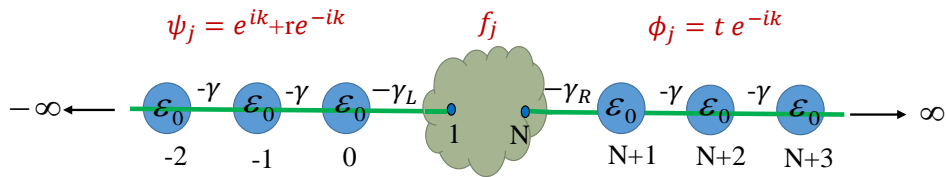


Figure 3.6.1. Tight-binding representation of a one dimensional arbitrarily scattering region attached to one dimensional lead.

Considering the nanoscale junction in Figure (3.6.1), where an arbitrary scattering region with Hamiltonian H is connected to two one dimensional leads. On-site energies

and coupling in the left (right) lead $L(R)$ are ε_L (ε_R) and $-\gamma_L$ ($-\gamma_R$), respectively, and the leads are connected to the site 1 and N of the scattering region.

If the wave function in the left, the right and the scattering region are $\psi_j = e^{ikj} + re^{-ikj}$, $\phi_j = te^{ikj}$ and f_j respectively, the Schrödinger equation for the left and right lead and the scattering region with connection points could be written as:

$$\varepsilon_0\psi_j - \gamma\psi_{j-1} - \gamma\psi_{j+1} = E\psi_j \quad \text{for } j \leq 0 \quad (3.6.1)$$

$$\varepsilon_0\psi_0 - \gamma\psi_{-1} - \gamma\psi_1 = E\psi_0 \quad \text{for } j = 0 \quad (3.6.2)$$

$$\sum_{j=1}^N h_{ij}f_j - \gamma_L\psi_0\delta_{i1} - \gamma_R\phi_{N+1}\delta_{iN} = Ef_i \quad \text{for } 0 \leq j \leq N + 1 \quad (3.6.3)$$

Also,

$$\varepsilon_0\phi_{N+1} - \gamma_R f_N - \gamma\phi_{N+2} = E\phi_{N+1} \quad \text{for } j = N + 1 \quad (3.6.4)$$

$$\varepsilon_0\phi_j - \gamma\phi_{j-1} - \gamma\phi_{j+1} = E\phi_j \quad \text{for } j > N + 1 \quad (3.6.5)$$

Equation (3.6.3) can be written as:

$|f\rangle = g|X\rangle$ where $g = (E - h)^{-1}$ is the Green's function and $|X\rangle$ called source which is a zero vector with non-zero elements only in the connection points at site $j = 0$ and $j = N + 1$. For the junction in figure (3.6.1), $|X\rangle$ has only two non-zero elements due to the source.

$$\begin{pmatrix} f_1 \\ f_N \end{pmatrix} = \begin{pmatrix} g_{11} & g_{1N} \\ g_{N1} & g_{NN} \end{pmatrix} \begin{pmatrix} X_0 \\ X_{N+1} \end{pmatrix} \quad (3.6.6)$$

Where $X_0 = \gamma_L\psi_0$ and $X_{N+1} = \gamma_R\phi_{N+1}$.

By using the recurrence relation, I get:

$$\gamma\phi_N = \gamma_R f_N \quad (3.6.7)$$

$$\gamma\psi_1 = \gamma_L f_1 \quad (3.6.8)$$

$$\phi_N = \phi_{N+1} e^{-ik} \quad (3.6.9)$$

$$\psi_1 = 2isink + \psi_0 e^{-ik} \quad (3.6.10)$$

By combine these four equations with equation (3.6.6) I get:

$$\begin{pmatrix} \frac{\gamma}{\gamma_L} e^{-ik} - g_{11} \gamma_L & -g_{1N} \gamma_R \\ -g_{N1} \gamma_L & -g_{NN} \gamma_R - \frac{\gamma}{\gamma_R} e^{-ik} \end{pmatrix} \begin{pmatrix} \psi_0 \\ \phi_{N+1} \end{pmatrix} = \frac{\gamma}{\gamma_L} (2isink) \begin{pmatrix} 1 \\ 0 \end{pmatrix} \quad (3.6.11)$$

Therefore

$$\begin{pmatrix} \psi_0 \\ \phi_{N+1} \end{pmatrix} = \frac{\gamma}{\gamma_L} (2isink) \frac{1}{d} \begin{pmatrix} -\frac{\gamma}{\gamma_R} e^{-ik} - g_{NN} \gamma_R \\ -g_{N1} \gamma_L \end{pmatrix}$$

The transmission t and reflection r amplitudes could be obtained:

$$t = iv \left[\gamma_L g_L \left(\frac{g_{N1}}{\Delta} \right) \gamma_R g_R \right] \quad (3.6.12)$$

Where $g_{L,R} = \frac{e^{ik_{L,R}}}{-\gamma_{L,R}}$ (3.6.13)

This is the surface Green's function in the left and right leads and:

$$\Delta = (1 - \Sigma_L g_{11} - \Sigma_R g_{NN} + \Sigma_L \Sigma_R (g_{11} g_{NN} - g_{1N} g_{N1})) \quad (3.6.14)$$

Where $\Sigma_{L,R} = \gamma_{L,R}^2 g_{L,R}$ are called self-energies due to the left and right contacts.

The transmission probability is:

$$T(E) = |\phi_{N+1}|^2 = |t|^2 \quad (3.6.15)$$

Then,

$$T(E) = \left(\frac{\gamma_L}{\gamma} \right)^2 \left(\frac{\gamma_R}{\gamma} \right)^2 v^2 \left(\frac{g_{N1}}{\Delta} \right)^2 \quad (3.6.16)$$

Equation (3.6.16) is the most general formula to calculate the transmission probability for any scattering region connected to identical leads.

The completely general technique for calculating Green's function and a scattering S matrix and transport coefficient of a finite super-lattice connected to crystalline semi-infinite leads can be found in ⁹.

3.7 Features of the Transport Curve

The main feature of electron transport through single molecules and phase coherent nanostructures is the appearance of transport resonances and anti-resonances associated with quantum interference. Deep understanding of the transmission process can be achieved by looking at the properties of these resonances. Here, I will briefly discuss different kinds of resonances, which are: Breit-Wigner resonances¹⁰, anti-resonances^{11,12} and Fano resonances^{13,14}.

3.7.1 Breit-Wigner Resonance

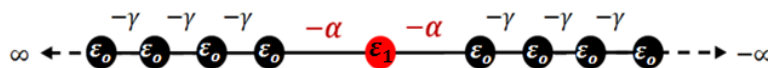


Figure 3.7.1: Simple model to study a Breit-Wigner resonance, a scattering region with a single impurity placed between two one-dimensional semi-infinite chains

To study the behaviour of resonances for transmission function $T(E)$, figure (3.7.1) shows a one-dimensional crystalline linear chain with a single impurity placed in the middle of the chain as a defect which is coupled to the left and right of semi-infinite

crystalline chains by hopping elements $-\alpha$. Then, the transmission probability could be expressed by a Lorentzian function, via the Breit-Wigner formula as:

$$T(E) = \frac{4\Gamma_1\Gamma_2}{[(E-\varepsilon_n)^2+(\Gamma_1+\Gamma_2)^2]} \quad (3.7.1)$$

Therefore, within this formula, the transmission coefficient $T(E)$ of the single molecular junction can be described by two parameters: (Γ) and (ε_n) where (Γ) is the strength of the coupling between the molecule and the electrodes (labeled 1 and 2 in equation (3.7.1)) and $\varepsilon_n = E_n - \Sigma$ is the eigen energy E_n of the molecular orbital shifted slightly by an amount Σ due to the coupling of the orbital to the electrodes⁵. Transmission coefficient $T(E)$ has Breit-Wigner-type resonances showing the maximum value when the electron resonates with the molecular orbital (i.e. when $E = \varepsilon_n$).

The formula is valid when the energy E of the electron is close to an Eigen energy E_n of the isolated molecule, and if the level spacing of the isolated molecule is larger than $(\Gamma_1 + \Gamma_2)$. In the case of a symmetric molecule attached symmetrically to identical leads (i.e. $\Gamma_1 = \Gamma_2$) and again when $(E = \varepsilon_n)$, $T(E) = 1$. The width of the resonance depends on the coupling component α where if the coupling element α is large, the resonances are wider.

If a bound state (e.g. a pendant group ε_2) is coupled (by coupling integral β) to a continuum of states as shown in figure (3.7.2), Fano resonances could occur. Fano resonance contains an anti-resonance followed by a resonance with an asymmetric line profile in between.

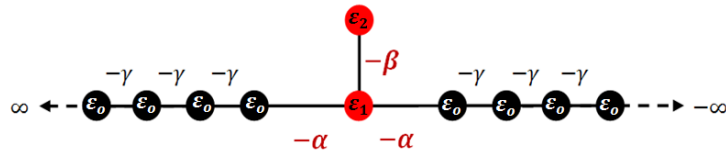


Figure 3.7.2: Tight binding model to study Fano resonances. Two one-dimensional semi-infinite chains coupled to a scattering region of site energy ϵ_0 by hopping elements $-\gamma$ where an extra energy level is attached to the scattering region.

Also, an anti-resonance could appear in the transmission probability when the system is multi-branched and destructive interference occurs between propagating waves at the nodal point. A simply example is shown in figure (3.7.3)

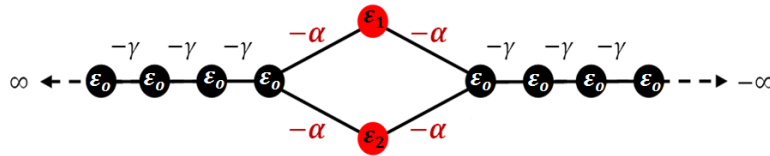


Figure 3.7.3: Tight binding model to study anti-resonance. Two one-dimensional semi-infinite chains coupled to the scattering region.

Figure 3.7.4 shows the general shape of the transmission probability related to this kind of resonances.

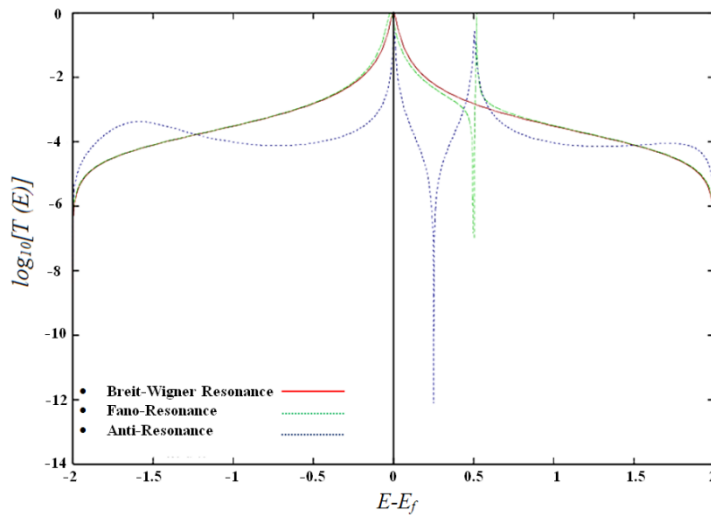


Figure 3.7.4: Transmission coefficients for the systems describe in sections 3.7.1 (Red), 3.7.2 (Green) and 3.7.3 (Blue).

Bibliography

- (1) Schrödinger, E. An Undulatory Theory of the Mechanics of Atoms and Molecules. *Phys. Rev.* **1926**, 28 (6), 1049.
- (2) Landauer, R. Spatial Variation of Currents and Fields Due to Localized Scatterers in Metallic Conduction. *IBM J. Res. Dev.* **1957**, 1 (3), 223–231.
- (3) Büttiker, M.; Imry, Y.; Landauer, R.; Pinhas, S. Generalized Many-Channel Conductance Formula with Application to Small Rings. *Phys. Rev. B* **1985**, 31 (10), 6207.
- (4) Cuevas, J. C.; Scheer, E.; Cao, G.; Wang, Y.; Diagnostics, P. M. World Scientific Series in Nanoscience and Nanotechnology. **2010**.
- (5) Lambert, C. J. Basic Concepts of Quantum Interference and Electron Transport in Single-Molecule Electronics. *Chem. Soc. Rev.* **2015**, 44 (4), 875–888.
- (6) Paxton, A. T.; others. An Introduction to the Tight Binding Approximation--Implementation by Diagonalisation. *NIC Ser.* **2009**, 42, 145–176.
- (7) Datta, S. *Electronic Transport in Mesoscopic Systems*; Cambridge university press, 1997.
- (8) Fisher, D. S.; Lee, P. A. Relation between Conductivity and Transmission Matrix. *Phys. Rev. B* **1981**, 23 (12), 6851.
- (9) Sanvito, S.; Lambert, C. J.; Jefferson, J. H.; Bratkovsky, A. M. General Green's-Function Formalism for Transport Calculations with Spd Hamiltonians and Giant Magnetoresistance in Co-and Ni-Based Magnetic Multilayers. *Phys. Rev. b* **1999**, 59 (18), 11936.
- (10) Breit, G.; Wigner, E. Capture of Slow Neutrons. *Phys. Rev.* **1936**, 49 (7), 519.
- (11) Ke, S.-H.; Yang, W.; Baranger, H. U. Quantum-Interference-Controlled Molecular Electronics. *Nano Lett.* **2008**, 8 (10), 3257–3261.

- (12) Stadler, R. Quantum Interference Effects in Electron Transport through Nitrobenzene with Pyridil Anchor Groups. *Phys. Rev. B* **2009**, *80* (12), 125401.
- (13) Fano, U. Effects of Configuration Interaction on Intensities and Phase Shifts. *Phys. Rev.* **1961**, *124* (6), 1866.
- (14) Papadopoulos, T. A.; Grace, I. M.; Lambert, C. J. Control of Electron Transport through Fano Resonances in Molecular Wires. *Phys. Rev. b* **2006**, *74* (19), 193306.

Chapter 4

The Conductance of Porphyrin-Based Molecular Nanowires Increases with Length

The conductance of a classical metallic wire is inversely proportional to its length. In contrast, molecular wires usually act as tunnelling barriers where the conductance decays exponentially with length. In contrast, in this chapter, the conductance of fused-oligo-porphyrin nanowires is examined theoretically, and I demonstrate the conductance increase with length at room temperature. The results presented in this chapter were published in Norah Algethami, et al 'The Conductance of Porphyrin-Based Molecular Nanowires Increases with Length' Nano Letter 2018, 18 (7), 4482–4486.

4.1. Introduction

The search for molecular nanowires, whose electrical conductance decays slowly with length has been subject to many studies in the last couple of decades¹⁻⁶. Single-molecule wires typically act as tunnel barriers and their conductance G decays exponentially by molecular length^{7,8} L as $G = A e^{-\beta L}$ where A is pre-factor and β is the decay (attenuation) factor. Molecular wires usually possess a high beta factor, which limits their potential as interconnects in future molecular-scale circuitry. For example, measured room-temperature values of β range from 2.0 - 3.4 nm^{-1} for OPEs⁹, 3.3 nm^{-1} for OAEs¹⁰, 1.7 - 1.8 nm^{-1} for OPVs¹¹, 4.9 nm^{-1} for acenes¹², 1.7 - 3.1 nm^{-1} for oligoynes^{11,13} and 8.4 nm^{-1} for alkanes¹⁴ depending on their precise anchor groups to gold electrodes.

The aim of this chapter is to identify molecular wires with vanishing or even a negative value of β , motivated by measurements of molecular wires based on porphyrin derivatives¹⁵⁻²⁰, which exhibit exceptionally low attenuation factors, due to their highly conjugated electronic structure. For example, scanning tunnelling microscope (STM) measurements using a gold tip and substrate revealed that molecular wires formed from porphyrin units connected to each other through acetylene linkers exhibit a low attenuation factor of $\beta = 0.4 \text{ nm}^{-1}$ with both pyridyl and thiol anchors^{2,21} and fused-oligo-porphyrin wires with pyridyl anchors²² exhibited an even lower value of $\beta = 0.2 \text{ nm}^{-1}$. The agreement between these experiments and theories based on phase coherent transport suggests that the electron-phonon interaction²³ is not a dominant effect in porphyrin nanowires up to $\sim 4 \text{ nm}$. In what follows, I demonstrate that by employing different anchors, this fascinating family of molecular wires can exhibit vanishing or negative attenuation factors. I demonstrate that a negative attenuation factor is an intrinsic property of the fused-oligo-porphyrins, which arises from the strong coupling

between neighbouring porphyrin oligomers and a resulting strong decrease in their HOMO–LUMO gap with length. This behaviour is in marked contrast the anomalous conductance trends measured in oligothiophenes,²⁴ which are attributed to extrinsic factors, such as conformational changes of the molecule in the junction,²⁵ or a peculiarity of iodide anchor groups, which cause short oligomers to lie flat on the substrate electrode²⁶.

4.2. Molecular Structure

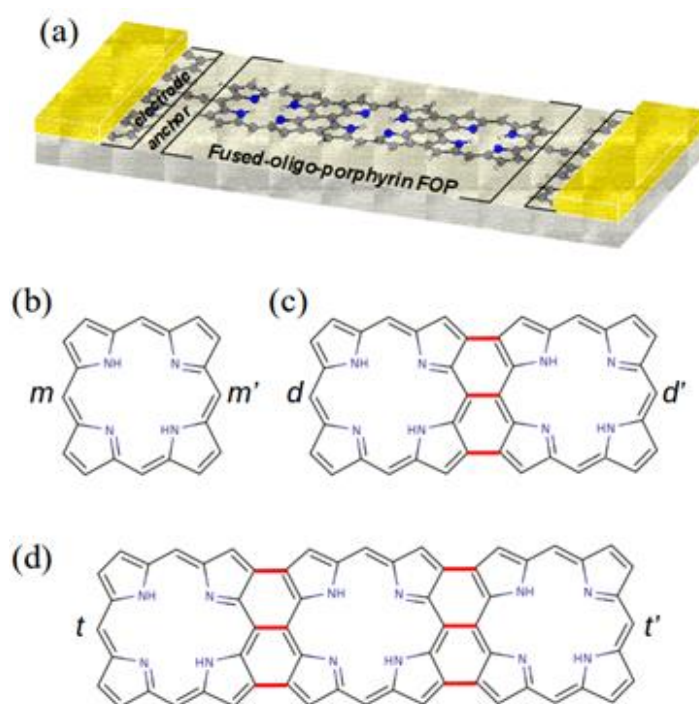


Figure 4.2.1. A schematic of a generic molecular junction and FOP monomer, dimer, and trimer molecular wires. (a) The schematic of a generic molecular junction containing a fused porphyrin trimer. (b) A porphyrin monomer connected to electrodes from m and m' connection points. (c) A fused porphyrin dimer, comprising two monomers connected to each other through three single bonds (red bonds) and connected to electrodes from d and d' connection points. (d) A fused porphyrin trimer connected to electrodes from t and t' connection points.

Figure 4.2.1 shows the molecular structure of a porphyrin monomer, a fused dimer and a fused trimer, in which two or three porphyrins are connected to each other through three single bonds (shown by red lines in figure 4.2.1 (c), (d)).

To gain a deeper insight into electrical transport properties for this molecule, the computational modelling has been used. Before computing transport properties, all molecules were initially geometrically relaxed in isolation to yield the geometries shown in figure 4.2.1. These geometry of each structure for porphyrin molecule was relaxed to a force tolerance of 20 meV/\AA using the SIESTA implementation of density functional theory (DFT) which has been presented in details in chapter (2), with a double- ζ polarized basis set (DZP) and generalized gradient functional approximation (GGA-PBE) for the exchange and correlation functional and a real space grid was defined with an equivalent energy cutoff 150 Ry.

Table 4.2.1 shows the plots orbitals of the highest occupied molecular orbital (HOMO) and lowest unoccupied molecular orbital (LUMO). By comparing the topology of the HOMO and LUMO orbitals for the oligo-fused porphyrin as shown in table 4.2.1 with the molecular orbitals for non-fused porphyrin as shown in table 4.2.2, from the first figure, because the fused porphyrin is fully conjugated electronic structure, I see the charge density is distributed and extended across the length of all the molecule (Monomer, Dimer and Trimer).

Table 4.2.1. The wave functions of HOMO-2, HOMO-1, HOMO, LUMO, LUMO+1 and LUMO+2 levels orbitals for fused oligo porphyrin.

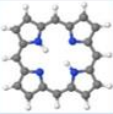
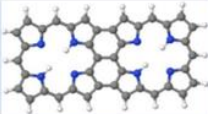
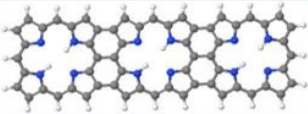
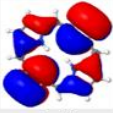
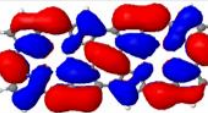
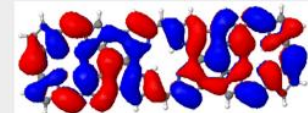
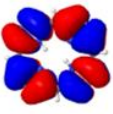
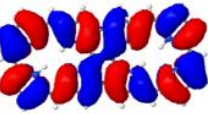
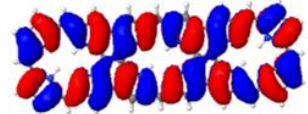
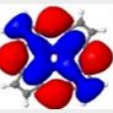
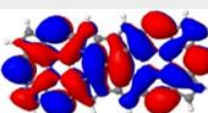
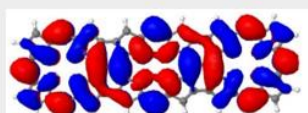

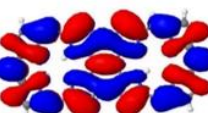
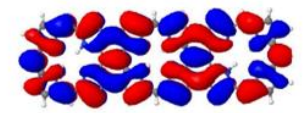

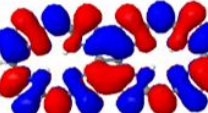
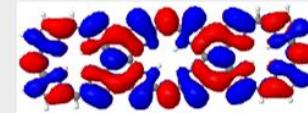
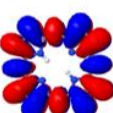
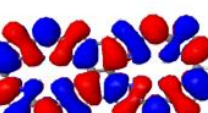
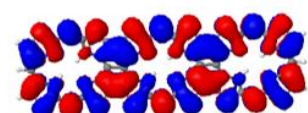
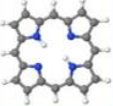
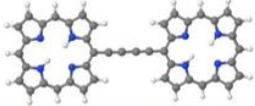
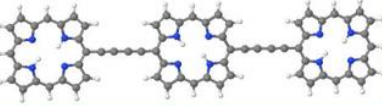
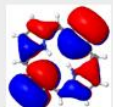
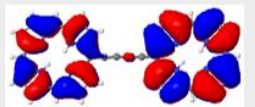
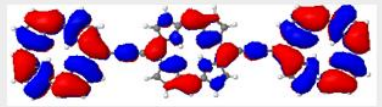
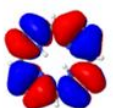
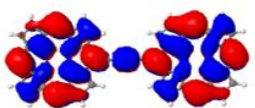
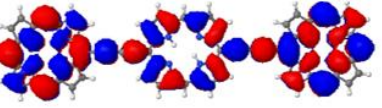
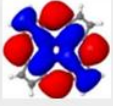
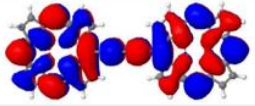
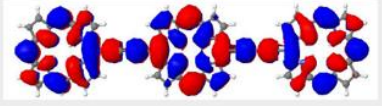
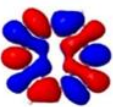
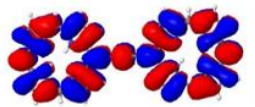
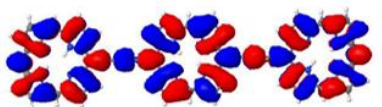
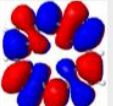
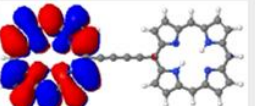
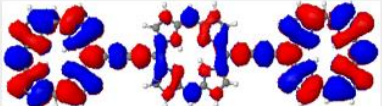
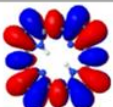
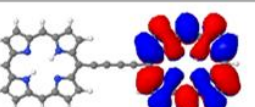
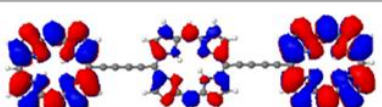
Structure	 $E_F = -3.73 \text{ eV}$	 $E_F = -3.76 \text{ eV}$	 $E_F = -3.88 \text{ eV}$
HOMO-2	 -5.33 eV	 -4.89 eV	 -4.58 eV
HOMO-1	 -4.76 eV	 -4.41 eV	 -4.30 eV
HOMO	 -4.51 eV	 -4.21 eV	 -4.13 eV
LUMO	 -2.62 eV	 -3.33 eV	 -3.55 eV
LUMO+1	 -2.58 eV	 -2.82 eV	 -2.93 eV
LUMO+2	 -1.31 eV	 -2.45 eV	 -2.92 eV

Table 4.2.2: The wave functions of HOMO-2, HOMO-1, HOMO, LUMO, LUMO+1 and LUMO+2 levels orbitals for Non-Fused Porphyrin.

Structure	 $E_F = -3.73$ eV	 $E_F = -3.34$ eV	 $E_F = -3.79$ eV
HOMO-2	 -5.33 eV	 -4.87 eV	 -4.91 eV
HOMO-1	 -4.76 eV	 -4.81 eV	 -4.57 eV
HOMO	 -4.51 eV	 -4.27 eV	 -4.22 eV
LUMO	 -2.62 eV	 -3.09 eV	 -3.29 eV
LUMO+1	 -2.58 eV	 -2.70 eV	 -2.93 eV
LUMO+2	 -1.31 eV	 -2.68 eV	 -2.74 eV

4.3. Results and discussion

I compute the electrical conductance of the highly conjugated porphyrin wires shown in figure 4.2.1, in which neighbouring porphyrins are fused to each other via three single bonds (shown in red in figure 4.2.1). I systematically examined fused-oligo-porphyrin

(FOP) wires with different lengths connected to different electrodes with different anchors and consistently found that the conductance of these fused-oligo-porphyrin (FOP) wires can increase with length and that they possess a negative attenuation factor. This is first time that negative β -factor wires have been identified and is significant, because these wires are stable and therefore ideal candidates for low-conductance interconnects. To demonstrate that this result is generic and occurs for different electrode materials and anchor groups, I study quantum transport through FOPs (figure 4.2.1 (a)) with three different lengths (figure 4.2.1 (b), (c), (d)) sandwiched between either gold electrodes^{27,28} with thiol or acetylene anchors. I also study FOPs between graphene electrodes^{17,29,30} with either direct carbon-carbon bonds to the edges of the graphene or non-specific, physisorbed coupling to the graphene.

From the molecular structure of a porphyrin monomer, a fused dimer and a fused trimer as shown in figure 4.2.1, I first consider molecular junctions in which the carbon atoms labelled (m,m') , (d,d') and (t,t') respectively are connected to electrodes via acetylene linkers as shown in figure 4.3.1 which illustrate the molecular structure junction of porphyrin wires in case of Monomer, Dimer and trimer in figure 4.3.1 (a), (b), (c) where the porphyrin wires are connected to the edges of rectangular shaped graphene electrodes with periodic boundary conditions in the transverse direction.

To calculate the room temperature electrical conductance G , we calculate the electron transmission coefficient $T(E)$ using the Gollum transport code combined with the material specific mean field Hamiltonian obtained from SIESTA implementation of density functional theory (DFT) and then evaluate G using the Landauer formula (as explain in chapter 2). Results for the monomer, dimer and trimer attached to graphene electrodes figure 4.3.1 (a), (b), (c) are shown in figure 4.3.1(d).

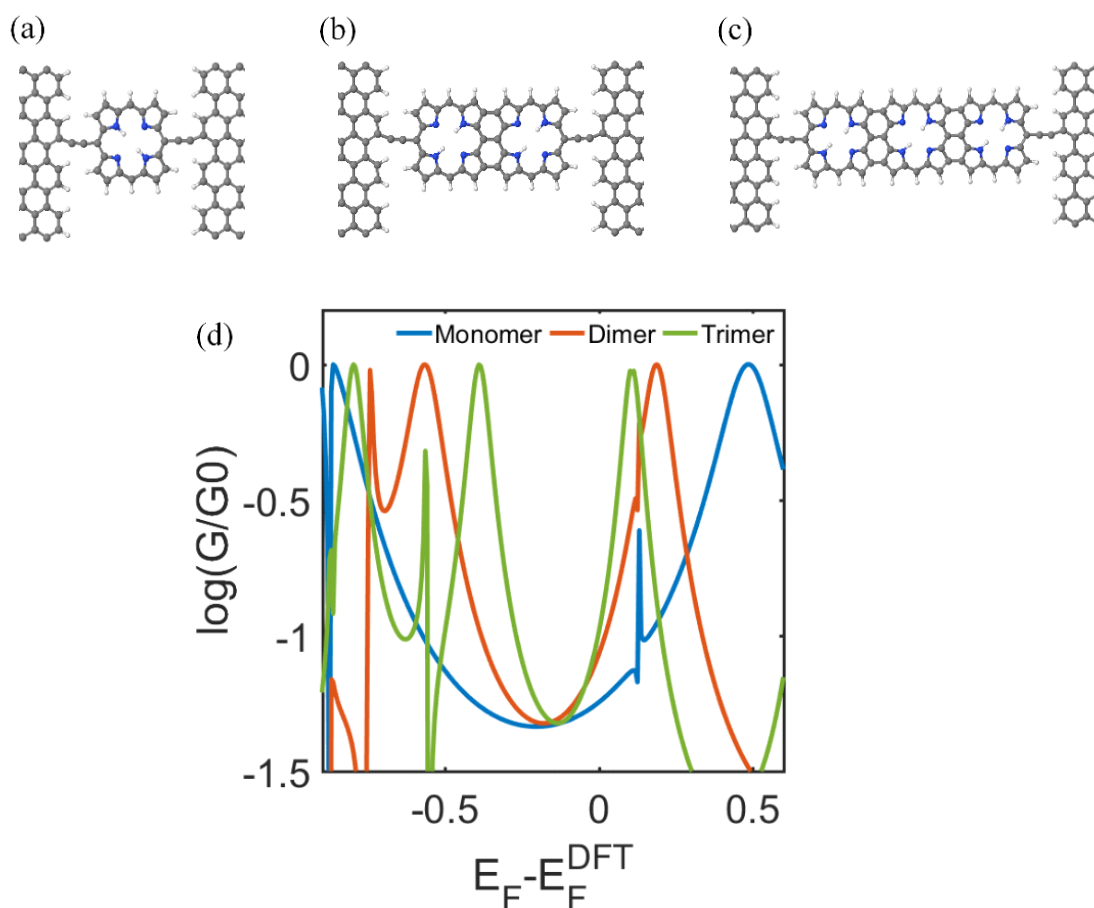


Figure 4.3.1: Transport through monomer, dimer and trimer molecular wires attached to two graphene electrodes. (a),(b),(c) A fused porphyrin molecular wire connected to graphene electrodes via acetylene linkers through monomer, dimer and trimer respectively. (d) The room temperature electrical conductance for the porphyrin monomer (blue curve), porphyrin dimer (red curve) and porphyrin trimer (green curve) as a function of the electrode Fermi energy E_F , in units of the conductance quantum $G_0 = 77$ microsiemens.

For these highly-conjugated wires, the energy level spacing decreases as their size increases. Therefore, the energy gap between the highest occupied molecular orbital (HOMO) and lowest unoccupied molecular orbital (LUMO) of the dimer is smaller than that of the monomer and in turn, the HOMO-LUMO (HL) gap of the trimer is smaller than that of the dimer. This behaviour is reflected in the conductance resonances of figure 4.3.1 (d), which are furthest apart for the monomer (blue curve)

and closest together for the trimer (green curve). This can be understood by starting from a chain of N isolated monomers. Because each monomer has a HOMO energy E_H^0 and a LUMO energy E_L^0 , the isolated chain has N -fold degenerate HOMO and N -fold degenerate LUMO. When the monomers are coupled together to form a fused wire, the degeneracies are lifted, to yield a HOMO, N -tuplet with molecular orbital energies $E_H^1 < E_H^2 < \dots < E_H^0 \dots < E_H^N$ and a LUMO, N -tuplet $E_L^1 < E_L^2 < \dots < E_L^0 \dots < E_L^N$. Consequently, the new HL gap $\Delta(N) = E_L^1 - E_H^N$ is lower in energy than that of the monomer.

Figure 4.3.1(d) shows the electrical conductance as a function of the electrode Fermi energy E_F , plotted relative to the value E_F^{DFT} predicted by DFT for pristine electrodes. The precise value of the electrode Fermi energy E_F can depend on many environmental factors, but unless the molecular energy levels are shifted by an electrostatic or electrochemical gate, it always lies within the H-L gap of the contacted molecule. If $E_F - E_F^{DFT}$ is approximately -0.18 eV, then all three curves in figure 4.3.2 (d), coincide and the monomer, dimer and trimer will possess the same conductance. For any other value within the HL gap (i.e. between the resonant peaks in the range -0.4 eV to +0.1 eV) the conductance of the trimer exceeds that of the dimer, which in turn exceeds that of the monomer. Consequently, we predict that β is negative or zero.

To demonstrate that negative values of β are a generic feature of FOP molecular wires and occur for different choices of electrode or anchor groups, we calculate their electrical conductances when connected to gold electrodes through thiol anchors as shown in figure 4.3.3 (a), (b), (c) respectively and calculated their electrical conductances as shown in figure 4.3.3 (d). I also computed their conductances when coupled to graphene electrodes without a conventional anchor group as shown in figure 4.3.4.

For these molecular junctions, figure 4.3.3 (d) show the electrical conductance for the gold junctions with thiol anchors, if $E_F - E_F^{DFT}$ is lower than the mid-gap (0.18 eV) of the trimer, β is zero or slightly positive, otherwise β is negative.

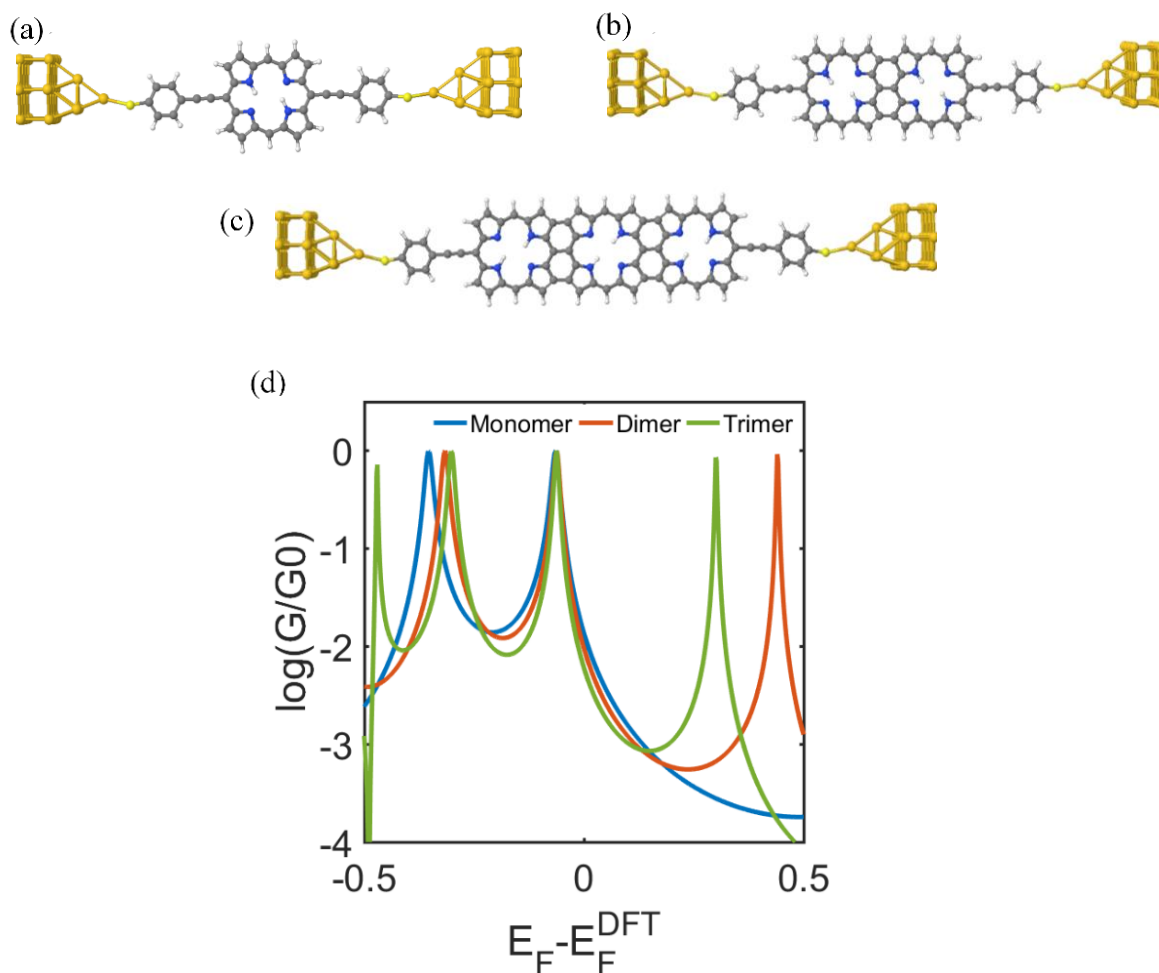


Figure.4.3.3: Transport through monomer, fused dimer and trimer porphyrin wires sandwiched between two graphene or gold electrodes. (a),(b),(c) A gold/FOPs/gold junction with thiol anchors. (d) The electrical conductances of the gold/monomer, dimer or trimer/gold junctions with thiol anchors. The distance between the molecules with gold electrodes and sulfur atom is 0.26 nm.

In the graphene junctions without specific anchoring as shown in figure 4.3.4, where the overall conductance is low due to the weak physisorbed nature the coupling to the

electrodes, the electrical conductances of FOPs within the HL gap of the trimer are again found to increase with length. This unconventional negative beta factor is clearly independent of the connection point to the electrodes, because in the structure junctions of figure 4.3.4 (a), (b), (c) there is no specific connection point between the electrode surfaces and the molecules. The results of figure 4.3.3 and 4.3.4 demonstrate that low or negative β factors are a common feature of fused oligo-porphyrins and occur for different modes of anchoring to electrodes.

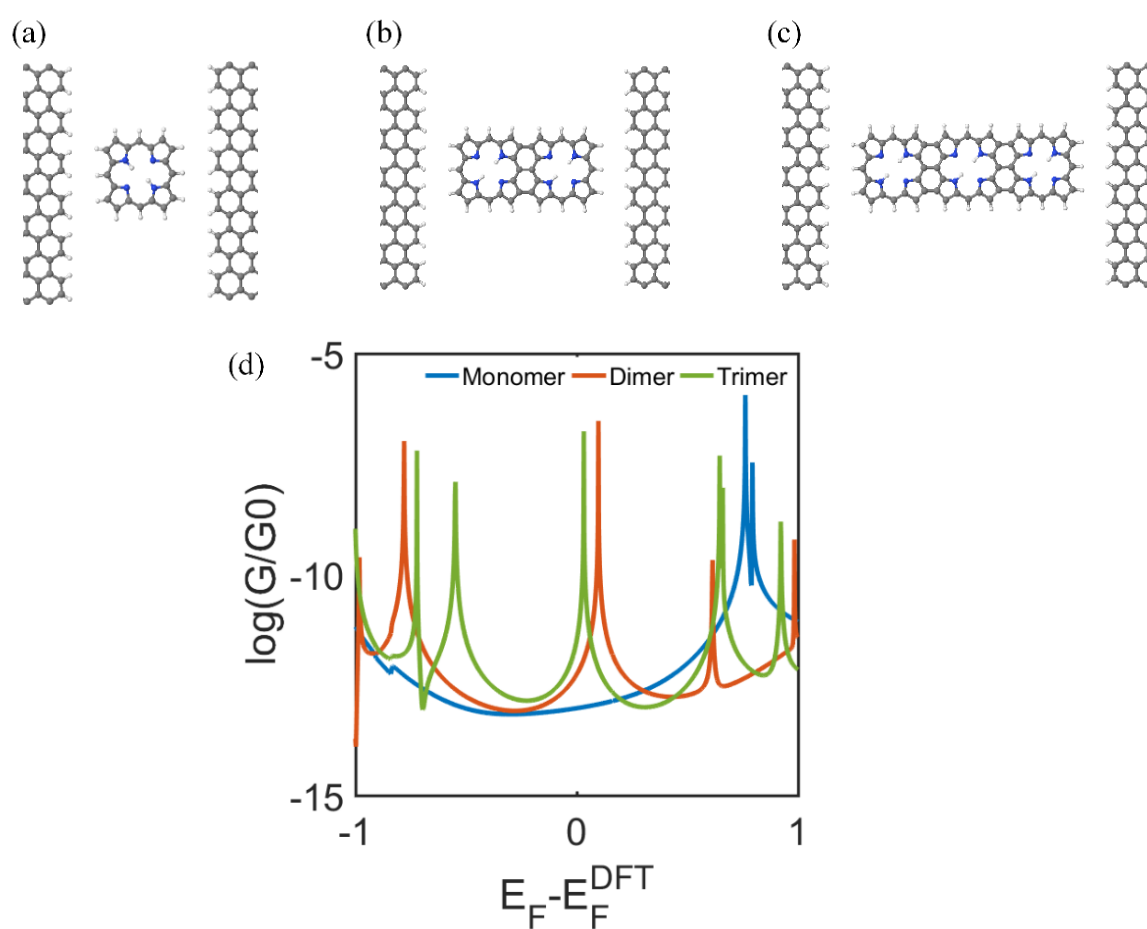


Figure.4.3.4: The molecular junction of graphene/monomer, dimer or trimer/graphene junctions without specific anchoring to the graphene shows in (a), (b), (c) respectively. The distance between FOP and graphene electrodes are 0.3 nm. (d) The electrical conductances graphene/monomer, dimer or trimer/graphene junctions without specific anchoring to the graphene.

To clarify why the conductance increases with length, we constructed a simple tight-binding model, in which a single p orbital per atom interacts with nearest neighbour orbitals only. The energy origin is chosen such that all on-site energies $\varepsilon = 0$ and $-0.5/\gamma$ for carbon and nitrogen respectively and nearest-neighbour couplings $\gamma = -1$ for both C-C and C-N bonds.

I calculated the transmission function $T(E)$ between two ends of the wires e.g. (with contact atoms (m, m') , (d, d') and (t, t') for the monomer, dimer and trimer respectively, as shown in figure 4.1.1 I then examined the effect of varying the coupling parameter α between neighbouring porphyrin units which shown by red bonds in figure 4.1.1 (c), (d). The different curves in figure 4.3.5(a) show that for a value $\alpha = -0.65\gamma$ where $\gamma = -1$ is coupling integrals between p orbitals of any neighboring C-C atoms, the curves overlap and for more negative values of α , the transmission coefficient increases with length for energies within the HL gap of the trimer as shown in figure 4.3.5 (a), in agreement to the above DFT results. To demonstrate that the decrease in the HL gap is due to a splitting of the HOMO and LUMO degeneracies, figure 4.3.5 (b) shows the transmission curves of the trimer over a larger range of energy, for a series of values of the coupling α . For small α , the HOMO and LUMO are each almost triply degenerate and as the magnitude of α increases, the degeneracy is increasingly lifted, leading to a reduction in the HL gap.

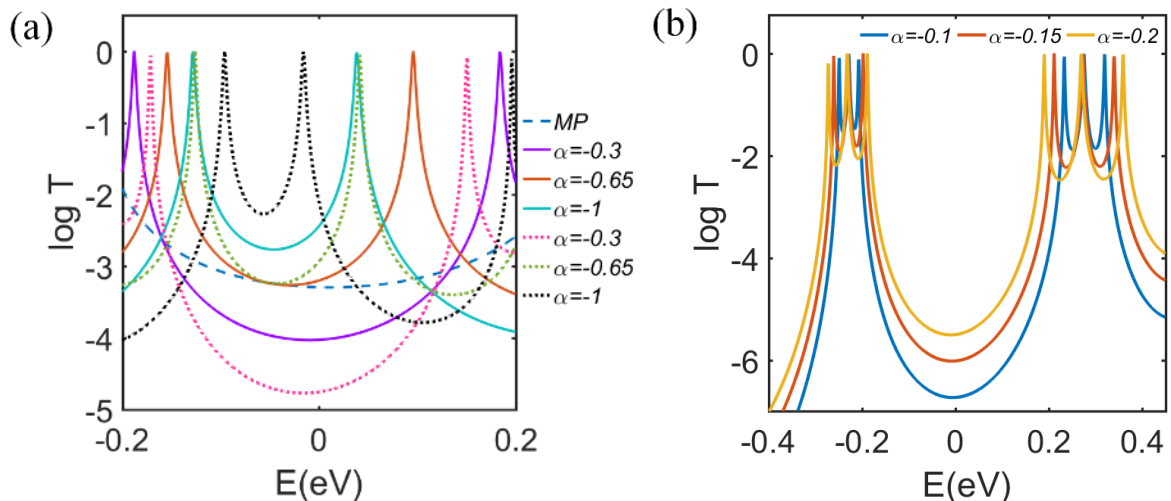


Figure. 4.3.5: The transmission coefficient for three connections point (m,m') , (d,d') and (t,t') shown in figure. 4.2.1 (b), (c) and (d) respectively, obtained using a simple tight binding TB model of FOP junctions. (a) The dash line curve shows the transmission coefficients for the monomer. The solid and dotted lines show the transmission coefficient for the dimer and trimer respectively. The solid red and dotted green curves show the transmission coefficient for the dimer and trimer when $\alpha=-0.65$. (b) The transmission coefficient of the trimer for values of $\alpha = -0.1, -0.15, -0.2$.

For $\alpha=0.65\gamma$, figure 4.3.6 shows that this increase in conductance with length persists even if the number of fused porphyrin units increased to 4, 5 and 6 units.

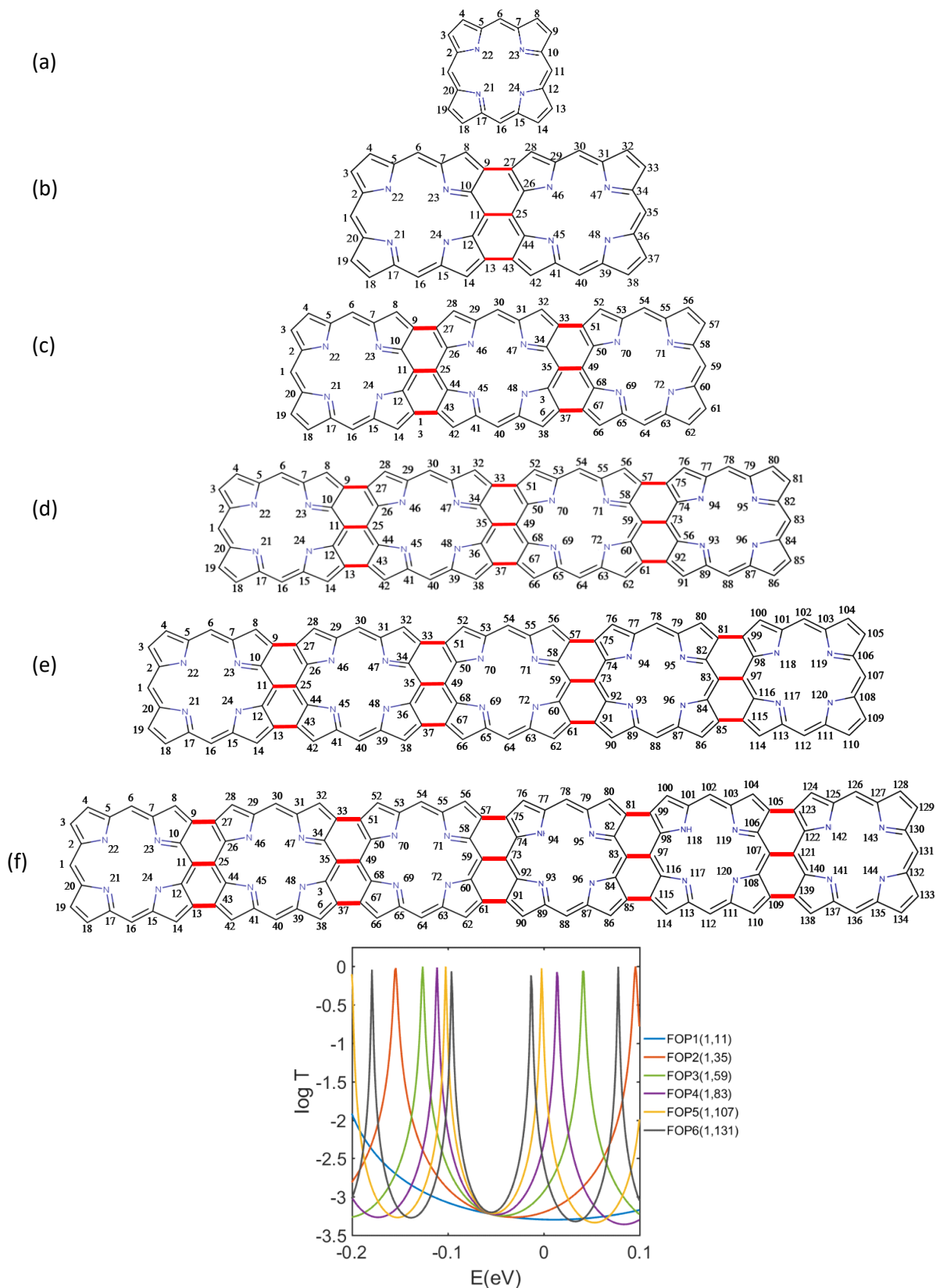


Figure. 4.3.6: Transmission coefficient for fused oligo porphyrins with different length upto 6 ((a)to(f)) porphyrin units calculated using simple tight binding model. The red bonds are chosen to be $\alpha = -0.65$.

On the other hand, figure 4.3.7 shows that the band structure of an infinitely-periodic fused porphyrin wire, calculated using density functional theory, the k-point grid of $1 \times 1 \times 20$ was chosen for band structure calculation possesses a small energy gap of about $\sim 100\text{meV}$. Therefore, fused porphyrin ribbons are narrow-gap semiconductors, meaning that eventually the conductance will begin to decrease with length. In practice, this decrease is likely to be slower than exponential, because at room temperature and large enough length scales, inelastic scattering will become significant and a cross-over from phase-coherent tunnelling to incoherent hopping will occur^{10,31}.

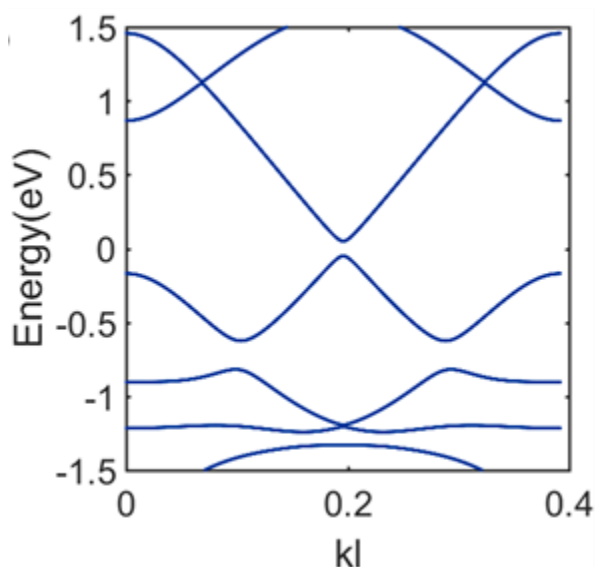


Figure 4.3.7: Band structure of fused porphyrin nanoribbon.

For comparison, figure 4.3.8 shows the transmission curves for butadiyne-linked porphyrin monomer, dimer and trimer molecular wires, for which the attenuation factor β is clearly positive for a wide range of energies within the HL gap of the trimer by tight binding model in agreement with the DFT calculation³² and also with reported measured values²¹⁻³².

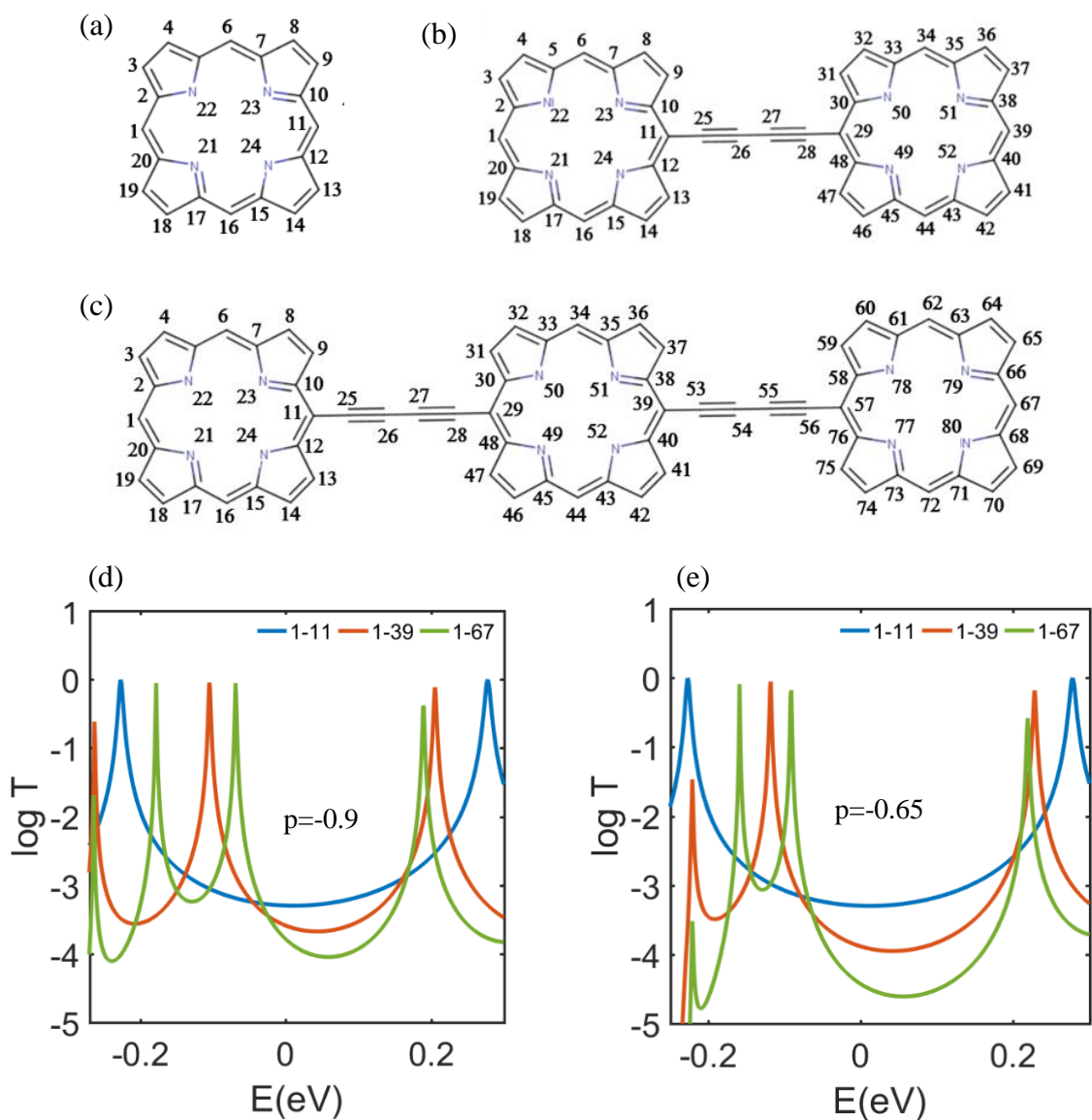


Figure 4.3.8: (a), (b) and (c) are the schematic of Non-Fused porphyrin monomer, dimer and trimer molecular structure. (d), (e) are the transmission curves for the non-fused porphyrin calculated by TBM in case of the oligoyne bond between two or three Monomer (p) are (-0.9) and (-0.65) respectively.

The fact that fused porphyrin ribbons are narrow-gap semiconductors means that for a finite oligomer, when electrons tunnel through the gap there will be contributions to the transmission coefficient from both the HOMO and the LUMO bands. As described in

the next section, the qualitative features of Figure 4.3.5(a) and Figure 4.3.1(d) can be obtained by summing these two contributions.

4.3.1. A simple model based on coupling the frontier orbitals of a chain of monomers

Here I note that the qualitative features of the figure 4.3.1(d) can be reproduced by a simple tight binding model of independent transport through the HOMOs and LUMOs. Let $T(E, n, -\gamma_L, \varepsilon_L)$ be the transmission coefficient for a chain of n monomer LUMOs, with energies ε_L and coupled by nearest neighbour matrix elements $-\gamma_L$. Similarly let $T(E, n, +\gamma_H, \varepsilon_H)$ be the transmission coefficient of an independent chain of monomer HOMOs, with energies ε_H and coupled by nearest neighbour matrix elements $+\gamma_H$. Note that from figure 4.3.5 (b), since the splitting of the LUMO resonances is greater than that of the HOMO resonances, $\gamma_L > \gamma_H$.

Then if we assume no interference between the HOMO and LUMO, the total transmission coefficient is

$$T(E, n) = T(E, n, -\gamma_L, \varepsilon_L) + T(E, n, +\gamma_H, \varepsilon_H) \quad (4.3.1)$$

Without loss of generality, we choose $\varepsilon_H = -\varepsilon_L$, which fixes the energy origin. As shown in figure 4.3.10, with an appropriate choice of parameters, this simple model captures the qualitative features of figure 4.3.1(d) and the tight-binding results of figure 4.3.5(a).

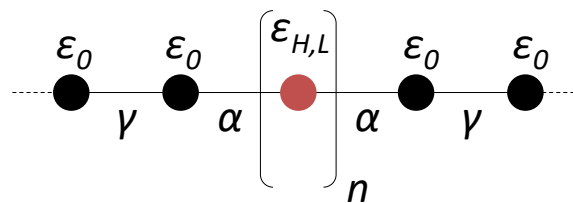


Figure 4.3.9. A tight binding (Hückel) model of 1, 2 or 3 site scattering regions (depicted in red), coupled to one-dimensional leads. The scattering region represents either a chain of coupled monomer LUMOs or a chain of coupled monomer HOMOs. After calculating their separate transmission coefficients, they are simply added to give the total transmission coefficient.

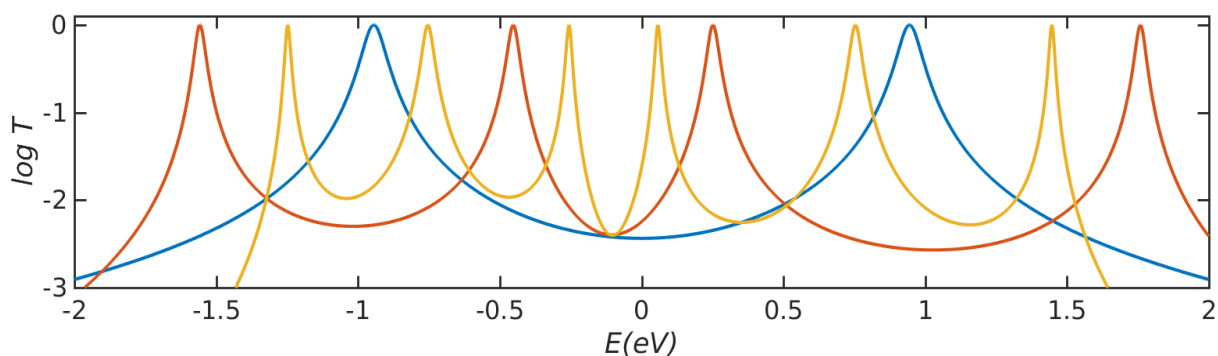


Figure 4.3.10. Sum of transmission coefficient $T(E, n) = T(E, n, -\gamma_L, \epsilon_L) + T(E, n, +\gamma_H, \epsilon_H)$ through independent HOMO and LUMO levels for a monomer $n=1$, dimer $n=2$ and trimer $n=3$. For the monomer, $\epsilon_L = 0.935$; for the dimer, $\epsilon_L = 1.0$, $\gamma_L = 0.75$, $\gamma_H = 0.55$ and for the trimer, $\epsilon_L = 0.75$, $\gamma_L = 0.5$, $\gamma_H = 0.35$. In these plots, the coupling between the molecule and the one-dimensional leads is $\alpha = -0.1$ and the leads are represented by a chain of sites with site energies $\epsilon_0 = 0$ and nearest neighbour couplings $\gamma = -1$.

The tight-binding results of figure 4.3.5 and the DFT results with a non-specific anchor (figure 4.3.4(d)) suggest that a negative beta factor is a generic feature of the fused porphyrin core, provided the centres of the HOMO-LUMO gaps of the monomer, dimer

and trimer are coincident. However, whether or not it is measured experimentally depends on level shifts of molecular orbitals after attaching to the electrodes. This is illustrated by the calculations shown in figure 4.3.11 using direct C-Au covalent anchoring to gold electrodes, where the HOMOs of the monomer, dimer and trimer coincide and therefore the centres of their HOMO-LUMO gaps are not coincident. This spoils the generic trend and leads to a positive beta factor.

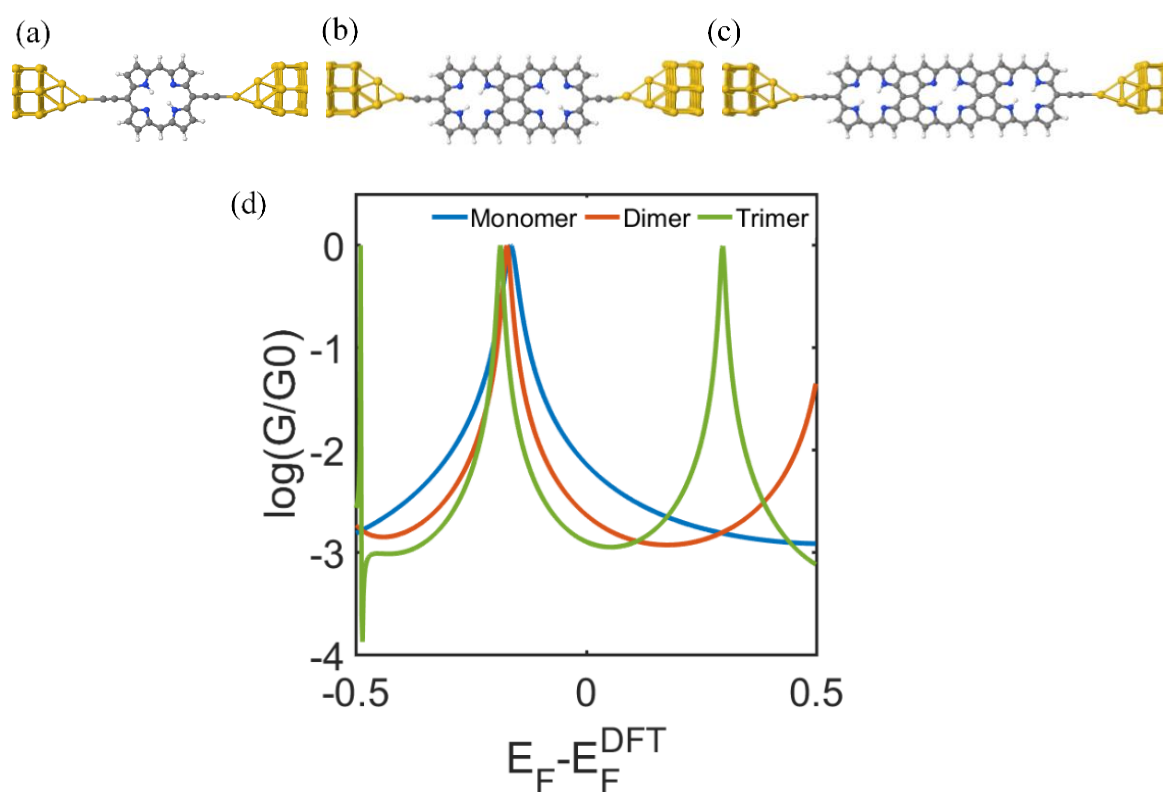


Figure 4.3.11. Transmission coefficient obtained from DFT Hamiltonian for three types of porphyrin connected to gold electrodes through a direct Au-C bond.

It is worth to mention that the magnitude of the electrical conductance is generally higher in the junctions formed by covalent bond to the graphene electrodes (Figure 4.3.1(d)) compared to junctions formed by gold electrodes (Figures 4.3.3(d) and 4.3.11 (d)). However, the predicted conductance for the gold junctions with the thiol and direct Au-C anchoring are similar. Depending on the choice of Fermi energy, one might be

higher than another as shown in figure 4.3.12 (a), (b) and (c) for thiol and direct Au–C anchoring for Monomer, Dimer and trimer respectively.

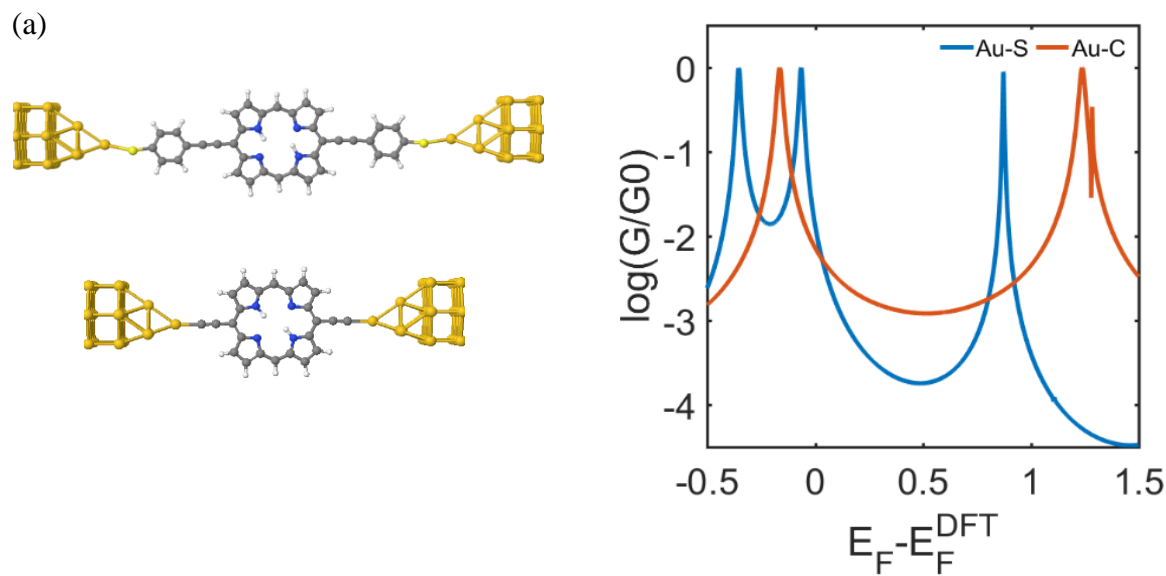


Figure 4.3.12 (a): Transmission coefficient obtained from DFT Hamiltonian for monomer porphyrin with thiol and direct Au–C anchors.

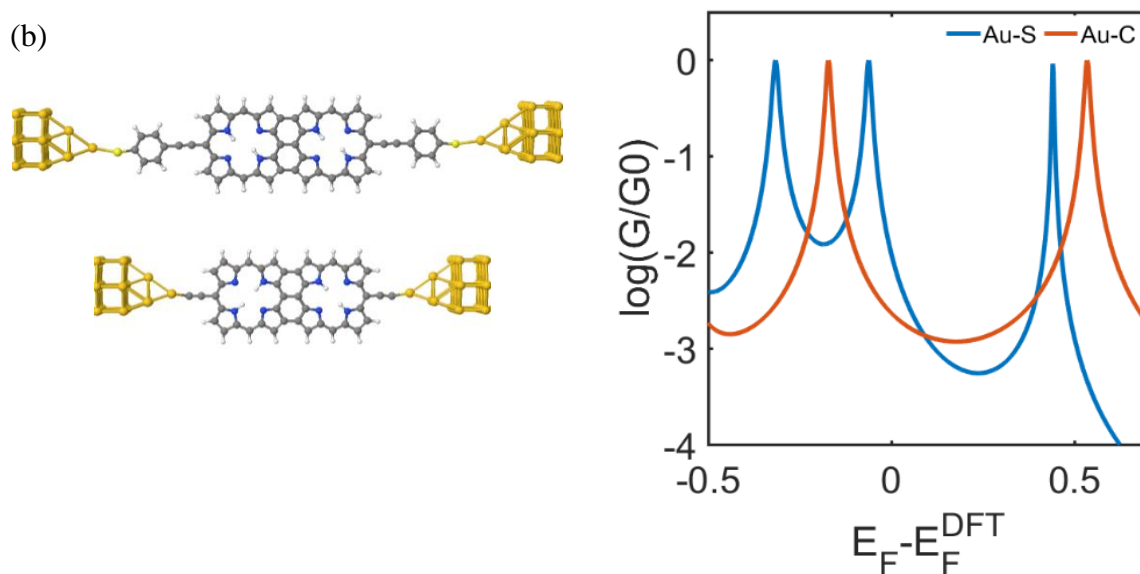


Figure 4.3.12 (b): Transmission coefficient obtained from DFT Hamiltonian for Dimer fused porphyrin with thiol and direct Au–C anchors.

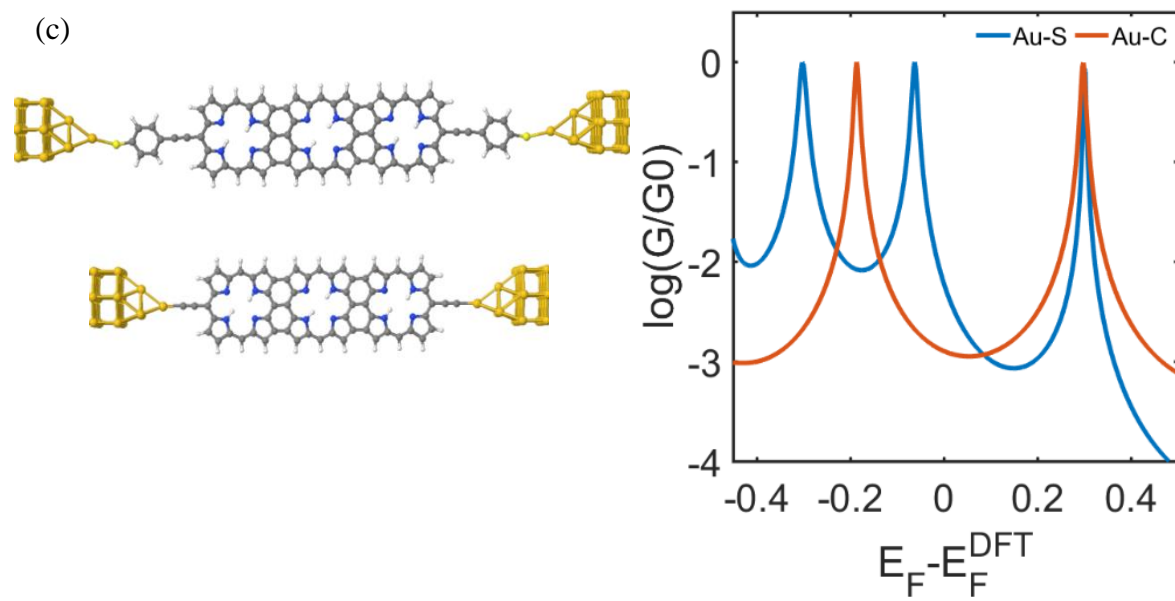


Figure 4.3.12 (c): Transmission coefficient obtained from DFT Hamiltonian for Trimer fused porphyrin with thiol and direct Au-C anchors.

Bibliography

- (1) Sadeghi, H.; Sangtarash, S.; Lambert, C. J. Robust Molecular Anchoring to Graphene Electrodes. *Nano Lett.* **2017**, *17* (8), 4611–4618.
- (2) Sedghi, G.; Sawada, K.; Esdaile, L. J.; Hoffmann, M.; Anderson, H. L.; Bethell, D.; Haiss, W.; Higgins, S. J.; Nichols, R. J. Single Molecule Conductance of Porphyrin Wires with Ultralow Attenuation. *J. Am. Chem. Soc.* **2008**, *130* (27), 8582–8583.
- (3) Fan, F. R. F.; Yang, J.; Cai, L.; Price, D. W.; Dirk, S. M.; Kosynkin, D. V.; Yao, Y.; Rawlett, A. M.; Tour, J. M.; Bard, A. J. Charge Transport through Self-Assembled Monolayers of Compounds of Interest in Molecular Electronics. *J. Am. Chem. Soc.* **2002**, *124* (19), 5550–5560.
- (4) Bergren, A. J.; McCreery, R. L.; Stoyanov, S. R.; Gusarov, S.; Kovalenko, A. Electronic Characteristics and Charge Transport Mechanisms for Large Area Aromatic Molecular Junctions. *J. Phys. Chem. C* **2010**, *114* (37), 15806–15815.
- (5) Ferreira, Q.; Bragança, A. M.; Alcácer, L.; Morgado, J. Conductance of Well-Defined Porphyrin Self-Assembled Molecular Wires up to 14 Nm in Length. *J. Phys. Chem. C* **2014**, *118* (13), 7229–7234.
- (6) Ashwell, G. J.; Urasinska, B.; Wang, C.; Bryce, M. R.; Grace, I.; Lambert, C. J. Single-Molecule Electrical Studies on a 7 Nm Long Molecular Wire. *Chem. Commun. (Camb)*. **2006**, No. 45, 4706–4708.
- (7) Sadeghi, H. Theory of Electron and Phonon Transport in Nano and Molecular Quantum Devices: Design Strategies for Molecular Electronics and Thermoelectricity. *arXiv Prepr. arXiv1607.02484* **2016**.
- (8) Sangtarash, S.; Vezzoli, A.; Sadeghi, H.; Ferri, N.; Brien, H. M. O. Gateway State-Mediated, Long-Range Tunnelling in Molecular Wires. 1 , 2. *Nanoscale*

2018, *10*, 3060–3067.

- (9) Kaliginedi, V.; Moreno-García, P.; Valkenier, H.; Hong, W.; García-Suárez, V. M.; Buitter, P.; Otten, J. L. H. H.; Hummelen, J. C.; Lambert, C. J.; Wandlowski, T. Correlations between Molecular Structure and Single-Junction Conductance: A Case Study with Oligo(Phenylene-Ethynylene)-Type Wires. *J. Am. Chem. Soc.* **2012**, *134* (11), 5262–5275.
- (10) Zhao, X.; Huang, C.; Gulcur, M.; Batsanov, A. S.; Baghernejad, M.; Hong, W.; Bryce, M. R.; Wandlowski, T. Oligo(Aryleneethynylene)s with Terminal Pyridyl Groups: Synthesis and Length Dependence of the Tunneling-to-Hopping Transition of Single-Molecule Conductances. *Chem. Mater.* **2013**, *25* (21), 4340–4347.
- (11) Moreno-García, P.; Gulcur, M.; Manrique, D. Z.; Pope, T.; Hong, W.; Kaliginedi, V.; Huang, C.; Batsanov, A. S.; Bryce, M. R.; Lambert, C.; et al. Single-Molecule Conductance of Functionalized Oligoynes: Length Dependence and Junction Evolution. *J. Am. Chem. Soc.* **2013**, *135* (33), 12228–12240.
- (12) Kim, B.; Beebe, J. M.; Jun, Y.; Zhu, X. Y.; Frisbie, G. D. Correlation between HOMO Alignment and Contact Resistance in Molecular Junctions: Aromatic Thiols versus Aromatic Isocyanides. *J. Am. Chem. Soc.* **2006**, *128* (15), 4970–4971.
- (13) Sadeghi, H.; Sangtarash, S.; Lambert, C. J. Oligoyne Molecular Junctions for Efficient Room Temperature Thermoelectric Power Generation. *Nano Lett.* **2015**, *15* (11), 7467–7472.
- (14) Liu, H.; Wang, N.; Zhao, J.; Guo, Y.; Yin, X.; Boey, F. Y. C.; Zhang, H. Length-Dependent Conductance of Molecular Wires and Contact Resistance in Metal-Molecule-Metal Junctions. *ChemPhysChem* **2008**, *9* (10), 1416–1424.

- (15) Li, Z.; Park, T. H.; Rawson, J.; Therien, M. J.; Borguet, E. Quasi-Ohmic Single Molecule Charge Transport through Highly Conjugated Meso-to-Meso Ethyne-Bridged Porphyrin Wires. *Nano Lett.* **2012**, *12* (6), 2722–2727.
- (16) Li, Z.; Borguet, E. Determining Charge Transport Pathways through Single Porphyrin Molecules Using Scanning Tunneling Microscopy Break Junctions. *J. Am. Chem. Soc.* **2012**, *134* (1), 63–66.
- (17) Mol, J. A.; Lau, C. S.; Lewis, W. J. M.; Sadeghi, H.; Roche, C.; Cnossen, A.; Warner, J. H.; Lambert, C. J.; Anderson, H. L.; Briggs, G. A. D. Graphene-Porphyrin Single-Molecule Transistors. *Nanoscale* **2015**, *7* (31), 13181–13185.
- (18) Winters, M. U.; Dahlstedt, E.; Blades, H. E.; Wilson, C. J.; Frampton, M. J.; Anderson, H. L.; Albinsson, B. Probing the Efficiency of Electron Transfer through Porphyrin-Based Molecular Wires. *J. Am. Chem. Soc.* **2007**, *129* (14), 4291–4297.
- (19) Grozema, F. C.; Houarner-Rassin, C.; Prins, P.; Siebbeles, L. D. A.; Anderson, H. L. Supramolecular Control of Charge Transport in Molecular Wires. *J. Am. Chem. Soc.* **2007**, *129* (44), 13370–13371.
- (20) Li, Z.; Smeu, M.; Ratner, M. A.; Borguet, E. Effect of Anchoring Groups on Single Molecule Charge Transport through Porphyrins. *J. Phys. Chem. C* **2013**, *117* (29), 14890–14898.
- (21) Sedghi, G.; García-Suárez, V. M.; Esdaile, L. J.; Anderson, H. L.; Lambert, C. J.; Martín, S.; Bethell, D.; Higgins, S. J.; Elliott, M.; Bennett, N.; et al. Long-Range Electron Tunnelling in Oligo-Porphyrin Molecular Wires. *Nat. Nanotechnol.* **2011**, *6* (8), 517–523.
- (22) Sedghi, G.; Esdaile, L. J.; Anderson, H. L.; Martin, S.; Bethell, D.; Higgins, S. J.; Nichols, R. J. Comparison of the Conductance of Three Types of Porphyrin-

- Based Molecular Wires: ??,Meso,??-Fused Tapes, Meso-Butadiyne-Linked and Twisted Meso-Meso Linked Oligomers. *Adv. Mater.* **2012**, *24* (5), 653–657.
- (23) Nitzan, A. Electron Transmission through Molecules and Molecular Interfaces. *Annu. Rev. Phys. Chem.* **2001**, *52* (1), 681–750.
- (24) Xu, B. Q.; Li, X. L.; Xiao, X. Y.; Sakaguchi, H.; Tao, N. J. Electromechanical and Conductance Switching Properties of Single Oligothiophene Molecules. *Nano Lett.* **2005**, *5* (7), 1491–1495.
- (25) Capozzi, B.; Dell, E. J.; Berkelbach, T. C.; Reichman, D. R.; Venkataraman, L.; Campos, L. M. Length-Dependent Conductance of Oligothiophenes. *J. Am. Chem. Soc.* **2014**, *136* (29), 10486–10492.
- (26) Xiang, L.; Hines, T.; Palma, J. L.; Lu, X.; Mujica, V.; Ratner, M. A.; Zhou, G.; Tao, N. Non-Exponential Length Dependence of Conductance in Iodide-Terminated Oligothiophene Single-Molecule Tunneling Junctions. *J. Am. Chem. Soc.* **2016**, *138* (2), 679–687.
- (27) Perrin, M. L.; Verzijl, C. J. O.; Martin, C. a.; Shaikh, A. J.; Eelkema, R.; Esch, J. H. Van; van Ruitenbeek, J. M.; Thijssen, J. M.; van der Zant, H. S. J.; Dulić, D.; et al. Large Tunable Image-Charge Effects in Single-Molecule Junctions. *Nat. Nanotechnol.* **2013**, *8* (4), 282–287.
- (28) Perrin, M. L.; Martin, C. A.; Prins, F.; Shaikh, A. J.; Eelkema, R.; van Esch, J. H.; van Ruitenbeek, J. M.; van der Zant, H. S. J.; Dulić, D. Charge Transport in a Zinc-Porphyrin Single-Molecule Junction. *Beilstein J. Nanotechnol.* **2011**, *2* (1), 714–719.
- (29) Sadeghi, H.; Mol, J. a; Lau, C. S.; Briggs, G. A. D.; Warner, J.; Lambert, C. J. Conductance Enlargement in Picoscale Electroburnt Graphene Nanojunctions. *Proc. Natl. Acad. Sci. USA* **2015**, *112* (9), 2658–2663.

- (30) Sadeghi, H.; Sangtarash, S.; Lambert, C. J. Electron and Heat Transport in Porphyrin-Based Singlemolecule Transistors with Electro-Burnt Graphene Electrodes. *Beilstein J. Nanotechnol.* **2015**, *6* (1), 1413–1420.
- (31) Choi, S. H.; Kim, B.; Frisbie, C. D. *Science* 2008, *320* (5882), 1482–1486.
- (32) Leary, E.; Limburg, B.; Alanazy, A.; Sangtarash, S.; Grace, I.; Swada, K.; Esdaile, L. J.; Noori, M.; Gonzalez, M. T.; Rubio-Bollinger, G.; et al. Bias-Driven Conductance Increase with Length in Porphyrin Tapes. *J. Am. Chem. Soc.* **2018**, *140* (40), 12877–12883.

Chapter 5

Quantum Interference Tuning in Single Molecular Junctions.

In this chapter I present the effect at different positions of pendant methoxyl groups (-OMe)) that enable the tuning of destructive quantum interference (DQI) features in meta-phenylene ethylene-type oligomers (m-OPE).

The results presented in this chapter were submitted to Chemical Science. This work is a collaboration work between (Lancaster University, Xiamen University, University of Western Australia and Durham University).

5.1. Introduction

The construction and electrical characterization of single-molecule junctions has underpinned rapid developments in the field of molecular electronics. The theoretical treatments and computational methods have given insight into the fundamentals of transmission of charge through single molecules. Recent developments include novel molecular wires,¹⁻³ molecular switches,^{4,5} molecular diodes⁶⁻⁸, molecular field-effect transistors⁹⁻¹⁰, and bio-molecule recognition^{11,12}. One of the most interesting aspects of single-molecular electronics is the phenomena of room-temperature quantum interference (QI), which has attracted increasing attention due to its potential for tuning charge transport through molecules¹³⁻¹⁷. QI affects electron transport, because when a molecule is bonded to the electrodes, the de Broglie waves of electrons passing through the molecule from one side to the other side, causes complicated interference patterns within the molecule¹⁸⁻²⁰. Consequently, strategies for controlling the QI-induced interference pattern may provide mechanisms for changing the conductance of a single molecule without changing molecular backbone structure. Based on the concept and principles of QI, constructive QI (CQI) occurs when the interference pattern has a large amplitude at both the source and drain electrodes, causing high conductance, whereas destructive QI (DQI) occurs when the amplitude is small at one of the electrodes causing extremely low conductance.^{21,22}

Recently a number of studies have contributed to the development of tuning mechanisms of single-molecule electronic junction, including the impact of anchoring groups,^{23,24} the position of heteroatoms^{25,26} and the effect of molecular backbone²⁷. Although much of research has been devoted to the investigation of QI patterns,^{28,29} few papers have reported the effect of controlling these patterns by varying the locations of additional substituent pendant groups. Consequently, the aim of this study

is to investigate whether or not the introduction of pendant groups could provide a new strategy for tuning QI.

5.2. Molecular Structures

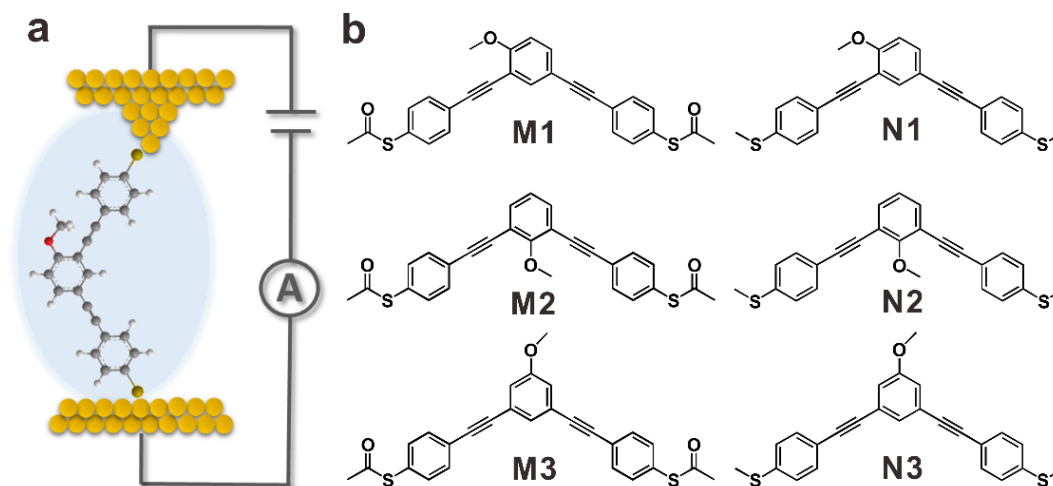


Figure 5.2.1. (a) Diagram of STM-BJ setup and (b) chemical structures of the investigated molecules.

5.3. Results and Discussion

In this study, single-molecule charge transport in a series of meta-phenylene ethylene-type oligomer (m-OPE) molecules, which were modified by a pendant methoxyl group (-OMe) placed at different positions is investigated. (As shown in Figure 5.2.1(b)). The three molecules **M1**, **M2**, **M3** have the same molecular backbone structure with the same anchor groups. The only difference between these molecules is the substitutional position of the pendant -OMe. The influence of anchor groups was also taken into consideration by utilizing either sulphur acetyl (-SAc) anchor groups (**M1**, **M2**, **M3**) or the methyl sulfide (SMe) anchor groups (**N1**, **N2**, **N3**) to further confirm that the ability

to tune QI by varying the position of the pendant-OMe is independent of the anchor group.

The above choice of molecules is informed by magic ratio theory³⁰⁻³², which describes QI in the central ring and views the moieties to the left and right as “compound electrodes,” which inject and collect electrons via triple bonds into pi orbitals labelled i and j respectively, as shown in Figure 5.3.1.

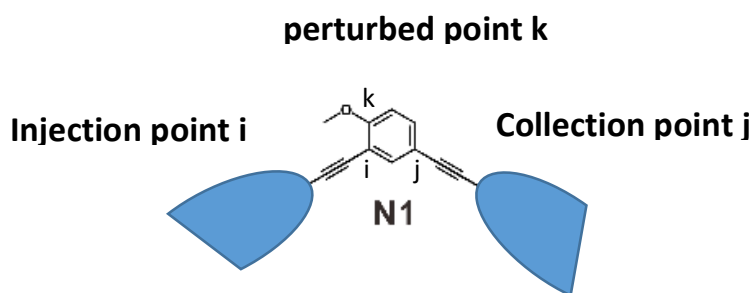


Figure 5.3.1. A conceptual view of eg. molecule N1. The blue regions represent compound electrodes, which inject and collect electrons via triple bonds into pi orbitals labelled i and j respectively. The perturbation is on site k .

Since i and j are in meta positions relative to each other, then in the absence of the pendant group, the bare ‘parent’ molecule will exhibit DQI. If a perturbation such as a pendant group is imposed on pi orbital k , to yield a ‘daughter’ molecule such as those shown in figure 5.2.1, then magic ratio theory predicts the following:

1. If, as in M3 and N3, k is meta to both i and j , then the pendant group will have only a small effect on conductance.
2. If, as in M1 and N1, k is ortho to i and para to j , then the pendant group will affect the conductance by shifting the DQI feature to a higher or lower energy.
3. If, as in M2 and N2, k is ortho to both i and j , then the pendant group will affect the conductance by shifting the DQI feature in an opposite direction to case 2.

This behavior is confirmed by density functional theory (DFT) calculations presented below and the MCBJ measurements carried out in Xiamen University. The experimental measurement shows the molecular conductance peaks were observed at $10^{-5.64\pm 0.37} G_0$, $10^{-4.95\pm 0.51} G_0$ and $10^{-5.36\pm 0.39} G_0$ for **M1-3**, and $10^{-5.70\pm 0.22} G_0$, $10^{-5.01\pm 0.37} G_0$ and $10^{-5.36\pm 0.47} G_0$ for **N1-3**, respectively as shown in figure (5.3.2).

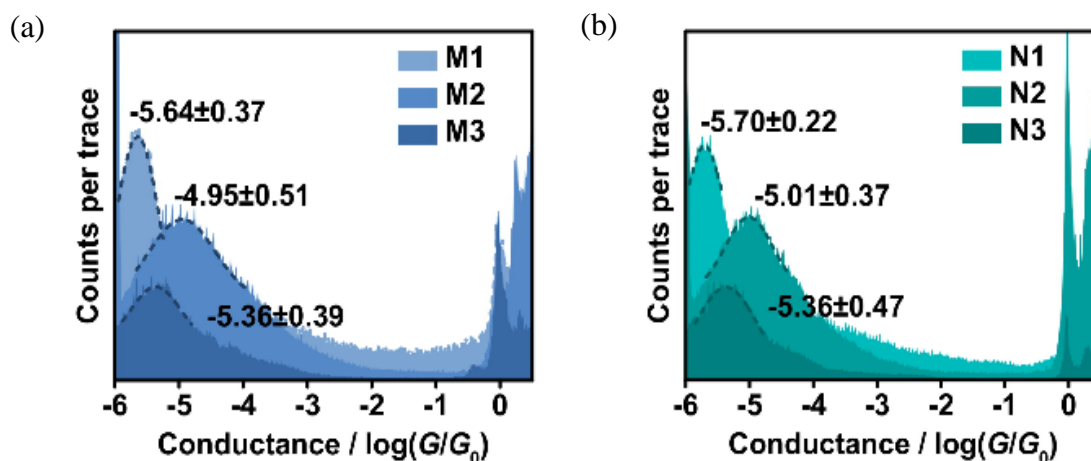


Figure 5.3.2. Typical individual conductance-distance for (a) sulphur acetyl (-SAc) anchor groups (**M1**, **M2**, **M3**) and (b) the methyl sulfide (-SMe) anchor groups (**N1**, **N2**, **N3**).

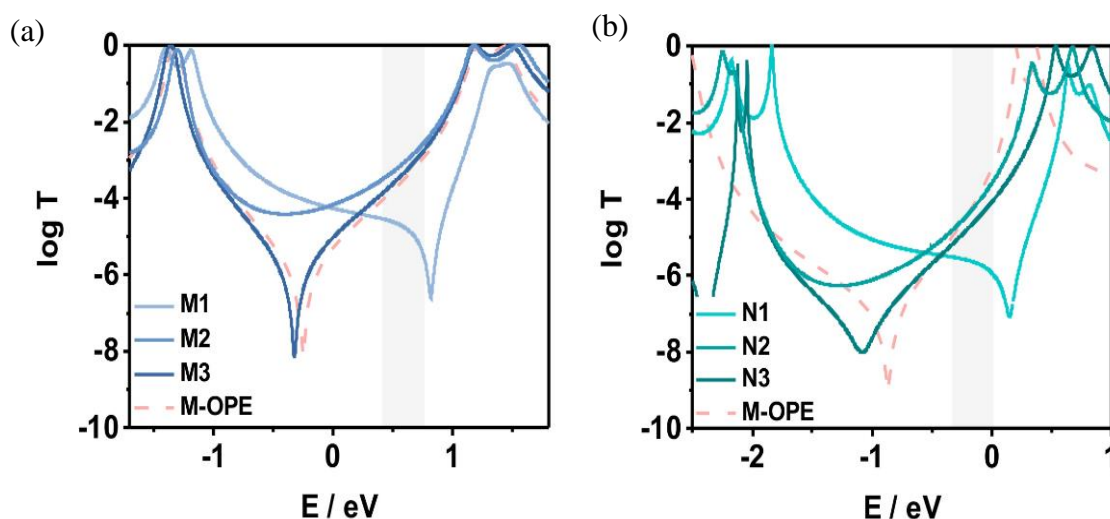


Figure 5.3.3. Transmission coefficients of (a) molecules **M1-M3** and (b) **N1-N3** compared with the parent meta OPE (which contains no pendant group).

To demonstrate how pendant groups, control QI within this series of molecules, I used DFT to optimize geometry and ground state Hamiltonian with overlap matrix elements of each structure combined with the quantum transport code Gollum to compute the transmission coefficient of the systems. SIESTA employs pseudo-potentials to account for the core electrons and linear combinations of atomic orbitals to construct the valence states. The generalized gradient approximation (GGA) of the exchange and correlation functional is used with the parameterization (PBE), a double- ζ polarized (DZP) basis set and a real-space grid defined with an equivalent energy cut-off of 150 Ry. The geometry optimization for each structure is performed to the forces is 20 meV/Ang.

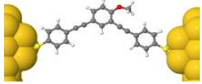
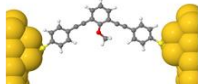
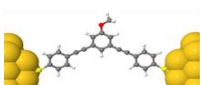
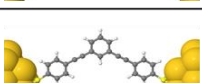
Second column of Table 5.3.1 (a) and (b) shows geometry-optimized structures used to obtain the DFT transmission coefficient of the systems illustrated in figure 5.3.3 (a) and (b) respectively. In agreement with magic ratio theory, Figure 5.3.3 (a) and (b) shows that the transmission dips of M3 and N3, (which are the signatures of DQI) are close to the transmission dips of their parents (shown as pink dashed curves) and therefore as expected, the pendant group has only a small effect on conductance. In contrast, the transmission dips of M1 and N1, are shifted to higher energies relative to the parental DQI dip, as expected. Furthermore, the transmission dips of M2 and N2, are shifted to much lower energies and no longer appear within the HOMO-LUMO gap.

The presence or otherwise of DQI transmission dips is also consistent with a recently highlighted orbital product rule, which states that if the HOMO amplitudes at the ends of a molecule have the same sign (opposite signs) then the HOMO is assigned an “orbital product” a_H , which is positive (negative). Similarly, if the LUMO amplitudes at the ends of a molecule have the same sign (opposite signs) then the LUMO is assigned an orbital product a_L , which is positive (negative). Finally if the a_H and a_L possess the

same sign (ie if $a_{H.AL}$ is positive) then the transmission function will possess a DQI dip, otherwise CQI occurs and there will be no dip. Example of HOMOs and LUMOs are shown in Table 5.3.2, which demonstrates that the presence or otherwise of DQI features indeed follow this product rule. Further examples are shown in tables 5.3.3 and 5.3.4. Tables (5.3.1) (a) and (b) shows relaxed structures of these molecules and calculated molecular length using DFT for thiol and SMe anchor group respectively.

Table 5.3.1. The geometry-optimized structures used to obtain the DFT results for (a) molecules M1-M3 and (b) N1-N3 with calculate the molecule with the junction distances.

(a)

Name	structure	Calculated Length	
		Au-Au (nm)	S-S (nm)
M1		2.205	1.79
M2		2.172	1.759
M3		2.181	1.768
M-OPE		2.178	1.757

(b)


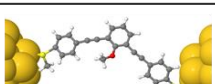
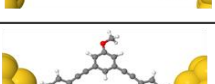
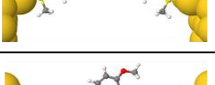
Name	structure	Calculated Length	
		Au-Au (nm)	S-S (nm)
N1		2.15	1.629
N2		2.199	1.767
N3		2.126	1.598
M-OPE		2.154	1.832

Table 5.3.2: HOMO and LUMOs of molecules N1-N3 and M-OPE. Blue regions are positive and red regions are negative. As an example, for N1 the HOMO at the left end of the molecule is positive (+) and at the right end it is negative (-). Therefore, since these have opposite signs, a_H is negative (-). Similarly, for N1, a_L is negative. Since the product of $a_H \cdot a_L$ is positive (+), N1 will exhibit DQI.

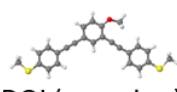
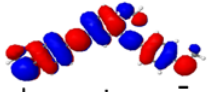
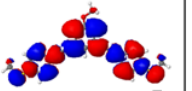
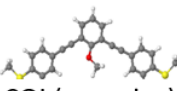
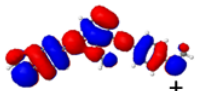
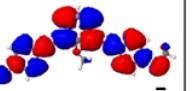
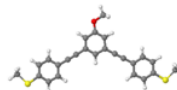
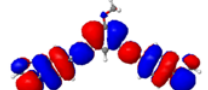
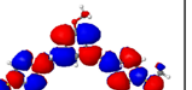
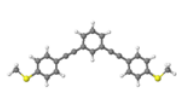
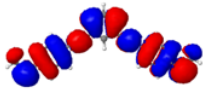
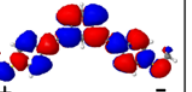
	Structure	HOMO	LUMO
N1	 DQI ($a_H \cdot a_L$ is +)	 + a_H is - -	 + a_L is - -
N2	 CQI ($a_H \cdot a_L$ is -)	 + a_H is + +	 + a_L is - -
N3	 DQI ($a_H \cdot a_L$ is +)	 - a_H is - +	 + a_L is - -
M-OPE	 DQI ($a_H \cdot a_L$ is +)	 + a_H is - -	 + a_L is - -

Table 5.3.3: The Molecular orbitals of the molecules with SMe anchor.

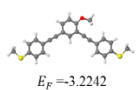
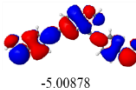
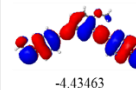
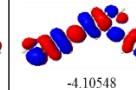
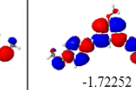
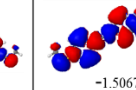
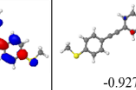
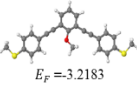
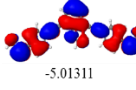
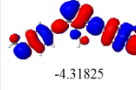
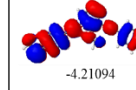
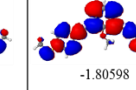
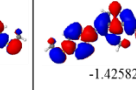
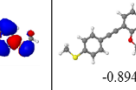
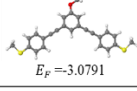
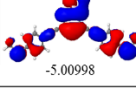
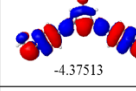
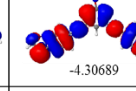
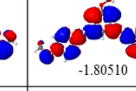
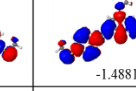
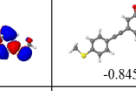
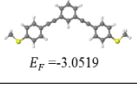
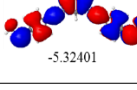
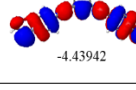
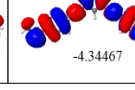
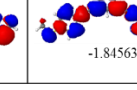
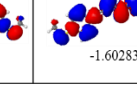
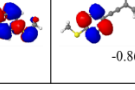
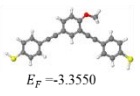
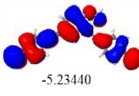
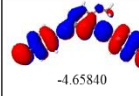
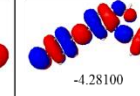
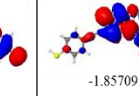
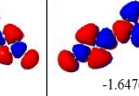
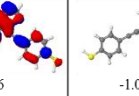
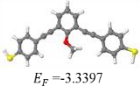
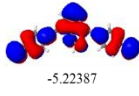
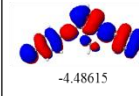
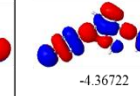
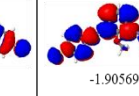
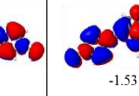
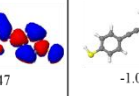
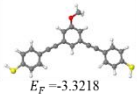
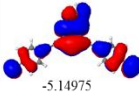
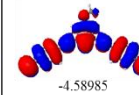
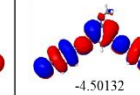
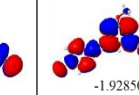
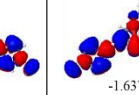
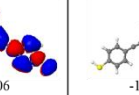
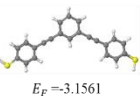
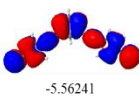
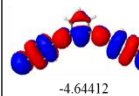
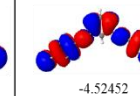
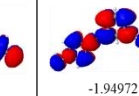
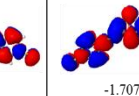
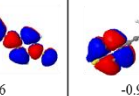
	Structure	HOMO-2	HOMO-1	HOMO	LUMO	LUMO+1	LUMO+2
N1	 $E_F = -3.2242$	 -5.00878	 -4.43463	 -4.10548	 -1.72252	 -1.50678	 -0.92720
N2	 $E_F = -3.2183$	 -5.01311	 -4.31825	 -4.21094	 -1.80598	 -1.42582	 -0.89469
N3	 $E_F = -3.0791$	 -5.00998	 -4.37513	 -4.30689	 -1.80510	 -1.48815	 -0.84549
M-OPE	 $E_F = -3.0519$	 -5.32401	 -4.43942	 -4.34467	 -1.84563	 -1.60283	 -0.86211

Table 5.3.4: The Molecular orbitals of the molecules with thiol anchor

	Structure	HOMO-2	HOMO-1	HOMO	LUMO	LUMO+1	LUMO+2
M1	 $E_F = -3.3550$	 -5.23440	 -4.65840	 -4.28100	 -1.85709	 -1.64766	 -1.08515
M2	 $E_F = -3.3397$	 -5.22387	 -4.48615	 -4.36722	 -1.90569	 -1.53147	 -1.00977
M3	 $E_F = -3.3218$	 -5.14975	 -4.58985	 -4.50132	 -1.92850	 -1.63706	 -1.00300
M-OPE	 $E_F = -3.1561$	 -5.56241	 -4.64412	 -4.52452	 -1.94972	 -1.70796	 -0.98211

Since the electrical conductance G (in units of the conductance quantum) is approximately $T(E_F)$, where E_F is the Fermi energy of the electrodes, a comparison with experiment requires knowledge of E_F . In Figure 5.3.3, the energy E is plotted relative to the DFT-predicted value of E_F , which is close to the LUMO (HOMO) resonance for –SMe-anchored (-S-anchored) molecules. Figure 5.3.3 shows that for a wide range of Fermi energies within the HOMO-LUMO gaps, the conductances are predicted to follow the trend **M2>M3** and **N2>N3**, in agreement with experimental results. The predicted conductance values of **M1** and **N1** are more sensitive to precise value of E_F , which is sensitive to unknowns such as the shape of the electrode tip and is not necessarily predict accurately by DFT. The experimental measurement tends of **M3>M1** and **N3>N1** suggest that the Fermi energies lie in the vicinity of the grey regions marked in Figure 5.3.3.

Bibliography

- (1) Algethami, N.; Sadeghi, H.; Sangtarash, S.; Lambert, C. J. The Conductance of Porphyrin-Based Molecular Nanowires Increases with Length. *Nano Lett.* **2018**.
- (2) Sedghi, G. G. Sedghi, VM Garcia-Suarez, LJ Esdaile, HL Anderson, CJ Lambert, S. Martin, D. Bethell, SJ Higgins, M. Elliott, N. Bennett et Al., Nat. Nanotechnol. 6, 517 (2011). *Nat. Nanotechnol.* **2011**, 6, 517.
- (3) Gunasekaran, S.; Hernangómez-Pérez, D.; Davydenko, I.; Marder, S. R.; Evers, F.; Venkataraman, L. Near Length-Independent Conductance in Polymethine Molecular Wires. *Nano Lett.* **2018**.
- (4) Jia, C.; Migliore, A.; Xin, N.; Huang, S.; Wang, J.; Yang, Q.; Wang, S.; Chen, H.; Wang, D.; Feng, B.; et al. Covalently Bonded Single-Molecule Junctions with Stable and Reversible Photoswitched Conductivity. *Science* (80-.). **2016**, 352 (6292), 1443–1445.
- (5) Alqahtani, J.; Sadeghi, H.; Sangtarash, S.; Lambert, C. J. Breakdown of Curly Arrow Rules in Anthraquinone. *Angew. Chemie* **2018**.
- (6) Chen, X.; Roemer, M.; Yuan, L.; Du, W.; Thompson, D.; del Barco, E.; Nijhuis, C. A. Molecular Diodes with Rectification Ratios Exceeding 10^5 Driven by Electrostatic Interactions. *Nat. Nanotechnol.* **2017**, 12 (8), 797.
- (7) Nerngchamnong, N.; Yuan, L.; Qi, D.-C.; Li, J.; Thompson, D.; Nijhuis, C. A. The Role of van Der Waals Forces in the Performance of Molecular Diodes. *Nat. Nanotechnol.* **2013**, 8 (2), 113.
- (8) Vezzoli, A.; Brooke, R. J.; Higgins, S. J.; Schwarzacher, W.; Nichols, R. J. Single-Molecule Photocurrent at a Metal--Molecule--Semiconductor Junction.

Nano Lett. **2017**, *17* (11), 6702–6707.

- (9) Cho, K.; Pak, J.; Kim, J.-K.; Kang, K.; Kim, T.-Y.; Shin, J.; Choi, B. Y.; Chung, S.; Lee, T. Field-Effect Transistors: Contact-Engineered Electrical Properties of MoS₂ Field-Effect Transistors via Selectively Deposited Thiol-Molecules (Adv. Mater. 18/2018). *Adv. Mater.* **2018**, *30* (18), 1870129.
- (10) Jia, C.; Famili, M.; Carlotti, M.; Liu, Y.; Wang, P.; Grace, I. M.; Feng, Z.; Wang, Y.; Zhao, Z.; Ding, M.; et al. Quantum Interference Mediated Vertical Molecular Tunneling Transistors. *Sci. Adv.* **2018**, *4* (10), eaat8237.
- (11) Im, J.; Biswas, S.; Liu, H.; Zhao, Y.; Sen, S.; Biswas, S.; Ashcroft, B.; Borges, C.; Wang, X.; Lindsay, S.; et al. Electronic Single-Molecule Identification of Carbohydrate Isomers by Recognition Tunnelling. *Nat. Commun.* **2016**, *7*, 13868.
- (12) Zhao, Y.; Ashcroft, B.; Zhang, P.; Liu, H.; Sen, S.; Song, W.; Im, J.; Gyarfas, B.; Manna, S.; Biswas, S.; et al. Single-Molecule Spectroscopy of Amino Acids and Peptides by Recognition Tunnelling. *Nat. Nanotechnol.* **2014**, *9* (6), 466.
- (13) Garner, M. H.; Li, H.; Chen, Y.; Su, T. A.; Shangguan, Z.; Paley, D. W.; Liu, T.; Ng, F.; Li, H.; Xiao, S.; et al. Comprehensive Suppression of Single-Molecule Conductance Using Destructive σ -Interference. *Nature* **2018**, *1*.
- (14) Cardamone, D. M.; Stafford, C. A.; Mazumdar, S. Controlling Quantum Transport through a Single Molecule. *Nano Lett.* **2006**, *6* (11), 2422–2426.
- (15) Frisenda, R.; Janssen, V. A. E. C.; Grozema, F. C.; van der Zant, H. S. J.; Renaud, N. Mechanically Controlled Quantum Interference in Individual π -Stacked Dimers. *Nat. Chem.* **2016**, *8* (12), 1099.

- (16) Guédon, C. M.; Valkenier, H.; Markussen, T.; Thygesen, K. S.; Hummelen, J. C.; Van Der Molen, S. J. Observation of Quantum Interference in Molecular Charge Transport. *Nat. Nanotechnol.* **2012**, *7* (5), 305.
- (17) Aradhya, S. V.; Meisner, J. S.; Krikorian, M.; Ahn, S.; Parameswaran, R.; Steigerwald, M. L.; Nuckolls, C.; Venkataraman, L. Dissecting Contact Mechanics from Quantum Interference in Single-Molecule Junctions of Stilbene Derivatives. *Nano Lett.* **2012**, *12* (3), 1643–1647.
- (18) Lambert, C. J. Basic Concepts of Quantum Interference and Electron Transport in Single-Molecule Electronics. *Chem. Soc. Rev.* **2015**, *44* (4), 875–888.
- (19) Su, T. A.; Neupane, M.; Steigerwald, M. L.; Venkataraman, L.; Nuckolls, C. Chemical Principles of Single-Molecule Electronics. *Nat. Rev. Mater.* **2016**, *1* (3), 16002.
- (20) Xiang, D.; Wang, X.; Jia, C.; Lee, T.; Guo, X. Molecular-Scale Electronics: From Concept to Function. *Chem. Rev.* **2016**, *116* (7), 4318–4440.
- (21) Borges, A.; Fung, E.-D.; Ng, F.; Venkataraman, L.; Solomon, G. C. Probing the Conductance of the σ -System of Bipyridine Using Destructive Interference. *J. Phys. Chem. Lett.* **2016**, *7* (23), 4825–4829.
- (22) Zhang, Y.; Ye, G.; Soni, S.; Qiu, X.; Krijger, T. L.; Jonkman, H. T.; Carlottti, M.; Sauter, E.; Zharnikov, M.; Chiechi, R. C. Controlling Destructive Quantum Interference in Tunneling Junctions Comprising Self-Assembled Monolayers via Bond Topology and Functional Groups. *Chem. Sci.* **2018**, *9* (19), 4414–4423.
- (23) Leary, E.; La Rosa, A.; González, M. T.; Rubio-Bollinger, G.; Agrat, N.; Martín, N. Incorporating Single Molecules into Electrical Circuits. The Role of

- the Chemical Anchoring Group. *Chem. Soc. Rev.* **2015**, *44* (4), 920–942.
- (24) Kiguchi, M.; Ohto, T.; Fujii, S.; Sugiyasu, K.; Nakajima, S.; Takeuchi, M.; Nakamura, H. Single Molecular Resistive Switch Obtained via Sliding Multiple Anchoring Points and Varying Effective Wire Length. *J. Am. Chem. Soc.* **2014**, *136* (20), 7327–7332.
- (25) Miguel, D.; de Cienfuegos, L.; Martín-Lasanta, A.; Morcillo, S. P.; Zotti, L. A.; Leary, E.; Burkle, M.; Asai, Y.; Jurado, R.; Cardenas, D. J.; et al. Toward Multiple Conductance Pathways with Heterocycle-Based Oligo (Phenyleneethynylene) Derivatives. *J. Am. Chem. Soc.* **2015**, *137* (43), 13818–13826.
- (26) Sangtarash, S.; Sadeghi, H.; Lambert, C. J. Connectivity-Driven Bi-Thermoelectricity in Heteroatom-Substituted Molecular Junctions. *Phys. Chem. Chem. Phys.* **2018**, *20* (14), 9630–9637.
- (27) Li, X.-F.; Qiu, Q.; Luo, Y. Tuning Electron Transport through a Single Molecular Junction by Bridge Modification. *J. Appl. Phys.* **2014**, *116* (1), 13701.
- (28) Xie, Z.; Baldea, I.; Oram, S.; Smith, C. E.; Frisbie, C. D. Effect of Heteroatom Substitution on Transport in Alkanedithiol-Based Molecular Tunnel Junctions: Evidence for Universal Behavior. *ACS Nano* **2016**, *11* (1), 569–578.
- (29) Danilov, A.; Kubatkin, S.; Kafanov, S.; Hedegård, P.; Stuhr-Hansen, N.; Moth-Poulsen, K.; Bjørnholm, T. Electronic Transport in Single Molecule Junctions: Control of the Molecule-Electrode Coupling through Intramolecular Tunneling Barriers. *Nano Lett.* **2008**, *8* (1), 1–5.
- (30) Liu, X.; Sangtarash, S.; Reber, D.; Zhang, D.; Sadeghi, H.; Shi, J.; Xiao, Z.-Y.;

Hong, W.; Lambert, C. J.; Liu, S.-X. Gating of Quantum Interference in Molecular Junctions by Heteroatom Substitution. *Angew. Chemie Int. Ed.* **2017**, *56* (1), 173–176.

- (31) Sangtarash, S.; Huang, C.; Sadeghi, H.; Sorohhov, G.; Hauser, J.; Wandlowski, T.; Hong, W.; Decurtins, S.; Liu, S.-X.; Lambert, C. J. Searching the Hearts of Graphene-like Molecules for Simplicity, Sensitivity, and Logic. *J. Am. Chem. Soc.* **2015**, *137* (35), 11425–11431.
- (32) Geng, Y.; Sangtarash, S.; Huang, C.; Sadeghi, H.; Fu, Y.; Hong, W.; Wandlowski, T.; Decurtins, S.; Lambert, C. J.; Liu, S.-X. Magic Ratios for Connectivity-Driven Electrical Conductance of Graphene-like Molecules. *J. Am. Chem. Soc.* **2015**, *137* (13), 4469–4476.

Chapter 6

Large amplitude, high-frequency single-molecule switch.

In this chapter, I demonstrate theoretically that 2-(methylthio)thiophene units not only act as contact groups but can reversibly switch between a monodentate configuration (MeS-only) and a bidentate configuration (MeS- and thienyl S) upon junction compression; as the junction is compressed the electrical conductance increases greatly with the increased molecule-contact interaction. This means that such molecules show a large-amplitude mechanical switching behaviour. Results are compared with recent experimental work carried out in the Chemistry department of the University of Liverpool.

6.1. Introduction

Changes of electrical conductance associated with the stretching or compression of a single-molecule junction sheds light on force-induced enhancement of molecular transport resonance,¹ electron transfer reactions,² spin transitions of an organometallic Fe(II) complex,³ stereoelectronic effects⁴ and quantum interference features.⁵ Alterations of the molecule-metal contact configuration⁶⁻⁹ upon junction stretching or compression are another important class of phenomena which translates into mechanoresistive behaviour. Enhanced overlap of π -orbitals with the metallic electrodes in a compressed junction results, for instance, in higher conductance in thiophenol-terminated molecular wires,^{10,11} or a rheostat-like behaviour in long oligoenes,¹² demonstrating the importance of weak interactions at the nanoscale. Such interactions are however ill-defined in nature, and to date, the conductance changes upon junction size modulation are only moderate.

6.2. Molecular Structure

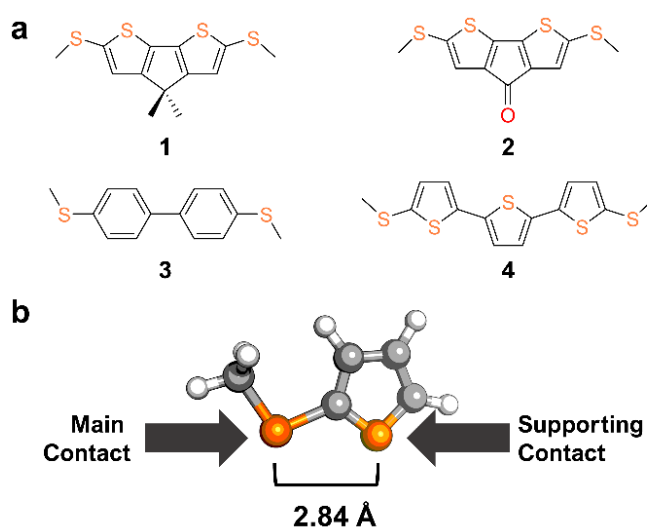
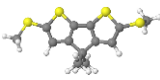
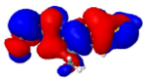
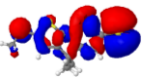
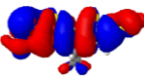
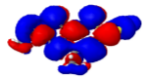
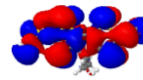
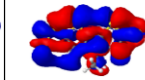
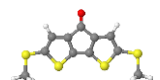
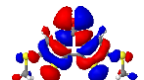
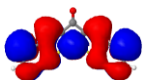

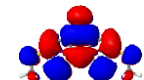
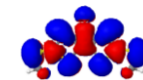
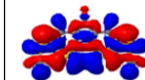
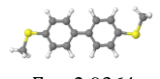
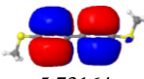

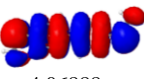
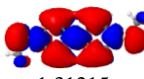
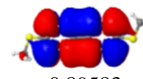
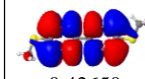
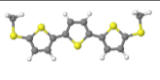
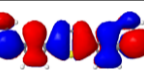
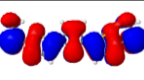
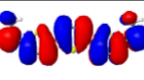
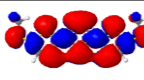
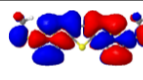
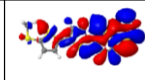


Figure 6.2.1: Structures and numbering of the compounds presented in this study (a) and schematics of the designed (thiomethyl)thiophene contact, with the two binding sites highlighted. Key: H = white, C = grey, S = orange.

All components of the molecules were initially geometrically relaxed to yield the optimized geometries and ground state Hamiltonian shown in table 6.2.1. Table 6.2.1. also shows the molecular orbitals of the systems where all the HOMO and LUMO are extended across the backbone.

Table 6.2.2. Molecular orbitals of HOMO-2, HOMO-1, HOMO, LUMO, LUMO+1 and LUMO+2 for the four components.

	Structure	HOMO-2	HOMO-1	HOMO	LUMO	LUMO+1	LUMO+2
Component 1	 $E_F = -3.1002$	 -5.21112	 -4.69876	 -3.86010	 -1.47812	 -0.16646	 0.08596
Component 2	 $E_F = -3.0725$	 -4.94524	 -4.90568	 -3.71151	 -2.49278	 -0.66719	 -0.43625
Component 3	 $E_F = -2.9364$	 -5.73164	 -4.76349	 -4.06888	 -1.31215	 -0.89583	 -0.42650
Component 4	 $E_F = -2.0720$	 -5.35988	 -4.39534	 -3.60843	 -1.70557	 -0.72441	 -0.17093

6.3. Results and Discussion

This study presents a molecular wire with improved mechanoresistive behaviour, based on a methyl thioether and thienyl moiety bidentate contact configuration. The former acts as primary contact and grants strong mechanical and electrical coupling, while the latter can interact with a metallic electrode through the lone pair on its sulfur atom and provide the additional electronic coupling to enhance conductance in the compressed junction as shown in figure 6.2.1(b). Thiophenes are known to make contact to Au electrodes,¹³ but the interaction is presented as being weaker than traditional contact groups,¹⁴ thus making it an ideal “supporting” molecular contact to the stronger methyl thioether.

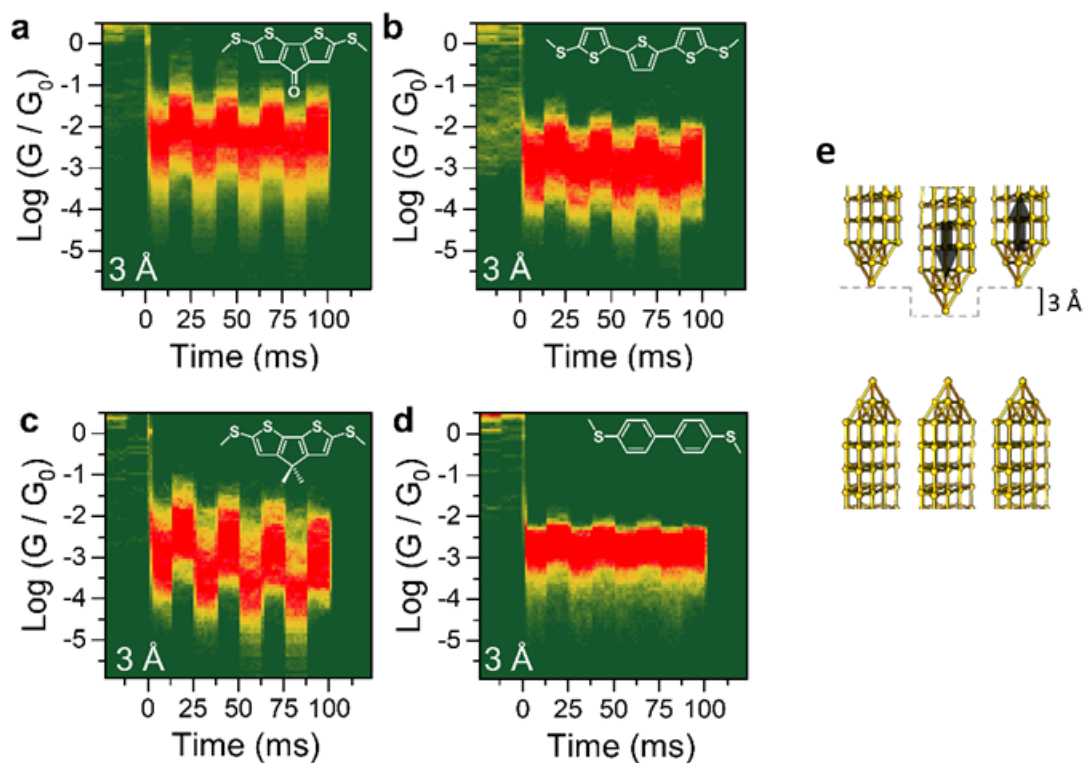


Figure 6.3.1: Conductance vs time density maps for compound **2** (a) and **4** (b) and compound **1** (c) and **3** (d) under square-wave modulation of 3 Å which is idealised position of the electrodes during the modulation is depicted in (e). The structure of the molecular wire is superimposed to its density map of the four compounds presented in this study. The fluctuation in conductance after modulation several times represents the high level which shows on-state in a switched molecule corresponding to a compressed junction, and the low level which shows off-state corresponding to an extended junction.

As can be observed in the experimental results from colleagues at Liverpool University shown in figure 6.2.1(b), after a push-pull process to get the electrode separation results and defined changes in the conductance of **1** as shown in figure 6.3.1 (c). For comparison, the biphenyl-based compound **3** showed very little conductance change as shown in figure 6.3.1 (d), consistent with increased interactions of the electrodes with the aromatic π -system as their junction is compressed. The striking difference in behaviour between these two simple biaryl compounds suggests that the thienyl moiety

is responsible for the mechanoresistive phenomenon. To better characterise this behaviour, two other compounds (**2** and **4**) are investigated, to test the versatility of 2-(methylthio)thiophene as a switching contact moiety. In compound **2** the carbonyl substituent has an electron withdrawing effect, and therefore would result in reduced thiophene-electrode coupling, thereby decreasing the switching magnitude. Compound **4** is a longer oligothiophene, and its purpose is to test whether mechanoresistive behaviour is retained in longer molecular wires. By using the same method is observed the conductance changes of greatly reduced magnitude in **2** as expected as shown in (a), and well-defined conductance variations in **4** which shown in figure 6.3.1 (b).

The overall results confirm that the thienyl moiety as responsible for the observed behaviour, with **1** being the compound providing the largest conductance variation upon modulation of the electrode position, as evidenced by analysing the modulation profile as shown in (c). Therefore, this unprecedented high conductance modulation has been exploited to test the effect of more incremental compression/elongation (push/pull) cycles, and thereby assess the potentiometric behaviour of such single-molecule junctions.

To better understand the phenomena leading to conductance modulation, I used density functional theory (DFT) to optimize geometry and compute the conductance versus electrode separation for all the molecules. SIESTA employs pseudo-potentials to construct the valence states. The generalized gradient approximation (GGA) of the exchange and correlation functional is used with the parameterization (PBE), a double- ζ polarized (DZP) basis set and a real-space grid defined with an equivalent energy cut-off of 150 Ry. The geometry optimization for each structure is performed to the forces is 20 meV/Ang. (See Method in chapter 2). The quantum transport code Gollum¹⁵ was used to calculate the transmission coefficient $T(E)$ for electrons of energy E passing

from the source to the drain electrode via the molecule. If $T(E)$ varies slowly on the scale of $k_B T$ at room temperature T , then $G = G_0 T(E_F)$, where E_F is the Fermi energy of the gold electrodes. Using compound **4** as example as shown in figure 6.3.2 (a), the prediction at small tip-tip distances, the gold electrodes interact with both thienyl and thioether sulfurs, resulting in high molecule-electrode coupling and a high transmission coefficient within the gap between the highest occupied molecular orbital (HOMO) and lowest unoccupied molecular orbital (LUMO) resonances as shown in figure 6.3.3 (a). As the electrode separation is increased, the coupling to the thiophene moiety is reduced and therefore the value of transmission coefficient decreases.

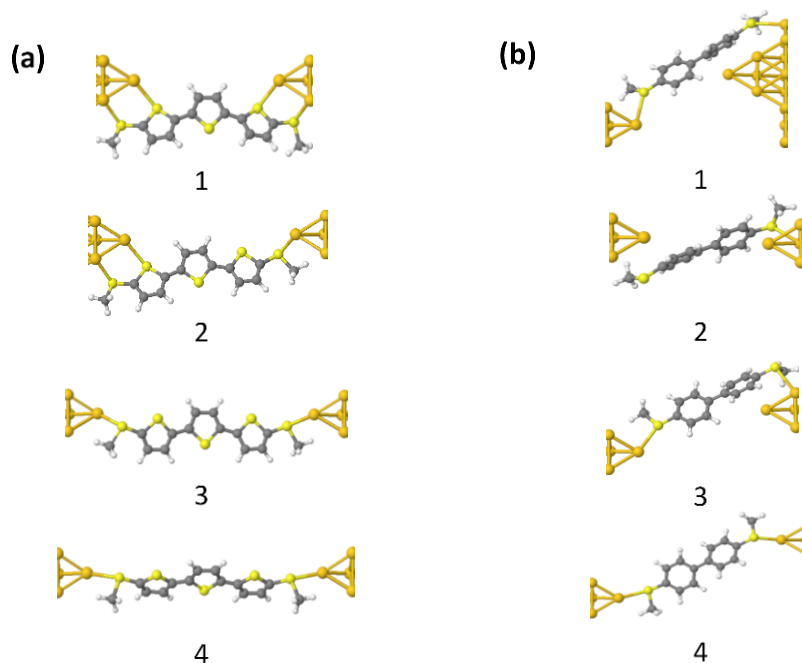
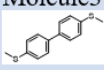
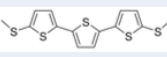


Figure 6.3.2: Relaxed structure of molecule **4** (a) and **3** (b) between two Au electrodes, at various tip-tip distances (11 and 8 Å respective starting separation, increased at any step by 2 Å). Key: H = white, C = grey, S = orange, Au = yellow.

The binding energy of these two of molecule **4** and **3**, at different tip-tip gold electrodes distances are shown in Table 6.3.1.

Table 6.3.1 binding energy calculations for the different binding positions for molecule 3 and 4.

	(Compressed) length1	length2	length3	(Stretched) length4
Molecule3 	-0.049205	-0.775394	-0.854444	-0.989522
Molecule4 	-0.006054	-0.116311	-0.677452	-0.916135

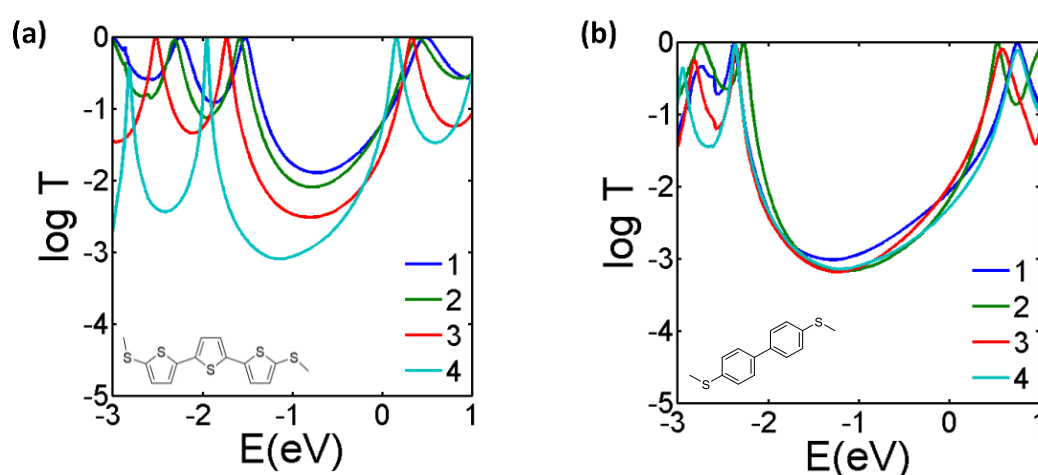


Figure 6.3.3: The transmission coefficient $T(E)$ versus electron energy of compound 4 (a) and 3 (b) at the four tip-tip distances. E is plotted relative to the DFT-predicted Fermi energy of gold (as $E - E_F$).

To predict the effect on the conductance $G = G_0 T(E_F)$, a value for E_F is needed. In figure 6.3.3 (a) and (b), the HOMO and LUMO levels correspond to the resonances in the transmission plots $T(E)$ located immediately below and above $E - E_F = 0$ respectively. The precise values of the HOMO and LUMO levels relative to E_F (and therefore the exact zero of the horizontal axis) depend on environmental conditions and on the unknown shape of the electrodes. However, since the molecules are neither

oxidised nor reduced, E_F lies within the energy gap between the HOMO and the LUMO, and the qualitative change in the conductance with tip-tip distance is determined by the behaviour of $T(E)$ within the gap.

In compound **4**, the additional thiophene-Au interactions described earlier result in large variations of the mid-gap value of $T(E)$ as the electrode position is modulated, and therefore the conductance is also expected to exhibit large variations. In compound **3**, which lacks a thiophene moiety, the value of $T(E)$ within the gap does not change significantly, and the conductance is predicted to be almost independent of the electrode separation.

The process was repeated for compounds **1** and **2** as presented in figures 6.3.4 and 6.3.5. In agreement with experimental results, compressing the electrodes leads to strong interactions between the electrodes and the thiophene moieties, causing significant variations of the transmission coefficient over a wide range of energies within the HOMO-LUMO gap. Overall the amplitude of transmission coefficient values correlates well with the experimental data, with compound **1** having the largest variations in $T(E)$ as the electrode separation is modulated, and compound **3** showing little or no effect.

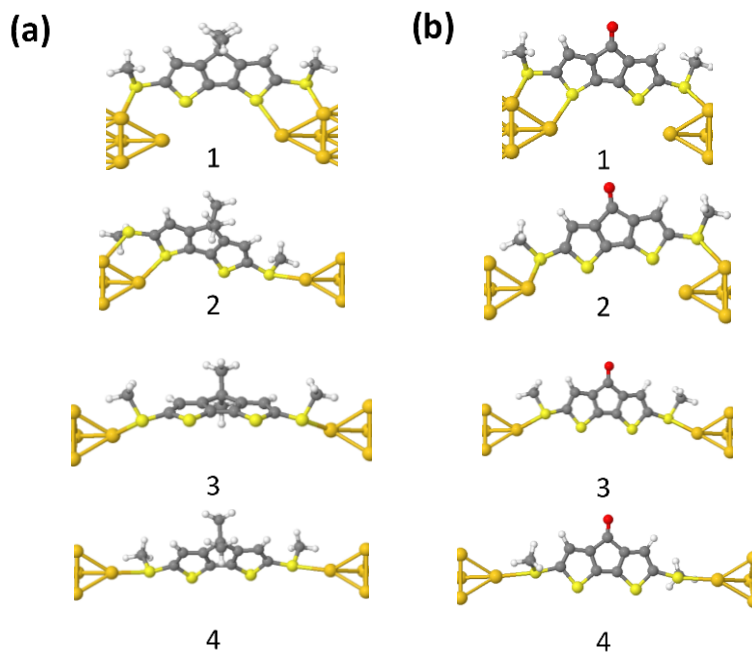


Figure 6.3.4: Relaxed structure of molecule **1** (a) and **2** (b) in a junction where the tip to tip distances is 7 Å for junction 1 and is stretched by ~ 2 Å at any step for junction 2-4. Key: H = white, C = grey, S = orange, Au = yellow and O=red.

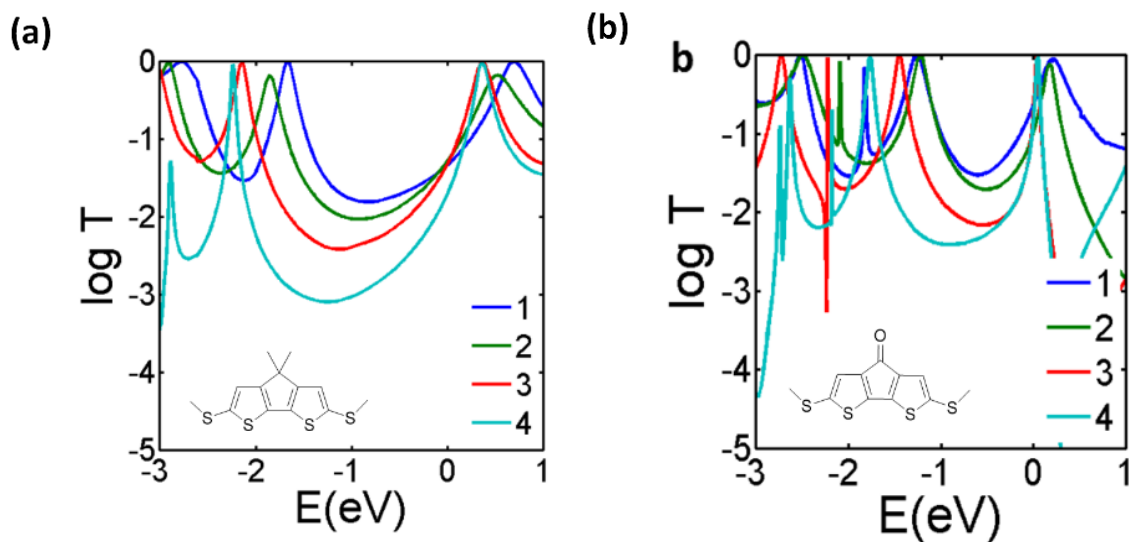


Figure 6.3.5: Transmission coefficient of compounds **1** (a) and **2** (b), calculated from the structures shown in Figure 6.3.6.

All calculations show a significant broadening of the transport resonances as the junction is compressed, further confirming that the change in molecule-contact interactions is indeed responsible for the switching phenomena.

Bibliography

- (1) Bruot, C.; Hihath, J.; Tao, N. Mechanically Controlled Molecular Orbital Alignment in Single Molecule Junctions. *Nat. Nanotechnol.* **2012**, *7* (1), 35.
- (2) Li, Y.; Haworth, N. L.; Xiang, L.; Ciampi, S.; Coote, M. L.; Tao, N. Mechanical Stretching-Induced Electron-Transfer Reactions and Conductance Switching in Single Molecules. *J. Am. Chem. Soc.* **2017**, *139* (41), 14699–14706.
- (3) Frisenda, R.; Harzmann, G. D.; Celis Gil, J. A.; Thijssen, J. M.; Mayor, M.; van der Zant, H. S. J. Stretching-Induced Conductance Increase in a Spin-Crossover Molecule. *Nano Lett.* **2016**, *16* (8), 4733–4737.
- (4) Su, T. A.; Li, H.; Steigerwald, M. L.; Venkataraman, L.; Nuckolls, C. Stereoelectronic Switching in Single-Molecule Junctions. *Nat. Chem.* **2015**, *7* (3), 215.
- (5) Stefani, D.; Weiland, K. J.; Skripnik, M.; Hsu, C.; Perrin, M. L.; Mayor, M.; Pauly, F.; van der Zant, H. S. J. Large Conductance Variations in a Mechanosensitive Single-Molecule Junction. *arXiv Prepr. arXiv1804.10789* **2018**.
- (6) Wang, K.; Hamill, J.; Zhou, J.; Guo, C.; Xu, B. Measurement and Control of Detailed Electronic Properties in a Single Molecule Break Junction. *Faraday Discuss.* **2014**, *174*, 91–104.
- (7) Yoshida, K.; Pobelov, I. V.; Manrique, D. Z.; Pope, T.; Mészáros, G.; Gulcur, M.; Bryce, M. R.; Lambert, C. J.; Wandlowski, T. Correlation of Breaking Forces, Conductances and Geometries of Molecular Junctions. *Sci. Rep.* **2015**, *5*, 9002.

- (8) Quek, S. Y.; Kamenetska, M.; Steigerwald, M. L.; Choi, H. J.; Louie, S. G.; Hybertsen, M. S.; Neaton, J. B.; Venkataraman, L. Mechanically Controlled Binary Conductance Switching of a Single-Molecule Junction. *Nat. Nanotechnol.* **2009**, *4* (4), 230.
- (9) Ismael, A. K.; Wang, K.; Vezzoli, A.; Al-Khaykanee, M. K.; Gallagher, H. E.; Grace, I. M.; Lambert, C. J.; Xu, B.; Nichols, R. J.; Higgins, S. J. Side-Group-Mediated Mechanical Conductance Switching in Molecular Junctions. *Angew. Chemie Int. Ed.* **2017**, *56* (48), 15378–15382.
- (10) Diez-Perez, I.; Hihath, J.; Hines, T.; Wang, Z.-S.; Zhou, G.; Müllen, K.; Tao, N. Controlling Single-Molecule Conductance through Lateral Coupling of π Orbitals. *Nat. Nanotechnol.* **2011**, *6* (4), 226.
- (11) Ramachandran, R.; Li, H. B.; Lo, W.; Neshchadin, A.; Yu, L.; Hihath, J. An Electromechanical Approach to Understanding Binding Configurations in Single-Molecule Devices. *Nano Lett.* **2018**.
- (12) Meisner, J. S.; Kamenetska, M.; Krikorian, M.; Steigerwald, M. L.; Venkataraman, L.; Nuckolls, C. A Single-Molecule Potentiometer. *Nano Lett.* **2011**, *11* (4), 1575–1579.
- (13) Harzmann, G. D.; Frisenda, R.; van der Zant, H. S. J.; Mayor, M. Single-Molecule Spin Switch Based on Voltage-Triggered Distortion of the Coordination Sphere. *Angew. Chemie Int. Ed.* **2015**, *54* (45), 13425–13430.
- (14) Bejarano, F.; Olavarria-Contreras, I. J.; Droghetti, A.; Rungger, I.; Rudnev, A.; Gutiérrez, D.; Mas-Torrent, M.; Veciana, H. S. J.; Rovira, C.; et al. Robust Organic Radical Molecular Junctions Using Acetylene Terminated Groups for C-Au Bond Formation. *J. Am. Chem. Soc.* **2018**, *140* (5), 1691–1696.

- (15) Ferrer, J.; Lambert, C. J.; García-Suárez, V. M.; Manrique, D. Z.; Visontai, D.; Oroszlany, L.; Rodríguez-Ferradás, R.; Grace, I.; Bailey, S. W. D.; Gillemot, K.; et al. GOLLUM: A next-Generation Simulation Tool for Electron, Thermal and Spin Transport. *New J. Phys.* **2014**, *16*, 093029.

Chapter 7

Conclusions and Future Work

1.1. Conclusions

In conclusion, by using DFT and Green's function methods as well as a simple tight binding method (TBM) as presented in chapter 2 and 3 respectively, I theoretically investigated transport properties of molecular scale junctions and achieved qualitative agreement with experimental data. Consequently, theory and experiment could effectively communicate and help each other to finally explain physics and chemistry phenomena at the molecular scale.

In chapter 4, I demonstrated that the electrical conductance of fused oligo porphyrin molecular wires can either *increase* with increasing length or be length independent in junctions formed with graphene electrodes. This is due to alignment of the middle of the HOMO-LUMO gap of the molecules with the Fermi energy of the graphene electrodes. In addition, I showed that in junctions formed with gold electrodes, this generic feature is anchor group dependent. This negative attenuation factor is due to the quantum nature of electron transport through such wires and arises from the narrowing of the HOMO-LUMO gap as the length of the oligomers increases.

In chapter 5, the possibility of tuning DQI within m-OPE molecules was investigated by placing -OMe pendant groups at different positions within the central phenyl ring. The results demonstrate that the introduction of -OMe at different locations has a significant impact on DQI and provides a promising route to tuning the charge transport properties of the compounds, without altering molecular backbone configurations or the surrounding environment. The DFT calculations reveal that this fine tuning of charge transport through the single-molecule junctions occurs, because the attachment of -OMe causes a significant shift the energetic location of transmission dips arising from DQI. More interestingly, the conductance of **M2** was almost five-fold higher than **M1**, indicating that the simple positional switch of -OMe can achieve a large change of molecular conductance. This work presents a simple and convenient strategy for tuning room-temperature DQI at a single-molecule level and demonstrates a new strategy for designing molecular materials and devices with desirable functions.

Finally, in chapter 6, a series of single-molecule mechanoresistive junctions was designed and characterised, based on a bidentate contact moiety that exploits the weak interactions of thienyl sulfurs with Au electrodes. The functional moiety is a (methylthio)thiophene, which is directly responsible for the observed high sensitivity behaviour by providing multiple anchoring points (the thienyl and thioether sulfurs) for the metallic electrodes. This study presents a novel strategy for the introduction of electromechanical functionality in molecular wires and highlights the importance of weak interactions at the electrode interface. Furthermore, as (methylthio) thiophenes and thiophenethiols are widely used as molecular wire termini in molecular electronics, that results shed more light on their unusual electromechanical properties.

1.2. Future Work

For the future, the following aspects deserve further attention: (1) the electronic properties of Porphyrin with different connectivities to the electrodes such as connectivities 1-11 versus 6-11 in figure 4.3.6 (a) (2) To examine the effect of negative attenuation factor in fused porphyrins on their thermoelectric performance^{1,2} and study the effect of metallic centre in metalloporphyrin such as Nickel and Cobalt element (3) a systematic study of the effect of different anchor groups such as Thiol (S), Amino (NH₂), Dihydrobenzo thiophene (BT), Direct carbon (C), methyle sulphide (SMe), Pyridine, Cyano (CN) on the transport properties^{3,4} and attenuation factor of molecular junctions formed by porphyrin or thiophene molecular cores.(4) examine the effect of different pendant group to the central ring of OPE3 such as NH₂, CF₃ on destructive quantum interference through meta connectivity.

The field of molecular thermoelectrics is in its infancy and ongoing studies are needed to highlight how chemical modifications of molecules and new combinations of molecules and electrode materials can be used to tune electrical properties. For the future, it would be of interest to study how transport properties change when alternative electrode materials are used such as platinum, palladium or iron^{5,6} or even superconducting electrodes⁷⁻⁹. For the purpose of computing thermal properties, it would be of interest to utilise methods for computing phonon transport through nanostructures^{10,11} to obtain the contribution from phonons to the thermal conductance through fullerene-based molecular junctions.

Bibliography

- (1) Liu, X.; Sangtarash, S.; Reber, D.; Zhang, D.; Sadeghi, H.; Shi, J.; Xiao, Z. Y.; Hong, W.; Lambert, C. J.; Liu, S. X. Gating of Quantum Interference in Molecular Junctions by Heteroatom Substitution. *Angew. Chemie - Int. Ed.* **2017**, *56* (1), 173–176.
- (2) Reddy, P.; Jang, S.-Y.; Segalman, R. A.; Majumdar, A. Thermoelectricity in Molecular Junctions. *Science (80-.)*. **2007**, *315* (5818), 1568–1571.
- (3) Moreno-García, P.; Gulcur, M.; Manrique, D. Z.; Pope, T.; Hong, W.; Kaliginedi, V.; Huang, C.; Batsanov, A. S.; Bryce, M. R.; Lambert, C.; et al. Single-Molecule Conductance of Functionalized Oligoynes: Length Dependence and Junction Evolution. *J. Am. Chem. Soc.* **2013**, *135* (33), 12228–12240.
- (4) Frisenda, R.; Tarkuç, S.; Galán, E.; Perrin, M. L.; Eelkema, R.; Grozema, F. C.; van der Zant, H. S. J. Electrical Properties and Mechanical Stability of Anchoring Groups for Single-Molecule Electronics. *Beilstein J. Nanotechnol.* **2015**, *6*, 1558.
- (5) García-Suárez, V. M.; Rocha, A. R.; Bailey, S. W.; Lambert, C. J.; Sanvito, S.; Ferrer, J. Single-Channel Conductance of H₂ Molecules Attached to Platinum or Palladium Electrodes. *Phys. Rev. B* **2005**, *72* (4), 45437.
- (6) García-Suárez, V. M.; Newman, C. M.; Lambert, C. J.; Pruneda, J. M.; Ferrer, J. Optimized Basis Sets for the Collinear and Non-Collinear Phases of Iron. *J. Phys. Condens. Matter* **2004**, *16* (30), 5453.
- (7) Fal'ko, V. I.; Lambert, C. J.; Volkov, A. F. Andreev Reflections and Magnetoresistance in Ferromagnet-Superconductor Mesoscopic Structures. *J. Exp. Theor. Phys. Lett.* **1999**, *69* (7), 532–538.
- (8) Lambert, C. J.; Raimondi, R.; Sweeney, V.; Volkov, A. F. Boundary Conditions

for Quasiclassical Equations in the Theory of Superconductivity. *Phys. Rev. B* **1997**, *55* (9), 6015.

- (9) Hui, V. C.; Lambert, C. J. Andreev Scattering, Universal Conductance Fluctuations and Phase Periodic Transport. *EPL (Europhysics Lett.)* **1993**, *23* (3), 203.
- (10) Fagas, G.; Kozorezov, A. G.; Lambert, C. J.; Wigmore, J. K.; Peacock, A.; Poelaert, A.; Den Hartog, R. Lattice Dynamics of a Disordered Solid-Solid Interface. *Phys. Rev. B* **1999**, *60* (9), 6459.
- (11) Han, H.; Zhang, Y.; Wang, N.; Samani, M. K.; Ni, Y.; Mijbil, Z. Y.; Edwards, M.; Xiong, S.; Sääskilahti, K.; Murugesan, M.; et al. Functionalization Mediates Heat Transport in Graphene Nanoflakes. *Nat. Commun.* **2016**, *7*, 11281.